Titre: Title:	New mixed oxide electrodes for the oxygen evolution reaction
Auteur: Author:	Hui Jun Miao
Date:	1993
Type:	Mémoire ou thèse / Dissertation or Thesis
Référence: Citation:	Miao, H. J. (1993). New mixed oxide electrodes for the oxygen evolution reaction [Ph.D. thesis, Polytechnique Montréal]. PolyPublie. https://publications.polymtl.ca/57982/

UNIVERSITÉ DE MONTRÉAL

NEW MIXED OXIDE ELECTRODES FOR THE OXYGEN EVOLUTION REACTION

par

Hui Jun MIAO

DÉPARTEMENT DE MÉTALLURGIE
ET DE GÉNIE DES MATÉRIAUX
ÉCOLE POLYTECHNIQUE

THÈSE PRÉSENTÉE EN VUE DE L'OBTENTION
DU GRADE DE PHILOSOPHIAE DOCTOR (Ph.D.)
(GÉNIE MÉTALLURGIQUE)
Mai 1993

ISBN 0-315-86555-5

Canada

me MIAO, HUI JUN

sertation Abstracts International is arranged by broad, general subject categories. Please select the one subject which most
ırly describes the content of your dissertation. Enter the corresponding four-digit code in the spaces provided.

Materials Science and Engineering.
SUBJECT TERM

0794
SUBJECT CODE

U·M·I

ɔject Categories

IE HUMANITIES AND SOCIAL SCIENCES

ıMUNICATIONS AND THE ARTS
ıitecture 0729
-listory 0377
ıma 0900
ce 0378
Arts 0357
ɪmation Science 0723
nalism 0391
ɔry Science 0399
s Communications 0708
ic 0413
ɔch Communication 0459
ıter 0465

CATION
eral 0515
ıinistration 0514
lt and Continuing 0516
cultural 0517
..... 0273
gual and Multicultural 0282
ness 0688
ımunity College 0275
ɨiculum and Instruction 0727
y Childhood 0518
ıentary 0524
ɲce 0277
dance and Counseling 0519
lth 0680
ıer 0745
ɔry of 0520
ıe Economics 0278
strial 0521
ɥuage and Literature 0279
ɦematics 0280
ic 0522
ɔsophy of 0998
ɨical 0523

Psychology 0525
Reading 0535
Religious 0527
Sciences 0714
Secondary 0533
Social Sciences 0534
Sociology of 0340
Special 0529
Teacher Training 0530
Technology 0710
Tests and Measurements 0288
Vocational 0747

LANGUAGE, LITERATURE AND LINGUISTICS
Language
- General 0679
- Ancient 0289
- Linguistics 0290
- Modern 0291

Literature
- General 0401
- Classical 0294
- Comparative 0295
- Medieval 0297
- Modern 0298
- African 0316
- American 0591
- Asian 0305
- Canadian (English) 0352
- Canadian (French) 0355
- English 0593
- Germanic 0311
- Latin American 0312
- Middle Eastern 0315
- Romance 0313
- Slavic and East European 0314

PHILOSOPHY, RELIGION AND THEOLOGY
Philosophy 0422
Religion
- General 0318
- Biblical Studies 0321
- Clergy 0319
- History of 0320
- Philosophy of 0322

Theology 0469

SOCIAL SCIENCES
American Studies 0323
Anthropology
- Archaeology 0324
- Cultural 0326
- Physical 0327

Business Administration
- General 0310
- Accounting 0272
- Banking 0770
- Management 0454
- Marketing 0338

Canadian Studies 0385
Economics
- General 0501
- Agricultural 0503
- Commerce-Business 0505
- Finance 0508
- History 0509
- Labor 0510
- Theory 0511

Folklore 0358
Geography 0366
Gerontology 0351
History
- General 0578
- Ancient 0579
- Medieval 0581
- Modern 0582
- Black 0328
- African 0331
- Asia, Australia and Oceania 0332
- Canadian 0334
- European 0335
- Latin American 0336
- Middle Eastern 0333
- United States 0337

History of Science 0585
Law 0398
Political Science
- General 0615
- International Law and Relations 0616
- Public Administration 0617

Recreation 0814
Social Work 0452
Sociology
- General 0626
- Criminology and Penology ... 0627
- Demography 0938
- Ethnic and Racial Studies 0631
- Individual and Family Studies 0628
- Industrial and Labor Relations 0629
- Public and Social Welfare 0630
- Social Structure and Development 0700
- Theory and Methods 0344

Transportation 0709
Urban and Regional Planning 0999
Women's Studies 0453

IE SCIENCES AND ENGINEERING

LOGICAL SCIENCES
ɨculture
- General 0473

Agronomy 0285
Animal Culture and Nutrition 0475
Animal Pathology 0476
Food Science and Technology 0359
Forestry and Wildlife 0478
Plant Culture 0479
Plant Pathology 0480
Plant Physiology 0817
Range Management 0777
Wood Technology 0746

ɔgy
- General 0306

Anatomy 0287
Biostatistics 0308
Botany 0309
Cell 0379
Ecology 0329
Entomology 0353
Genetics 0369
Limnology 0793
Microbiology 0410
Molecular 0307
Neuroscience 0317
Oceanography 0416
Physiology 0433
Radiation 0821
Veterinary Science 0778
Zoology 0472

ɨhysics
- General 0786

Medical 0760

TH SCIENCES
ɟeochemistry 0425
ɨchemistry 0996

Geodesy 0370
Geology 0372
Geophysics 0373
Hydrology 0388
Mineralogy 0411
Paleobotany 0345
Paleoecology 0426
Paleontology 0418
Paleozoology 0985
Palynology 0427
Physical Geography 0368
Physical Oceanography 0415

HEALTH AND ENVIRONMENTAL SCIENCES
Environmental Sciences 0768
Health Sciences
- General 0566
- Audiology 0300
- Chemotherapy 0992
- Dentistry 0567
- Education 0350
- Hospital Management 0769
- Human Development 0758
- Immunology 0982
- Medicine and Surgery 0564
- Mental Health 0347
- Nursing 0569
- Nutrition 0570
- Obstetrics and Gynecology .. 0380
- Occupational Health and Therapy 0354
- Ophthalmology 0381
- Pathology 0571
- Pharmacology 0419
- Pharmacy 0572
- Physical Therapy 0382
- Public Health 0573
- Radiology 0574
- Recreation 0575
- Speech Pathology 0460
- Toxicology 0383

Home Economics 0386

PHYSICAL SCIENCES
Pure Sciences
Chemistry
- General 0485
- Agricultural 0749
- Analytical 0486
- Biochemistry 0487
- Inorganic 0488
- Nuclear 0738
- Organic 0490
- Pharmaceutical 0491
- Physical 0494
- Polymer 0495
- Radiation 0754

Mathematics 0405
Physics
- General 0605
- Acoustics 0986
- Astronomy and Astrophysics 0606
- Atmospheric Science 0608
- Atomic 0748
- Electronics and Electricity 0607
- Elementary Particles and High Energy 0798
- Fluid and Plasma 0759
- Molecular 0609
- Nuclear 0610
- Optics 0752
- Radiation 0756
- Solid State 0611

Statistics 0463

Applied Sciences
Applied Mechanics 0346
Computer Science 0984

Engineering
- General 0537
- Aerospace 0538
- Agricultural 0539
- Automotive 0540
- Biomedical 0541
- Chemical 0542
- Civil 0543
- Electronics and Electrical 0544
- Heat and Thermodynamics ... 0348
- Hydraulic 0545
- Industrial 0546
- Marine 0547
- Materials Science 0794
- Mechanical 0548
- Metallurgy 0743
- Mining 0551
- Nuclear 0552
- Packaging 0549
- Petroleum 0765
- Sanitary and Municipal 0554
- System Science 0790

Geotechnology 0428
Operations Research 0796
Plastics Technology 0795
Textile Technology 0994

PSYCHOLOGY
General 0621
Behavioral 0384
Clinical 0622
Developmental 0620
Experimental 0623
Industrial 0624
Personality 0625
Physiological 0989
Psychobiology 0349
Psychometrics 0632
Social 0451

UNIVERSITÉ DE MONTRÉAL

ÉCOLE POLYTECHNIQUE

Cette thèse intitulée:

NEW MIXED OXIDE ELECTRODES FOR THE OXYGEN EVOLUTION REACTION

présentée par: **Hui Jun MIAO**

en vue de l'obtention du grade de: Philosophiae Doctor (Ph.D.)

a été dûment acceptée par le jury d'examen constitué de:

M. RIGAUD, Michel, D.Sc.A., président

M. PIRON, Dominique L., Ph.D., directeur de recherche

M. D'AMBOISE, Marius, Ph.D., examinateur externe

M. PERRIER, Michel, Ph.D., membre

To Jing Ren Tang

My wife whose cooperation and patience were strong supports to my completion of this thesis.

SOMMAIRE

La réaction de dégagement d'oxygène (RDO) est une importante réaction anodique dans l'électrolyse de l'eau, l'électrosynthèse et l'électroaffinage du Ni, Zn et Co. Dans ces procédés, le haut voltage de la cellule résultant d'une grande surtension produite par la réaction du dégagement d'oxygène donne un bas rendement de production. Une diminution de la surtension d'oxygène améliorerait le rendement énergétique.

Les techniques utilisées pour diminuer les surtensions de la RDO sont basées sur deux concepts: (a) l'utilisation de matériaux ayant une grande activité électrocatalytique et (b) l'utilisation des électrodes avec une grande surface réelle. Ces deux concepts ont été adoptés dans la présente étude afin de développer de nouvelles électrodes d'oxydes mixtes pour la RDO en solution alcaline. Le nickel a été choisi comme matériau de base des électrodes. Le Ni-Ir et le Ni-Ru ont été obtenus par électrodéposition. Les électrodes à base de composites de Ni, Co et de Fe ont également été fabriquées par déposition-composite.

L'activité électrocatalytique a été améliorée en utilisant des électrodes à base de nickel allié à des métaux de transition. Des électrodes de Ni-Ru et Ni-Ir obtenues par

codéposition ont été étudiées pour la RDO dans une solution de KOH 5M. Les caractéristiques électrochimiques ont montré, qu'en présence de Ru ou d'Ir, la couche d'oxyde mixte des électrodes de nickel a réduit la surtension et a augmenté la densité de courant pour la RDO. À 20 mA/cm^2, une diminution de la surtension d'environ 30 à 40 mV a été observée sur des électrodes d'alliages de nickel mentionnés. De plus, la densité de courant, avec une surtension de 0.4V sur les électrodes de Ni, a été multipliée par 3 et par 6 avec, respectivement, 2.2% en poids de Ru et 6.0% en poids d'Ir.

Les mesures de voltamétrie cyclique ont montré que l'addition de Ru ou d'Ir change la tension d'oxydation de la surface oxydée des électrodes de Ni. La surtension de la RDO peut être subdivisée en deux parties: $\eta = \Delta E_{ox} + \Delta E_{O2}$. Le ΔE_{ox}, qui caractérise la tension d'oxydation, est le plus bas dans le cas des oxydes mixtes de Ni-Ir; tandis que le ΔE_{O2}, qui représente la différence entre les tensions d'oxydation et de la RDO, est à son minimum dans le cas des oxydes mixtes de Ni-Ru. Il est donc suggéré que le mécanisme pour améliorer la performance des électrodes de Ni avec l'Ir soit différent de celui avec le Ru. L'Ir diminue la tension d'oxydation du Ni, tandis que le Ru abaisse la surtension de la RDO sur la surface oxydée. Tous les deux ont amélioré les propriétés catalytiques des électrodes de Ni.

Un nouveau procédé de déposition-composite a été étudié dans la fabrication des électrodes composite-revêtement. L'amélioration des propriétés catalytiques des électrodes composite-revêtement est attribuée à la porosité et à la rugosité élevées de la surface de ces dernières, et non pas à l'activation de la surface. Effectivement, des observations au MEB ont montré que les électrodes fabriquées selon la technique composite-revêtement présentent visiblement une surface rugueuse. De plus, cette rugosité de la surface augmente lorsqu'on ajoute des poudres de Ni, Co ou Fe dans le bain de déposition.

Les caractérisations d'impédance AC ont été effectuées sur les électrodes composite-revêtement dans une solution de KOH 5M à 25°C. Les spectres d'impédance ont été obtenus dans l'intervalle de fréquences variant de 10^{-3} à 10^{5} Hz pour la RDO et la RDH. Les comportements de l'impédance des électrodes furent théoriquement modélisés à l'aide d'un circuit équivalent constitué d'une R_{ct} et de la "Constante Phase Element" (CPE). Les données expérimentales des RDO et RDH correspondent très bien aux tracés des courbes produites à partir du circuit équivalent. Les caractérisations d'impédance montrent que la dimension fractionnaire, l'angle de dépression des points des plans complexes ainsi que le facteur de rugosité de la surface sur les électrodes à base de composite, ont été beaucoup plus élevés que pour les

électrodes de Ni. Ces mesures révèlent que l'augmentation de surface réelle d'une électrode à surface rugueuse est responsable de l'amélioration des performances pour la RDO et la RDH. Les meilleures performances pour la RDO et la RDH ont été obtenues sur des électrodes composites Ni-Fe. Les résultats ont montré que la valeur de l'angle de dépression des points des plans complexes n'est pas constante avec les variations de la surtension. Ces résultats ont aussi démontré que la capacité de la double couche varie, dépendant de la réaction (la RDO ou la RDH). Donc, il est possible d'utiliser l'angle de phase de l'impédance (paramètre dépendant de la fréquence) et l'angle de dépression (paramètre indépendant de la fréquence) pour caractériser les électrodes selon leur rugosité.

ABSTRACT

The objective of this study is to develop new mixed oxide electrodes for the oxygen evolution reaction (OER). A critical review of the most important aspects of the oxygen electrodes was presented in Chapter 2. Two techniques for reducing the oxygen overpotential have been adopted in this study. They are: (a) creating active centres on the electrode with catalytically active materials and (b) increasing electrode's real surface areas. Nickel was selected as the base material because of its relatively good electrocatalytical activity and stability in alkaline solutions. Electrolytic deposition was employed to prepare Ni-based electrodes. Ni-Ru and Ni-Ir electrodes were fabricated by codeposition. The Ni, Co and Fe composite-coating electrodes were prepared by the composite-deposition method.

The electrocatalytical activity on Ni-based electrodes were significantly improved by alloying with transition metals of less than 10 wt%, which is the new results for the Ni-based oxygen electrodes. Electrochemical characterizations showed that a decrease of 30 to 40 mV (at 20 mA/cm^2) of the OER overpotential was observed on the Ni-Ru and Ni-Ir mixed oxide electrodes in 5M KOH solution at 25°C. The electrode current density at 0.4 V of overpotential was increased threefold with 2.2 wt% Ru and 6-times with 6.0 wt% Ir.

Cyclic voltammetric measurements showed that the addition of Ru or Ir to Ni-based electrodes changed the surface oxidation peak potential. The OER overpotential can be divided into two parts: $\eta = \Delta E_{ox} + \Delta E_{O2}$. The ΔE_{ox}, which characterizes the peak potential, was the lowest on the Ni-Ir mixed oxide; the ΔE_{O2}, which represents the potential difference between the oxidation peak and the OER, was the lowest on the Ni-Ru mixed oxide. Therefore, it is suggested that the mechanism for improving the performance of the Ni electrode with Ir was different from that with Ru: Ir decreased the Ni oxidation potential while Ru lowered the overpotential on the oxidized surface. The presence of either Ru or Ir was, however, is beneficial to increase the Ni-based electrode's activity. This understanding is a new contribution to the knowledge of increasing the electrocatalyticalal activity of the oxygen electrodes.

A new process, namely composite-deposition, was employed to fabricate the composite-coating electrodes. It is very effective in fabricating an electrode with a very rough surface. Results showed that an improved catalytic property of the composite-coating electrodes was attributable to the very rough and porous surface, and not to surface activation. SEM examinations showed that the composite-coating electrode had a visibly rough surface, and the surface roughness on the coating increased when the electrode was prepared in the bath

with Ni, Co or Fe powders. The best performance for the OER and HER (hydrogen evolution reaction) in 5M KOH solution was obtained on the Fe composite-coating electrode.

AC impedance characterizations were carried out on the composite-coating electrodes in 5M KOH solution at 25°C. The impedance spectra were collected in the frequency range from 10^{-3} to 10^{5} Hz under the conditions for the OER and HER. It was found that impedance responses of the composite-coating electrode could not be modelled and fitted with a simple equivalent circuit, such as the R-C circuit. This suggests that the roughness of the composite-coating surface has an impact on the impedance response of the electrode at the tested frequency range. The depressed angle of semi-circular arc in the complex-plane plot was related to the electrode surface roughness. This behaviour has been taken as a measure of the impedance technique for characterization of the electrode surface roughness. This is one of the pioneer works to study the surface roughness by the impedance technique.

An equivalent circuit consisting of a charge transfer resistance (R_{ct}) and the "Constant Phase Element" (CPE) was used to model the electrode with a highly rough surface. Experimental data for the OER and HER corresponded very well with the curve fittings based on the equivalent circuit. Impedance characterizations showed that the fractal dimension,

the depression angle of the complex-plane plot and the surface roughness factor were sensitive indicators of the surface roughness on composite-coating electrodes. These measurements suggested that the high real surface area on the composite-coating electrode was responsible for the improvement of the electrode performance for the OER and HER. The results also demonstrated that the value of the depression angle of the complex-plane plot was not a constant as the overpotential changed; that the double-layer capacitance varied with electrochemical reactions, the OER or HER. Those are results first reported for oxygen and hydrogen electrodes. Therefore, it is possible to use the impedance phase angle (frequency-dependent parameter) and the depressed angle of the complex-plane plots (frequency-independent character) to characterize the electrode with a very rough surface.

RÉSUMÉ

La réaction de dégagement d'oxygène (RDO) est une importante réaction anodique dans l'électrolyse de l'eau, l'électrosynthèse et l'électroaffinage du Ni, Zn et Co. Dans ces procédés, le haut voltage de la cellule résultant d'une grande surtension produite par la réaction du dégagement d'oxygène donne un bas rendement de production. Une diminution de la surtension d'oxygène améliorerait le rendement énergétique.

L'étude bibliographique (Chapitre 2) traite des plus importants aspects relevant de l'électrocatalyse de la RDO. Les différents matériaux utilisés dans la fabrication des électrodes pour dégagement d'oxygène ont été classifiés et répertoriés. Une attention particulière a été donnée aux matériaux à base d'oxyde. Leur structure, leur méthode de préparation et leur activité électrocatalytique ont été discutées en détails. Les critères pris en considération pour le choix des matériaux utilisés dans la fabrication des électrodes sont: l'activité électrocatalytique, la résistance à la corrosion, la conductivité, la réaction sélective, le rapport entre la tension réversible de l'oxygène et la tension standard des électrodes, ainsi que la dépendance de l'activité électrocatalytique du phénomène d'adsorption-désorption des espèces réactantes.

Les techniques pour améliorer l'activité des électrodes pour la RDO seront citées ultérieurement. Le nickel en tant que matériau des électrodes a été revu. Les mécanismes de la RDO proposés par plusieurs auteurs ont été présentés dans l'étude bibliographique. Les paramètres électrochimiques des électrodes ainsi que l'évaluation de ses performances ont été résumés sommairement.

Les techniques utilisées pour diminuer les surtensions de la RDO sont basées sur deux concepts: (a) l'utilisation de matériaux ayant une grande activité électrocatalytique et (b) l'utilisation des électrodes avec une grande surface réelle. Ces deux concepts ont été adoptés dans la présente étude afin de développer de nouvelles électrodes d'oxydes mixtes pour la RDO en solution alcaline.

Le nickel a été choisi comme matériau de base des électrodes, vu sa bonne activité électrocatalytique et sa stabilité dans les solutions alcalines. Les électrodes à base de nickel sont préparées par des dépositions électrolytiques. Le Ni-Ir et le Ni-Ru ont été obtenus par électrodéposition. Les électrodes à base de composites de Ni, Co et de Fe ont également été fabriquées par déposition-composite. Ces électrodes ont été étudiées pour la RDO et la réaction de dégagement d'hydrogène (RDH) dans une solution de KOH 5M.

Les dépositions du nickel peuvent avoir lieu dans différents électrolytes. Les électrodes de nickel déposées à partir de sept (7) électrolytes ont été évaluées par analyse microscopique électronique à balayage (MEB). De plus, elles ont été caractérisées par les méthodes électrochimiques Une grande attention a été apportée aux propriétés catalytiques de la RDO. Les électrolytes chlorurés se sont avérés les plus performants pour la fabrication des électrodes de nickel. Elles ont révélé une densité de courant apparente assez élevée et une basse surtension avec une grande surface réelle basée sur les observations microscopiques et les caractéristiques électrochimiques.

L'activité électrocatalytique a été améliorée en utilisant des électrodes à base de nickel allié à des métaux de transition. Des électrodes de Ni-Ru et Ni-Ir obtenues par codéposition ont été étudiées pour la RDO dans une solution de KOH 5M à 25°C. Les caractéristiques électrochimiques ont montré, qu'en présence de Ru ou d'Ir, la couche d'oxyde mixte des électrodes de Ni a réduit la surtension et a augmenté la densité de courant pour la RDO. À 20 mA/cm^2, une diminution de la surtension d'environ 30 à 40 mV a été observée sur des électrodes d'alliages de nickel mentionnés. De plus, la densité de courant, avec une surtension de 0.4V sur les électrodes de Ni, a été multipliée par 3 et par 6 avec, respectivement, 2.2% en poids de Ru et 6.0% en poids d'Ir.

Les mesures de voltamétrie cyclique ont montré que l'addition de Ru ou d'Ir change la tension d'oxydation de la surface oxydée des électrodes de Ni. La surtension de la RDO peut être subdivisée en deux parties: $\eta = \Delta E_{ox} + \Delta E_{O2}$. Le ΔE_{ox}, qui caractérise la tension d'oxydation, est le plus bas dans le cas des oxydes mixtes de Ni-Ir; tandis que le ΔE_{O2}, qui représente la différence entre les tensions d'oxydation et de la RDO, est à son minimum dans le cas des oxydes mixtes de Ni-Ru. Il est donc suggéré que le mécanisme pour améliorer la performance des électrodes de Ni avec l'Ir soit différent de celui avec le Ru. L'Ir diminue la tension d'oxydation du Ni, tandis que le Ru abaisse la surtension de la RDO sur la surface oxydée. Tous les deux ont amélioré les propriétés catalytiques des électrodes de Ni.

L'effet bénéfique sur la RDO a été observé avec une faible addition de Ru (<1% poids). Par contre, l'utilisation de grandes quantités de Ru se traduit par une dissolution sélective de ce dernier sur la surface des électrodes. En effet, nous avons observé en laboratoire que l'augmentation de Ru dans les électrodes de Ni se traduit par une accélération de la corrosion dans une solution de KOH 5M. Les tests de stabilité sur les électrodes d'oxyde mixte Ni-Ir ont montré que sa résistance à la corrosion est élevée et qu'elle conserve ses bonnes caractéristiques électrocatalytiques pendant au moins 24 heures.

Un nouveau procédé de déposition-composite a été étudié dans la fabrication des électrodes composite-revêtement. La simplicité, la déposition rapide, le contrôle facile des conditions d'opération ainsi que le faible coût de cette technique la rendent efficace pour la fabrication des électrodes à grande surface rugueuse. L'amélioration des propriétés catalytiques des électrodes composite-revêtement est attribuée à la porosité et à la rugosité élevées de la surface de ces dernières, et non pas à l'activation de la surface. Effectivement, des observations au MEB ont montré que les électrodes fabriquées selon la technique composite-revêtement présentent visiblement une surface rugueuse. De plus, cette rugosité de la surface augmente lorsqu'on ajoute des poudres de Ni, Co ou Fe dans le bain de déposition.

Les caractérisations d'impédance AC ont été effectuées sur les électrodes composite-revêtement dans une solution de KOH 5M à 25°C. Les spectres d'impédance ont été obtenus dans l'intervalle de fréquences variant de 10^{-3} à 10^{5} Hz pour la RDO et la RDH. Les comportements de l'impédance des électrodes furent théoriquement modélisés à l'aide d'un circuit équivalent constitué d'une R_{ct} et de la "Constante Phase Element" (CPE). Les données expérimentales des RDO et RDH correspondent très bien aux tracés des courbes produites à partir du circuit équivalent. Les caractérisations d'impédance montrent que la dimension fractionnaire, l'angle

de dépression des points des plans complexes ainsi que le facteur de rugosité de la surface sur les électrodes à base de composite, ont été beaucoup plus élevés que pour les électrodes de nickel. Ces mesures révèlent que l'augmentation de surface réelle d'une électrode à surface rugueuse est responsable de l'amélioration des performances pour la RDO et la RDH. Les meilleures performances pour la RDO et la RDH ont été obtenues sur des électrodes composites Ni-Fe. Les résultats ont montré que la valeur de l'angle de dépression des points des plans complexes n'est pas constante avec les variations de la surtension. Ces résultats ont aussi démontré que la capacité de la double couche varie, dépendant de la réaction (la RDO ou la RDH). Donc, il est possible d'utiliser l'angle de phase de l'impédance (paramètre dépendant de la fréquence) et l'angle de dépression (paramètre indépendant de la fréquence) pour caractériser les électrodes selon leur rugosité.

Finalement, les électrodes fabriquées par différentes méthodes ont été comparées et les mécanismes pour améliorer les performances des électrodes ont été discutés. Les avantages ainsi que les limites d'utilisation de ces techniques ont été discutés.

ACKNOWLEDGMENTS

I would like to thank the director of my thesis, Professor Dominique L. Piron, who introduced me to this interesting and challenging subject, for his continuous encouragement to me to undertake this study and for his many constructive discussions and valuable advice for improving the quality of publications and presentations related to this work and also this thesis.

I sincerely thank Professor Michel Rigaud for serving as chairman of the jury of the thesis examination, and Professor Marius d'Amboise and Professor Michel Perrier for accepting to be jury members. I am very pleased that they honour me with their valuable time.

A special thank goes to Mrs. Betsy Piron, for carefully reading and correcting all the manuscripts of my publications. Her work has improved the quality of my papers and this thesis.

I gratefully acknowledge the help from many friends of mine in the laboratory: M. Sider, J. Saint-Pierre, Kamiab Amuzgar, B. Behzadian, S. Sokolski, H-S. Lee, G. Kim, N. Massé, C. Llerena, M. Rojas, S. Abderrahman and Professor Hu Mao Pu. Especially, I would like to thank Dr. Chonglun Fan for

his constructive discussions during the development of this text. I also thank all the personnel, technicians and secretaries in the département de Métallurgie et de Génie des Matériaux for the agreeable environment they created. I equally thank Mr. Jean Claudinon, Ms. Josée Laviolette, Ms. Li Shiqiong, Mr. Hong Bin and Mr. Xia Jin for their kind assistance in microscopic examination and photo-processing.

I realize that I could not have completed this study without the enormous support and understanding of my parents, my parents-in-law, my brothers and sisters, and especially of my wife, Jing Ren Tang. The great joys from my son, Kevin, are unforgettable.

TABLE OF CONTENTS

LIST OF TABLES

LIST OF FIGURES

LIST OF SYMBOLS

α	Fractional exponent.
β	Exponent defined in Equation (5-3).
b	Tafel slope, mV/dec.
b_h	Tafel slope at high current density, mV/dec.
b_l	Tafel slope at low current density, mV/dec.
C	Constant defined in fractal model, $F/(cm^2\ S^{\alpha})$.
C_{dl}	Double-layer capacitance, $\mu F/cm^2$.
CPE	Constant phase element.
D	Fractal dimension.
E_{rev}	Oxygen reversible potential.
E_{sp}	Specific energy consumption, kWh/kg of metal.
ΔH	Apparent energy of activation, kJ/mol.
HER	Hydrogen evolution reaction.
f	Frequency, Hz.
ω	Angular frequency, rad/s.
ω_c	Angular frequency at the maximal phase angle, rad/s.
ϕ	Depression angle of impedance diagram, degree.
θ	Impedance phase angle, $tg\theta=Z''/Z'$, degree. also fraction of the surface coverage by absorbates.
η	Overpotential, V.
η_a	Anodic overpotential, V.
η_c	Cathodic overpotential, V.
η_{100}	Overpotential at a current density of 100 mA/cm^2, mV.
i_{-200}	HER current density at -200 mV overpotential, mA/cm^2.

i_{300}	OER current density under 300 mV overpotential, mA/cm^2.
i_{ex}	Exchange current density, mA/cm^2.
i_{dp}	Deposition current density, mA/cm^2.
i_L	Limited current density of nickel deposition, mA/cm^2.
IR	Ohmic drop, V.
OER	Oxygen evolution reaction.
P_e	Equivalent atomic weight.
R_F	Current efficiency, (%).
R_{ct}	Charge transfer resistance, Ω-cm^2.
RDS	Rate-determining step.
R_s	Solution resistance, Ω-cm^2.
S	Surface roughness factor, $C_{dl}/20$, dimensionless.
SCE	Saturated calomel electrode.
SHE	Standard hydrogen electrode.
V_{cell}	Electrolytic cell voltage, V.
Z'	Real component of the impedance, Ω-cm^2.
Z"	Imaginary component of the impedance, Ω-cm^2.
Z_{CPE}	Impedance of the constant phase element, Ω-cm^2.

CHAPTER 1

INTRODUCTION

1.1 SELECTION OF THE SUBJECT

1.1.1 Energy consumption in electrolysis

The water electrolysis for hydrogen production and the electrowinning process for zinc production, are high energy-consuming processes. Power consumption in a typical industrial water electrolyser is 4.5 kWh/M^3(1). In the electrowinning step of the sulfate process for zinc production, a typical value for specific energy consumption (E_{sp}) is around 3.1 kWh/kg zinc(2). This energy represents 60% of the total energy consumption for the production of zinc from ores, or 35% of the total cost of the electrolysis operation(3,4). The energy consumption costs will increase rapidly in the future. This raises an important concern about saving energy and keeping electrolytic production competitive.

To lower production costs, the current efficiency of the electrolytic process must be improved. It has been reported(5) that lowering the overpotential by 50 mV at both the anode and cathode (100 mV cell voltage) would result in savings of up to 1 million dollars on a 50 MW water electrolyser operated at 1000 A/M^2. In water electrolysis, the overvoltage on the anode is usually higher than that on the cathode(6). This suggests

that decreasing overpotential for the **oxygen evolution reaction** (OER), (which is an anodic reaction in the water electrolyser), is essentially important.

Improvements have been found for zinc electrowinning in the alkaline process. St-Pierre and Piron(7) reported an E_{sp} of 1.75 kWh/kg at the high current density of 1000 A/M^2 in 7.5 M NaOH solution. The low energy consumption of the process was partially attributed to the use of an oxide anode which catalyses the OER (which is the anodic reaction in the bath) and consequently lowers the anodic overpotential and energy consumption.

The E_{sp} is a measure of the energy consumed in the process, defined as(8):

$$E_{sp} = \frac{26.8 V_{cell}}{P_e R_F} \qquad (1\text{-}1)$$

where P_e is the equivalent atomic weight (g/mol); R_F the current efficiency (%); and V_{cell} the electrolytic cell voltage (V), which is expressed as:

$$V_{cell} = E_{A/C} + |\eta_a| + |\eta_c| + IR \qquad (1\text{-}2)$$

Here $E_{A/C}$ is the difference in the equilibrium electrode potentials between the anode and the cathode, η_a and η_c are the overpotentials at the anode and the cathode, respectively, and IR is the ohmic drop across the electrolysis cell and

other current-carrying cell components. In the Eq.(1-1), a decrease in the V_{cell} will result in a lower E_{sp}.

Table (1-1) lists typical data of the parameters in Eq.(1-2) for zinc electrowinning in the sulphate and the alkaline processes. The operating current density was 500 A/M^2. As we can see from the table, η_a is 25% of V_{cell} in the sulfate process, but only 9% of V_{cell} in the alkaline process. Although lowering the cell voltage of zinc electrowinning is an important achievement of the alkaline process, it should be noted that most of the V_{cell} decrease in this process comes from a decrease in the η_a. As can be seen in Table (1-1), as much as 55% decrease of the V_{cell} (compared with the sulphate process) is obtained by lowering η_a. This indicates that η_a is one of the most important factors to be considered in attempting to lower the cell voltage of zinc electrowinning in alkaline solutions. This clearly reflects the importance of the electrocatalyst in industrial applications.

An active electrocatalyst accelerates the electrochemical reaction and lowers the cell voltage. Developing electrocatalytically active materials and constructing the electrode with preferred surface conditions for gas evolution to achieve a low overpotential and a high reaction rate are, therefore, the key techniques for lowering the energy consumption for the production. Althrough the IR drop between

the anode and cathode contributs a part of the overpotential, it cannot be significantly decreased, as an anode-cathode gap must be maintained during electrolysis to allow zinc deposition and to avoid short circuits in the cell.

TABLE 1-1
OPERATING CONDITIONS FOR ZINC ELECTROWINNING(2,7)

CELL VOLTAGE (V)	SULFATE[1] PROCESS	ALKALINE[2] PROCESS	ΔV(1)-(2)	ΔV/1.16V (%)
$E_{a/c}$	1.99	1.62	0.37	32
η_a	0.84	0.20	0.64	55
η_c	0.06	0.05	0.01	1
IR	0.50	0.36	0.14	12
V_{cell}	3.39	2.23	1.16	100
η_a/V_{cell}	25%	9%	---	---

1.1.2 The oxygen evolution reaction

The OER takes place in all kinds of electrolytes, such as acid, alkaline, sulfate salt and neutral media. Table (1-2) lists the overall oxygen reactions in various aqueous media and the corresponding standard equilibrium potentials at 25°C.

TABLE 1-2
THE OER IN VARIOUS MEDIA

MEDIA	REACTION	POTENTIAL
Acid media:	$2H_2O = O_2 + 4H^+ + 4e^-$	1.229 V *vs. SHE*
Alkaline media:	$4OH^- = O_2 + 2H_2O + 4e^-$	0.401 V *vs. SHE*
Sulfate salt:	discharging SO_4^{2-} leading to the OER:	
	$2SO_4^{2-} = 2SO_3 + O_2 + 4e^-$	
	$2SO_3 + 2H_2O = 2SO_4^{2-} + 4e^-$	
Neutral media:	discharging H_2O or OH^-	

The OER is a multiple electron transfer process, and it is complicated by many mechanisms with various reaction paths and routes. Pletcher(9) has pointed out that intermediates in the process may play an important role in the electrode kinetics. The rate-determining step (RDS) of the OER can be charge transfer, adsorption, diffusion processes or a combination of these processes. Therefore, a study of the OER mechanism represents a fundamental aspect of electrochemistry.

1.1.3 Objective

Appleby(10) stated that electrocatalysis was a study of the influence of the electrode material and the structure of the electrode surface on an electrochemical reaction. The main objective of this study is to develop new electrocatalytic materials serving as electrodes for the oxygen evolution reaction in alkaline solutions. Although high catalytic activity is often found in noble metals, such as Pt, Ru, Ir, Rh etc., the high cost of these precious metals is a major drawback for applications in industry. My study, therefore, is focused on economical materials with good catalytic activity for the OER, such as oxides based on the transition metals (Ni, Co, Fe). Using a small quantity of noble transition metals to increase the electrode activity was also considered, but more efforts were devoted to improving the electrode performance by increasing the effective real surface areas. The OER mechanism was studied on these electrodes. Finally,

techniques for characterization of the electrode with a rough and porous surface were studied.

1.2 APPLICATIONS OF OXYGEN ELECTRODES

The oxygen electrode has a wide range of applications in various industrial sectors. The term "oxygen electrode" includes both the anode for the OER and the cathode for the oxygen reduction reaction. Water electrolysis and fuel cell are two of the most important applications for the oxygen electrode. In water electrolysis, the OER occurs on the anode, and the hydrogen evolution reaction (HER) occurs on the cathode. Therefore, some electrodes, such as composite-coating electrodes, were also investigated as the HER electrode. Research on oxygen electrodes in the past decade has been oriented mostly towards searches either for reversible oxygen electrodes or for the best oxygen reduction cathode for fuel cell and metal-air battery applications. More information about oxygen reduction cathodes can be found in Yeager's(11) review.

CHAPTER 2

CRITICAL LITERATURE REVIEW

The oxygen evolution reaction is a thoroughly studied subject. Many comprehensive reviews, reports and books on the subject can be found in the literature(10-19). Complete coverage and discussion of problems related to the subject are, therefore, impossible. Consequently, only the essentially important aspects relevant to our study are discussed in this chapter. Section 2.1 begins with a classification of materials investigated as oxygen electrocatalysts, with a special emphasis on oxide materials. Structure and preparation of the oxide electrode are discussed. The electrocatalytic activities of the oxide electrodes are evaluated as well. Section 2.2 is devoted to discussion of the selection of the oxygen electrode material. The selection criteria are based on the factors such as activity, corrosion resistance, conductivity, selectivity and the relationship between the oxygen reversible potential and the standard electrode potential, as well as dependence of the electrocatalytic activity on adsorption-desorption of the reactant species. The techniques for improving the electrode activity towards the OER are addressed in section 2.3. Nickel as an electrode material, because of its well-known catalytic property and stability as an electrocatalyst, has attracted the most attention. It is reviewed in section 2.4 of this chapter. The OER is a multiple-electron transfer reaction with

various reaction routes or steps. Identifying the reaction mechanism would improve our understanding of the effects of electrode structure on its activity and help us in developing the high-performance electrode. The OER mechanisms and paths proposed by many authors are presented in this section. The final step in studying an electrocatalyst is to evaluate electrode performance in specific conditions for particular reactions. How to evaluate electrode performance is an essential question. Finally, in section 2.5, the electrochemical parameters adopted for evaluating electrode performance are summarized and appraised with a discussion of the limiting conditions for application.

2.1 THE OXYGEN ELECTRODE MATERIALS

Various materials have been studied as electrodes for the OER. These materials can be classified into the categories of noble metals and their alloys, active metals and their oxides, oxide materials and other materials such as complexes, carbon and graphite, etc. The mixed oxides have attracted considerable attention in recent years due to their excellent catalytic properties and stability in electrolytes.

2.1.1 Active metals and their alloys

The oxygen reactions (both anodic evolution and cathodic reduction) on noble metals were reviewed by Hoare(18). The

standard potential of the oxygen electrode is 1.23 V *vs. SHE* (at pH=0). This potential is higher than the standard potential of most solid metal elements. The choice of a suitable metal support for the oxygen electrode is therefore limited. As we understand that at a potential higher than 1.23 V, oxides, not metals, are the stable state of materials. Many studies of oxygen electrocatalysts were focused on noble metals. The reason is related to the corrosion resistance of the electrode material and the reversible potential of the oxygen electrode. Almost all the noble metals have an excellent resistance to corrosion in aqueous solutions (20,21). Therefore, noble metals are a natural choice as an oxygen electrode in alkaline solution.

However, studies in the literature showed that the reversible potential of oxygen was not observed on electrodes fabricated with those noble metals. It became apparent that the noble metal was not truly inert and that it did interact with oxygen (17). Additional evidence given by Hoare(17) is that the oxygen reduction has been observed on the bare metal and on the oxide electrode, but the OER always occurs on an oxidized surface. This implies that searches for the reversible oxygen electrode should focus on oxide materials. This is why the oxide materials have attracted more attention than other forms of material for application in the oxygen electrocatalysts.

Pt, Au, Pd, Rh and Ir are well-known noble metals used as oxygen electrodes(17). However, high costs are the drawback for using these materials as successful electrodes. The technique of dispersing metal particles on carbon or silica glass was applied to limit the electrode cost. Pt is a metal being extensively investigated as an oxygen electrode, and its kinetics and the mechanism are well-established (17,18).

Noble metal alloys, Au-Pd(20), Ru-Pt, Ir-Pt, Pd-Pt(21) and Rh-Pt(21-23), have also been studied as oxygen electrodes. The OER overpotential on Pt-Rh and Pt-Pd alloys was lower than on the Pt electrode. Damjanovic et al(23) explained this by the maximum coverage of oxygen adsorption, which increased with Rh composition in a series of Rh-Pt alloys. Ru-Ir alloys were also investigated as anodes for the OER in 1N H_2SO_4(24), and it was shown that the Ru corrosion was significantly reduced by increasing Ir content. Simultaneously, the Tafel slope and overpotential for the OER were increased.

Active metals, such as Ag, Pb and Ni, have been studied as oxygen electrodes, with a special interest in battery systems(17). Since these metals form a thick oxide layer on the electrode surface when undergoing anodic polarization, they are practically treated as oxide electrodes. Generally, active metals are good electrocatalysts. Miles(25) has classified Fe, Ni, Rh, Pd and Ir as good electrocatalytic

materials in alkaline solution, and Pt and Au as relatively good ones. Nickel and Ni oxides are the materials most frequently used to fabricate anodes for the OER in alkaline media(17,26-30). Since the Ni oxides are formed at the potential at which the OER occurs, it will then be more reasonable to discuss it in a section on oxide materials.

2.1.2 Active metal oxides

PbO_2 was the first bulk oxide electrode investigated for its practical application in lead-acid batteries(31), metal electrowinning and chlorine production(32). Trasatti(14) said that although the electrocatalytic activity for the OER on the PbO_2 electrode is not excellent, its good corrosion stability has led to many industrial applications.

Ni oxide is a well-known catalytically active material for the OER. It is stable under the condition of the anodic polarization in alkaline media, and the η value of the OER is reasonably low(27,29,35,36). A typical η value at 100 mA/cm^2 is about 350 to 400 mV in alkaline solution(14). However, an unsatisfactory aspect is the problem associated with long-term industrial application: the potential is not stable and it drifts towards more positive values with time(28,29,37). Improvements of both catalytic activity and stability of the electrode potential were made by alloying Ni with elements such as Li(30), Fe(38-40), Cr (41), Ti, Ir, Ru, W(42) and

Co(43). Most of these works aimed to develop the anode for water electrolysis in alkaline media.

Lu and co-workers(29) studied the Ni-Ir(25-75%), Ni-Ru(25-75%) and the Ni-W(25-50%) alloys as electrocatalysts for the OER in alkaline solution. The O_2 overpotential decrease was observed on the alloys of 50Ni-50Ir and 75Ni-25Ru. The lowered η value was about 40 and 30 mV, respectively. It was found that the surface oxide film plays a major role in electrode performance. They stated(29) that the electrode surface of these alloys after prolonged anodization was predominantly composed of Ni oxide, which consequently determined the kinetic parameters of the OER.

Over 25% of the expensive transition elements (Ru, Ir) in alloys still cannot control the surface oxide catalytic property. It is therefore not wise to use a high content of the expensive metals to obtain a good catalyst. It is economically more attractive to use low contents of transition elements to improve the performance of the Ni electrode for industrial applications.

2.1.3 Oxide materials

Oxides investigated as oxygen electrodes can be put into three groups with different structures, that is: the rutile-type, the spinel-type, and the perovskite-type oxides.

A typical example of these oxides can be given as RuO_2, $NiCo_2O_4$ and Na_xWO_3, respectively. Comprehensive reviews of these oxides exist in the literature(14,44). The oxide structures, preparation methods and their catalytic activities will be presented in this section.

2.1.3.1 Rutile-type oxides

STRUCTURE--The structure of a rutile-type oxide is shown in Fig.2-1. It exhibits tetragonal symmetry, and the unit cell contains two element formulas MO_2. Each cation is the centre of an octahedron of oxygen atoms, each of which in turn is approximately in the centre of an equilateral triangle of metal atoms. The last shell of the electron configuration and the resistivity of some rutile-type oxides are listed in Table (2-1).

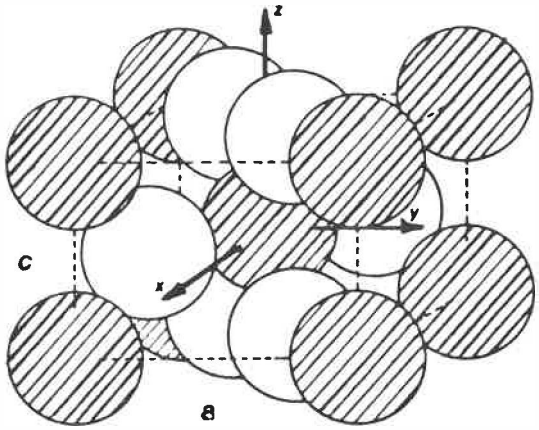

Fig.2-1 Crystal structure of rutile-type oxides, MO_2. (•) Metal atoms; (o) Oxygen atoms. From (44).

TABLE 2-1
STRUCTURE AND ELECTRONIC PARAMETERS OF RUTILE-TYPE OXIDES(44)

OXIDE	LAST SHELL CONFIGURATION	RESISTIVITY* ohm/cm	TYPE OF CONDUCTOR**
RuO_2	$4d^4$	$3\text{-}5X10^{-5}$	M
IrO_2	$5d^5$	$3\text{-}6X10^{-5}$	M
$MnO_2(\beta)$	$3d^3$	0.1-0.01	S
OsO_2	$5d^4$	$6X10^{-5}$	M
RhO_2	$4d^5$	$<10^{-4}$	M
TiO_2	$3d^0$	10^8	S
PtO_2	$5d^6$	10^6	S

* at room temperature. ** M = metal, S = semiconductor.

The general formula of this type of oxide is MO_2, where M could be a non-transition metal, such as Pb, Sn, Ge, Te and Si, or several transition metals with 3d, 4d, and 5d electron configurations (Ti, V, Cr, Mn, Nb, Mo, Tc, Ru, Rh, Ta, W, Re, Os, Ir, and Pt). Some oxides, such as GeO_2, SnO_2, TeO_2, SiO_2, VO_2, TiO_2, NbO_2, are not conductive; therefore, they have no application as catalytic electrodes. The conductivity of SnO_2 can, however, be improved by doping, and it is therefore used as an electrode. All others, with the exception of MnO_2 and PtO_2, can be classified as metallic conductors.

PREPARATION OF OXIDES--Thermal decomposition was the most popular method for preparing the rutile-type oxide. Other techniques, such as chemical vapour deposition, sputtering and electrodeposition have also been explored(44). The oxide prepared by thermal deposition satisfied most requirements for an electrocatalyst. The basic procedure for preparation of the

rutile-type oxide consists of dissolving a suitable chloride compound (e.g.,$RuCl_3*xH_2O$) in a solvent (water or alcohol), spreading it on a support and firing it in a furnace at a selected temperature (300~600°C). The choice of the firing temperature depends on the starting materials and the nature of the support. As a rule, the firing temperature must be high enough to ensure the maximum decomposition of the reactant but low enough to avoid excessive sintering and crystallization in the final products. The experimental conditions for preparing rutile-type oxide electrodes are summarized in Appendix I.

ELECTROCATALYTICAL ACTIVITY--Among the rutile-type oxides, only MnO_2, RuO_2 and IrO_2 have been practically investigated in detail for application of electrocatalysis, reported in literature(44). The most information available is on the RuO_2 electrode for the chlorine evolution reaction. The catalytic activity of the IrO_2 electrode for the OER is generally lower than that of the RuO_2 electrode. However, the IrO_2 electrode is a much more stable oxide in alkaline media. The reason for this behaviour was not explained in the literature. MnO_2 has been employed as an anode in a number of technological processes, such as the electrolysis of oxyacid and oxysalt(33), where Pb metal and its dioxide are rather unstable. Although MnO_2 is not a good electrocatalyst for the OER(14), the presence of this oxide in mixtures of RuO_2+TiO_2 and IrO_2+TiO_2 decreased the OER overpotential(34).

The electrocatalytic activity is characterized by the parameters of exchange current density (i_{ex}), Tafel slope (b) (when b is measured at low & high i, and is represented by b_L & b_H), Tafel parameter (a) and overpotential (η). Sometimes information on the electrode surface area (S) is provided. Table (2-2) lists the kinetic parameters for the OER. Several oxides prepared by thermal decomposition were tested in 30 wt% of KOH at 80°C by Miles and co-workers(45). A poor catalytic activity was observed on V, Cr, Mo, W, Mn and Re oxide electrodes. The electrocatalytic activity sequence (on the basis of b and i_{ex}) was reported in the following order:

Ru > Ir = Pt = Rh = Pd = Ni = Os >> Co >> Fe

TABLE 2-2
KINETIC PARAMETERS OF THE OER ON RUTILE-TYPE OXIDES(44)

TYPE OF METAL OXIDE	a mV	b mV/dec	i_{ex} A/cm^{-2}
Ru	37	67	3.0×10^{-6}
Ir	41	50	6.3×10^{-9}
Pt	41	46	1.2×10^{-9}
Rh	43	67	3.8×10^{-7}
Pd	45	67	1.9×10^{-7}
Ni	45	71	4.6×10^{-7}
Os	49	70	1.0×10^{-7}
Co	69	126	3.3×10^{-6}
Fe	91	191	1.7×10^{-5}

One of the most outstanding oxide electrodes with a rutile structure is the DSA^R-type electrode, which has been successfully used in the production of chlorine and chlorate through the electrolysis of brine. The DSA^R-type electrode, namely the dimensionally stable electrode, consists of a thin

noble metal oxide coating (RuO_2) supported by a valve metal such as Nb, Ta, Ti or Zr(44,46). Before 1960, graphite electrodes were generally used in chlorine production. The graphite anodes require frequent maintenance, but the DSA^R-type electrodes preserve both their shape and a low overpotential for the reaction. They are widely used today.

2.1.3.2 Spinel-type oxides

Among the oxide catalysts, complex oxides with spinel structure are of the greatest interest as oxygen electrodes. The main merits of these systems are their high activity, low cost, availability, and a satisfactory stability in alkaline media. The disadvantages are low specific surface and relatively high electric resistance. Since they dissolve in acid solutions, the field of application is mainly restricted to alkaline solutions(44).

STRUCTURE--Spinel is a binary system of metal oxides having the composition of $M'M_2O_4$, where M' and M correspond to different metals. Figure 2-2 shows an ideal structure of a spinel oxide, in which the O^{2-} anions form a fcc packing, while the M and M' cations are located in vacant lattice sites. Each unit cell contains eight formula units $M'M_2O_4$. The spinel oxides studied as electrocatalysts found in the literature are $NiCo_2O_4$, $MnCo_2O_4$, Co_3O_4, Fe_3O_4 and $M_xFe_{3-x}O_4$, where M=Mg, Zn, Mn, Co or Ni.

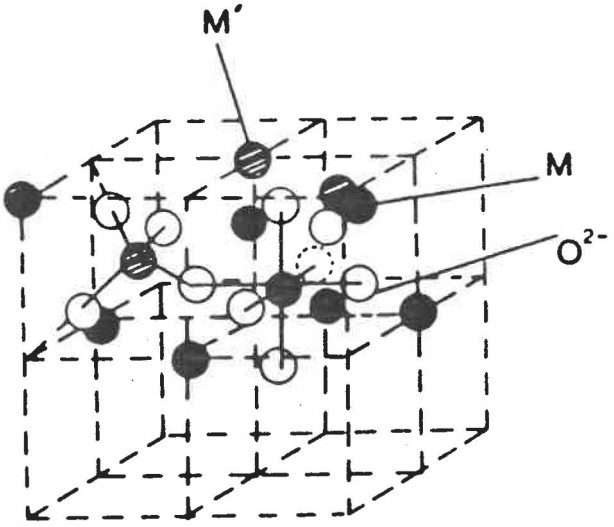

Fig.2-2 Crystal structure of spinel-type oxides, $M'M_2O_4$. From (44).

PREPARATION OF OXIDES--It was believed(14) that the structure of the spinel oxide was responsible for a high electrocatalytical activity on the spinel-type oxide electrodes. It is, therefore, important to obtain a spinel structure for achieving the highest activity on electrodes. There are various methods for preparing the spinel oxide. Some of them are suitable for preparing the electrocatalytical electrode. They were reviewed in the literature(44) and are adapted in Appendix I.

By comparing merits of the different preparation methods, we have found that thermal decomposition is considered as the most convenient and practical method for preparing spinel-type oxide electrodes.

It is believed(14) that stoichiometric nickel-cobalt spinel oxides give the best electrocatalytic performance for the OER. To prepare the Ni-Co oxide coating, $Ni(NO_3)_2*6H_2O$ and $Co(NO_3)_2*6H_2O$ are mixed in stoichiometric amounts (1:2, approximately), and dissolved in isopropanol alcohol ($CH_3CHOHCH_3$). The mixed solution is applied to the substrate by brushing or dipping. The dipping procedure generally gives more reproducible results and it is recommended in coating applications. Briefly, the substrate is dipped into the solution, dried 10 minutes in a dryer at a temperature between 70 and 100°C, then put into the electric furnace for decomposition at 400°C for 1 hour. Depending on catalytic material loadings, the above procedures are repeated 4-6 times for each electrode.

ELECTROCATALYTICAL ACTIVITY--The electrocatalytical activities for the OER on spinel-type oxide electrodes in terms of Tafel slope b (obtained at low & high E, b_L & b_H) and exchange current density i_{ex} (at low & high E) are listed in Table 2-3. Generally, the Tafel slope of the OER in the KOH solution on $NiCo_2O_4$ and Co_3O_4 oxide electrodes is in the range of 45 to 60 mV/dec. In some cases, the b changed at high η, and a different value of b (b_H) were reported (44). The exchange current densities were on the order of 10^{-10} to 10^{-8} A/cm^2 (high E).

TABLE 2-3
KINETIC PARAMETERS OF THE OER ON SPINEL-TYPE OXIDES(44)

SPINEL OXIDE	CONDITIONS	b_L (mV/dec)	b_H (mV/dec)
$NiCo_2O_4$	30% KOH,80°C	45	
	0.1mol/L KOH,60°C	50	90
Co_3O_4	0.1mol/L KOH,60°C	50	100
	0.1mol/L $KClO_4$,60°C	60	120
$MnCo_2O_4$	0.1mol/L KOH,60°C	50	100

SPINEL OXIDE	CONDITIONS	i_L(Low E) (A/cm^2)	i_H(High E) (A/cm^2)
$NiCo_2O_4$	30% KOH,20°C		$(1-9)\times10^{-10}$
$NiCo_2O_4$	30% KOH,80°C		7×10^{-10}-3×10^{-8}
	0.1mol/L KOH,60°C	3.2×10^{-13}	6.3×10^{-10}
Co_3O_4	0.1mol/L KOH,60°C	1.1×10^{-12}	4.5×10^{-10}
$MnCo_2O_4$	0.1mol/L KOH,60°C	1.3×10^{-11}	1.0×10^{-10}

2.1.3.3 Perovskite-type oxides

STRUCTURE--Perovskite-type oxides have a crystal structure similar to that of the mineral perovskite $CaTiO_3$ (44). The general chemical formula of perovskite oxide is ABO_3, where A is a larger cation; B is a small transition-metal cation. The sum of the valence state of the A and B cations should be +6 to preserve electrical neutrality. The ideal crystal structures of the perovskite oxide are cubic, as shown in Fig.2-3. The positions of A and B can be exchanged at the origin position, as shown in (a) and (b). (c) shows the unit cell of a perovskite $BaSr_{0.33}Ta_{0.67}O_3$ on a hexagonal basis in which the c-axis is taken along the [111] direction.

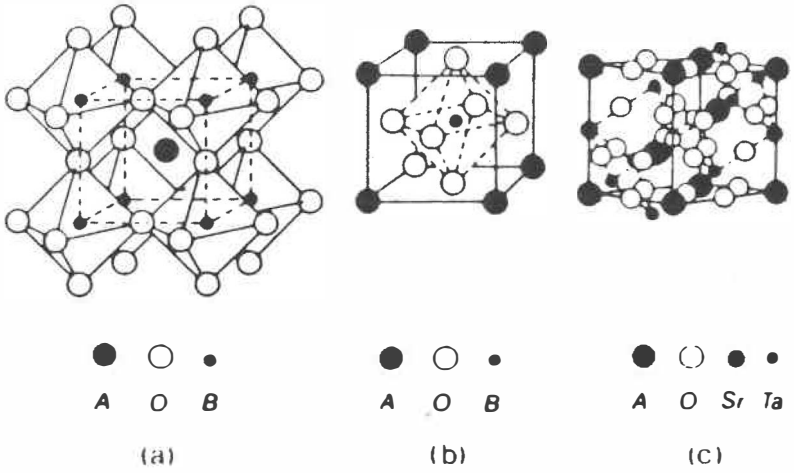

Fig.2-3 Crystal structures of perovskite-type oxides, ABO_3. (a) B cation at the origin; (b) A cation at the origin, (c) the unit cell of $BaSr_{0.33}Ta_{0.67}O_3$ on a hexagonal basis in which the c-axis is taken along the [111] direction. From (14).

PREPARATION OF OXIDES--Perovskite oxides are usually prepared by thermal decomposition of an appropriate mixture of metal salts or by the solid state reaction of metallic oxides. The conditions of thermal decomposition for the preparation of perovskite oxides are very similar to those for the rutile and spinel-type oxides. Table B in Appendix I lists preparation conditions for $LaNiO_3$, which is considered to be a typical perovskite oxide. Preparation conditions by high temperature solid-state reactions can be found in reference(47).

ELECTROCATALYTICAL ACTIVITY--The perovskite oxides exhibit good electrocatalytic properties for the OER and HER(44). The OER on the perovskite oxide electrodes was studied essentially in alkaline solutions, but only limited

kinds of oxides were tested electrochemically, with a focus on electrocatalysis. Those oxides are: $LaCoO_3$, NiM_2O_4 with M=La, Pr, Nd, $La_{1-x}Sr_xCoO_3$, $La_{1-x}Sr_xFeO_3$, $La_{1-x}Ba_xCoO_3$, $Nd_{1-x}Sr_xCoO_3$, and $SrFeO_3$. Preliminary results for the OER on the Ba- and Sr-doped $LaCoO_3$ have been reported(48). The observed b was from 57 to 74 mV/dec., and the i_{ex} was on the order of 10^{-7} to 10^{-8} A/cm^2. In comparison with the rutile and the spinel-type oxides, no superior activity for the OER was found for perovskite oxides.

2.1.3.4 Mixed oxide electrodes

There is an increasing tendency to use mixed oxides as electrocatalysts for the OER. RuO_2/TiO_2 is a typical case to show the superior performance and the stability of the mixed oxide over the single oxide(14,15,45,49,50). A similar result was obtained on the IrO_2/TiO_2 anode for the OER in acid solution(51). However, a study of the OER in 30 wt% KOH at 80°C(45) showed an increase in electrode resistance on other mixed metal oxides (except Ru) when mixed with TiO_2. In the case of $NiCo_2O_4$, NiO_x may co-exist with $NiCo_2O_4$. The behaviour of the electrode will then be represented as a mixture of these two oxides.

It should be noted that most conducting oxides are transition metal oxides, and their activity depends on the metal components. It was reported(12) that the unpaired d-

electrons in transition metals strongly affect the reaction mechanism by increasing oxygen adsorption. This will be discussed in more detail in Section 2.2.3.

2.1.4 Other materials

Metal phthalocyanines and porphyries, Co-Ag, Co-Fe, Co-Mn porphyries have been used as oxygen cathodes in fuel cell systems(11,52). The geometry of the compounds can affect the formation of intermediates in the reaction, and the intermediate can affect the catalytic property.

Because of their good electronic conductivity, carbon and graphite materials have been considered as good electrode materials for the OER. The carbon fibre electrode(52) behaves like a synthetic metal. The performance of the platinized carbon fibre is similar to that of the bulk Pt electrode. This shows an effective way to use the precious metals, like Pt, to construct high quality electrodes without losing electrode activity. The disadvantages of synthetic-type electrodes are that carbon consumption is high; they are not corrosion resistant in most electrolytes; contamination of the electrolyte exists; and extra caution is needed in preparing and handling(46).

2.1.5 Summary and comments

Searches for the OER catalyst began with noble metals,

with an initial interest in finding a reversible oxygen electrode. The oxygen reduction was observed on bare metal and oxide electrodes, but the OER always occurs on oxidized surfaces(17). This indicates that our solution to this problem may lie with oxide materials. This is why oxide materials have attracted more attention than other forms of materials in the role of oxygen electrocatalysts.

Three types of oxides with different structures (rutile, spinel and perovskite) were studied as OER electrodes. These works generally gave the values of b, i_{ex} and η. The importance of the oxide structure on catalytic activity was pointed out, but was not explained. It was claimed that the spinel structure might be responsible for good catalytic properties(14), but the role of the structure of the oxide in determining the activity is still not known.

On the other hand, the chemical composition, especially in the case of mixed oxide materials, may play an important role in determining electrode activity; however, the basis for its impact on the mixed oxide electrode activity is not clear. (This basis may simply be chemical composition or structure, surface adsorption coverage or change in the work functions.) Although some works link the electrode catalytic activity with work function and/or band structure of metals(44), these fundamental studies are far from giving us a satisfactory

prediction of the catalytic behaviour of an oxide electrode. Further, the morphology of the oxide is essentially important in determining electrode activity for an electrochemical reaction. In most cases, the information relating to the surface is not available; or is unclear. The surface state of the oxides prepared by different methods is different, resulting in variations in activity for an electrochemical reaction. However, research on the effect of the surface morphology and the state of electrode activity is scarcely seen in the literature.

2.2 SELECTION OF OXYGEN ELECTROCATALYSTS

The history of the development of the DSA^R (dimensionally stable anode) electrode is a typical example of invention of a high performance electrode for a specific electrochemical reaction. It has taken more than 15 years to complete the revolutionary invention of the DSA^R electrode(46), and it was neither simple nor easy. Over the decades, most R&D on new electrocatalysts has consisted in a try-and-see, cooking style approach, without theoretical and practical guidelines to direct studies. Developing a new electrode therefore involved an extraordinary number of tests and an exceedingly long time. Unfortunately, this situation has not changed much today. However, Tseung(37) gave the first discussion of the selection of conducting oxides as the OER electrode. His discussion

mainly addresses the relationship between the standard electrode potential and the oxygen reversible potential. It was a thermodynamic approach. The kinetics of forming oxides on the electrode is not treated at all. The OER is a reaction related to the adsorption-desorption of reactants, intermediates or other species during the reaction. Adsorption-desorption is quite an important phenomenon in this case. To make a correct choice of new electrode materials, it is necessary to understand the fundamental requirements of an electrocatalyst.

2.2.1 Requirements of an electrode

2.2.1.1 Electrocatalytical activity

Electrocatalysis is the acceleration of a particular electrode's reaction by an appropriate choice of electrode material(9). The primary function of an electrocatalyst then is catalysing selected electrode reaction. The best catalyst should therefore possess highly electrocatalytic properties based on a unit surface area. In most cases, a high real-surface-area electrode provides a larger current on the basis of apparent electrode surface than a smooth (or polished) electrode surface. On the basis of the definition of catalytic activity of a unit real surface area, this electrode is not necessarily an excellent electrocatalyst, but it does improve the electrode performance by providing a large real surface area for the electrode reaction.

2.2.1.2 Stability

The choice of an electrocatalyst for the OER is restricted by the extent of corrosion of the electrode material occurring at the potential and the condition at which the reaction occurs. It is important to know the stability of the considered oxide materials under the specific operating conditions (such as the alkaline water electrolysis, pH=14, E_{cell}=1.3 ~ 2 V, T=25 ~ 100°C). The long-term stability of the electrode for electrolysis and electrosynthesis is the most important property for a successful industrial electrode. Besides the chemical attack of alkaline solutions on the electrode material, especially under an anodic potential, the passivation of the electrode, either on the inter-surface between the substrate and the oxide coating or between coating layers, will significantly increase the resistance of the electrode(14,49,53,54). This diminishes the catalytic activity of an electrode by increasing overpotential. Mechanical wear of the electrode changes the dimensions of the electrode and increases the distance between the anode and cathode, and consequently the IR drop. From there, the stability of an electrode has a wide significance.

Any electrode wear may lead to contamination of products, early failure or short life of the electrode, and it causes additional electrode material and labour costs due to the need for its periodical replacement. To achieve economic success,

the high catalytic activity of an industrial electrode must be guaranteed by stability over a long period of service time. Stability of the electrode sometimes is even more important than catalytic activity, either to avoid contamination of products, or because of the special cell design and operational conditions required for a dimensionally stable electrode(55). Due to the great stability of DSA^{R}-type electrodes, it has become common to use such electrodes even where no special catalytic activity is shown or needed(9). Stability is related to the cost of the electrode material. High activity, stability over a long period and acceptable electrode material costs are the most important aspects of a successful electrocatalyst.

2.2.1.3 Conductivity

An electrochemical reaction involves the transfer of electrons. The electrode surface must therefore be a good electronic conductor, although the process may occur by a quantum mechanical tunnel through a thin surface film(12). Both electrode resistance and electrolyte resistance contribute to the IR drop in the cell. A high electrode conductivity means a low electrode resistance, and the resistance contribution to the IR drop across the electrode/electrolyte interface is low, and consequently a lower cell voltage would be achieved. The conductivity of an oxide can be improved by doping. A good example given by

Tseung and co-workers (30) was Li-doped NiO oxide. The resistivity of oxide materials is listed in Table (2-4).

2.2.1.4 Selectivity

Electrocatalytic selectivity is another important requirement. It is essential that an electrocatalyst catalyses only the desired reaction and inhibit unwanted side reactions. The selectivity of an electrode comes from favourable thermodynamic or kinetic conditions. One reaction proceeds as primary and faster on the electrode over another because of differences in the potential or the activation energy.

2.2.1.5 Surface structure

For a gas evolution reaction, an appropriate surface structure with facilely release of gas bubbles is a practical requirement for the electrode. The ohmic drop due to the gas bubble screening effects and concentration gradients in the electrolyte solution is another source of IR drop contribution to a high electrolysis cell voltage. The appropriate cell and electrode designs can lead to favourable conditions of wettability at the electrode/gas/electrolyte interfaces from which gas bubbles flow freely and can then decrease the IR drop related to the gas bubble screening effect.

Larger real surface areas are very effective for increasing the electrode's activity and for reducing the

electrode's overpotential. However, a porous electrode structure may trap a large amount of gas bubbles and partially block the reaction sites. Since increasing the real surface area of the electrode is not always effective in improving the electrode performance, it is necessary to have an appropriate surface structure to facilitate the release of gas bubbles from the surface. For example, a new type of PTFE-covered Ni gas-evolving electrode was prepared and tested for the hydrogen evolution reaction (56). Due to the hydrophobicity of the PTFE coverage, the gas bubble release rate from the electrode surface is increased with an average decrease in overvoltage of -100 mV (with respect to the polished electrode) for the HER.

2.2.2 Standard electrode potential

The fundamental requirements for the electrocatalyst give us a general rule in the search for a new electrocatalytically active material as the electrode. For a given electrode reaction, such as the OER, the standard electrode potential of the electrode material is linked to the oxygen reversible potential.

Hoare(17,18) has shown that in all metals studied, the oxygen produced on the electrode will initially react with the bare metal surface to form a surface oxide. Therefore, the potential at which the O_2 starts to evolve from the electrode

is related to the redox potential of the metal/metal oxide couple. If there is more than one form of oxide involved, this potential is related to the lower metal oxide/high metal oxide couple. Thus, an ideal electrode for the OER would be one which has an equilibrium potential lower or the same as the oxygen reversible potential (1.23 V *vs.SHE*). If the equilibrium potential of metal/oxide is higher than 1.23 V, the expected oxygen evolution potential would be even higher. Table (2-4) lists the equilibrium electrode potential of some oxides or oxide couples(37) which are candidates for OER electrodes.

On the basis of this potential criterion solely, Mn_2O_3/MnO_2 (E=+1.014 V), OsO_2/OsO_4 (+1.000 V), Ir_2O_3/IrO_2 (+0.930 V) and Cu_2O/CuO (+0.667 V) would be considered to be the most suitable oxide couples. CrO_3/CrO_2 (1.284 V), RuO_2/RuO_4 (1.387 V), low Co_2NiO_4/ high Co_2NiO_4 (1.4 V), Ni_2O_3/NiO_2 (1.434 V), Co_2O_3/CoO_2 (1.447 V), AgO/Ag_2O_3 (1.570 V) and PtO/PtO_2 (1.700 V) are the oxides that have a standard electrode potential slightly higher than 1.23 V. They are still close to the oxygen reversible potential, and could be accepted as potentially good catalysts. Since this potential criterion is only a thermodynamic approach for selecting the OER electrocatalysts, kinetics and corrosion resistance of the electrode material will play a more important role in determining the final choice.

TABLE 2-4
PROPERTIES OF SEMICONDUCTING OXIDES(37,44)

OXIDE	RESISTIVITY (Ω/cm)	CONDUC-TIVITY	CORROSION RESISTANCE*	STANDARD E (V *vs.SHE*)
La/La_2O_3		P	G	-2.069
Ti_2O_3/TiO_2	10^8		G	-0.556
V_2O_4/V_2O_5		P	P	-0.666
Cr_2O_3/CrO_2	$1.2\text{-}2.5X10^{-4}$		P	+1.284
MoO_2/MoO_3	$0.9\text{-}2X10^{-4}$		P	-1.090
W_2O_5/WO_3		P	P	-0.029
Mn_2O_3/MnO_2	0.1-0.01		U	+1.014
Co_2O_3/CoO_3		P	G	+1.447
Co_2NiO_4 (L/H)		G	G	+1.400
Ni_2O_3/NiO_2		P	G	+1.434
RuO_2/RuO_4	$3\text{-}5X10^{-5}$		P	+1.387
Rh_2O_3/RhO_2	$<10^{-4}$		U	+1.730
PdO_2/PdO_3		G	G	+2.030
OsO_2/OsO_4	$6X10^{-5}$		P	+1.000
Ir_2O_3/IrO_2	$3\text{-}6X10^{-5}$		P	+0.930
PtO/PtO_2	10^6		G	+1.700
Cu_2O/CuO	$1.7X10^{-6}$		U	+0.667
AgO/Ag_2O_3		G	P	+1.570
Au_2O_3/AuO_2		G	U	+2.630

* Evaluated at pH = 14, P=Poor; G=Good; and U=Uncertain.

2.2.3 Adsorption-desorption and catalytic activity

Adsorption-desorption is involved in the OER mechanism. The adsorption of reactants may be the first step and the desorption of oxygen bubbles may be the last step in the reaction sequence. When oxygen evolves from the electrode surface, adsorbates should not be too strongly chemisorbed on the surface, and should be easily desorbed from the surface. For an effective catalyst, the metal-adsorbed bond should be of intermediate strength. However, the adsorption-desorption level depends on the free energy of adsorption of the reactant species. If the free energy of adsorption is low, it will lead

to insufficient coverage by the adsorbate, thus diminishing the effectiveness of the electrocatalyst, and resulting in a slow reaction rate. If the free energy of adsorption is too high, it will cause the desorption rate to be too slow, resulting in a low reaction rate. The relationship between reaction rate and free energy adsorption is schematically represented in Fig.2-4. This curve, which has a shape of a "volcano", was introduced by Parson(57) in the discussion of the hydrogen evolution reaction. Similarly, a "volcano"-shaped curve was found between the overpotential of the OER as a function of activation energy (ΔH) (Fig.2-5)(14). In this figure, almost all oxides lie on the left-hand side of the curve, corresponding to weak adsorption. The oxides on the right side of the curve have a too strong adsorption and difficulty in desorption.

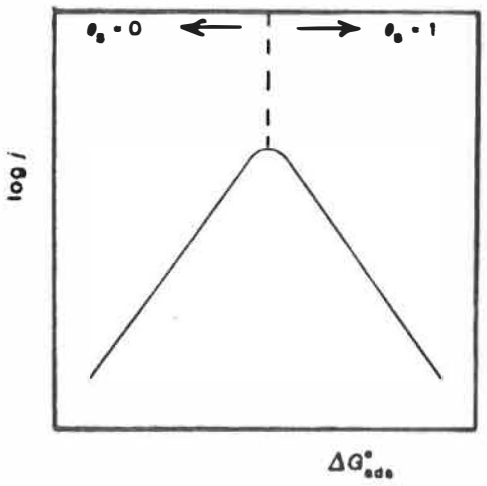

Fig.2-4 Schematic representation of the relationship between the reaction rate (i) and the free energy of adsorption (ΔG_{ads}).

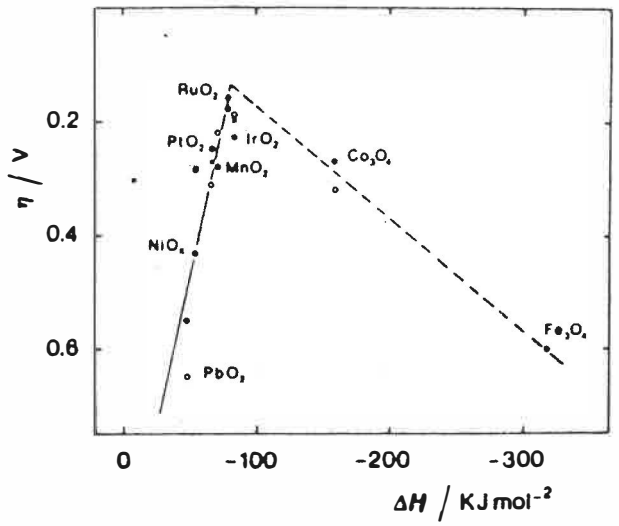

Fig.2-5 The OER overpotential (η) as a function of enthapy change (ΔH^0) for the low → high oxide transition. (•)in acid (○) alkaline media. From (44).

Study of the oxygen adsorption on some noble metals has shown that the maximum oxygen coverage on an electrode is related to transition metals and its number of unpaired *d*-electrons(12). Table (2-5) shows that as the number of unpaired *d*-electrons increase (Pa, Pt to Rh, 0.55 to 1.7), the oxygen adsorption coverage increases (from 0.22 to 0.90). An explanation of why transition metals have better catalytic properties can be given by the relationship between the electron configuration and the free energy of adsorption of these metals(44). The transition metals usually have unpaired *d*-electrons and unfilled *d*-orbital which are available for forming bonds with adsorbates. The free energy of adsorption will depend on the number of unpaired *d*-electrons per metal atom and on the energy levels(9). If the free energy of adsorption is changed, so is the activation energy of the

reaction and the reaction mechanisms or paths. The electrode reaction rate is altered by the transition metals.

TABLE 2-5
OXYGEN ADSORPTION ON SOME NOBLE METALS AND THEIR ELECTRON BAND CONFIGURATIONS (58)

METAL	O_2 COVERAGE $\mu F/cm^2$	O_2 MONOLAYER $\mu F/cm^2$	FRACTION COVERAGE	No. UNPAIRED *d*-ELECTRONS
Pa	110	510	0.22	0.55
Pt	135	500	0.27	0.6
Rh	480	530	0.90	1.7
Ir	440	525	0.84	1.7
Ru	500	530	0.95	2.2
Au	<15	---	<0.03	0

Figure 2-6 shows a linear variation of the maximum oxygen coverage (θ_{max}) with Pt-Rh alloy composition. When θ_{max} increases, the reaction rate can be increased and the Pt-Rh alloy has a higher activity than that of the Pt metal(21-23).

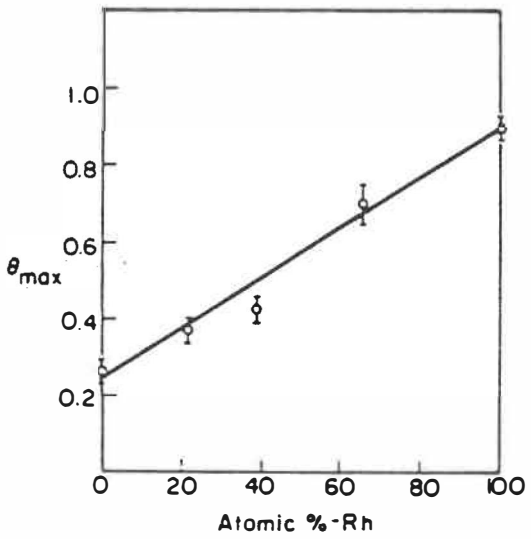

Fig.2-6 The linear variation of maximum oxygen coverage (θ_{max}) with Pt-Rh alloy composition (%) (the number of unpaired *d*-electrons increases from pure Pt to Rh). From (57).

Improvement of electrocatalytic activity can be based on the fact that different materials have varied ability to affect certain reactions. A Sn-Pt alloy was employed as a catalyst for methanol oxidation(59). The choice of this alloy was based on the concept that the organic molecules would be adsorbed on the Pt and the oxygen more readily adsorbed on the Sn. Increased adsorption of both organic and oxygen molecules on the electrode surface will lead to an increase in the reaction rate.

2.2.4 Summary and comments

The requirements for electrocatalytic electrodes were discussed in the literature(9,37,44). General considerations for selection of the OER electrode include: catalytic activity, stability, conductivity, selectivity and surface structure of the electrode. However, methods for measuring the electrode activity were not discussed, and there was no standard to unify the wide range of experimental data on electrode activity. This situation should be changed; more precise concepts about the requirements of the electrode should be developed.

The oxygen overpotential is related to the standard electrode potential. This link is based on thermodynamics. Some researchers already used this theory to look for electrocatalytic materials. The overpotential of the oxygen

reaction, one of the important parameters for characterizing electrode catalytic activity, also depends on electrode kinetics. Using thermodynamic results to predict electrode kinetic performance is limited. This type of discussion could be extended to the relationship between adsorption-desorption and catalytic activity. Adsorption or desorption depends on the free energy of adsorption, which is a thermodynamic value.

Some reports have suggested that metal oxidation from low valence oxides to higher ones (such as Ni, Ru and Ir oxides) was involved in the OER mechanism. In other words, oxidation was part of the OER process on the oxidized surface and was necessary for its completion. Some oxides thus obtained are stable, and others are not. They dissolve into the solution, as is the case of RuO_2 in alkaline solution. If the above suggestion is true, the kinetics of oxidation would strongly affect the kinetics of the OER. If this is not true, the process of oxidation of the electrode could be separated from the mechanism of the OER, and the standard electrode potential might have less importance in the oxygen reversible potential.

2.3 IMPROVING ELECTROCATALYTICAL ACTIVITY ON AN ELECTRODE

It is essential that an electrode have a high catalytic activity towards an electrochemical reaction. The primary reason for studying electrocatalysis is to find the material

with the best catalytic properties and/or to improve its catalytic activity. In Section 2.1, we have discussed oxygen evolution electrode materials. Here, our focus will be on improving the electrocatalytic activity of an electrode. Generally, improving electrocatalytic activity on an electrode can be realized in three ways: a) the kinetic approach, achieved by changing the reaction path and speeding the reaction rate; b) surface modifications, by producing active sites; and c) enlarging the real surface area on the electrode to deliver a higher current at lower overpotentials.

2.3.1 Kinetic approach

Improving electrode performance can be achieved by changing the reaction mechanism or altering the rate-determining step (RDS)(58). If the electrode reaction mechanism has a RDS in which the activation energy is high, it might be possible to rearrange the reaction route and to have the new RDS with a much lower activation energy. This results in an increase in the reaction rate. For example: the oxygen reduction reaction proceeds conventionally by an electrochemical route(58). However, a suitable redox system, the nitric acid-nitric oxide couple, might be introduced into this electrochemical reaction system (see Fig.2-7). The primary process in the new route is then the reduction of nitric acid, not the reduction of oxygen directly. The oxygen then oxidizes the nitric oxide formed back to nitric acid,

while it is being reduced itself. Since the electrochemical reduction of nitric acid and the chemical oxidation of nitric acid proceed considerably faster than the electro-reduction of oxygen, the total reaction rate is increased even if more steps are necessary to complete the reaction cycle. Increasing temperature, stirring and forcing solution flow are other methods for changing the kinetic conditions to favour the electrode reaction.

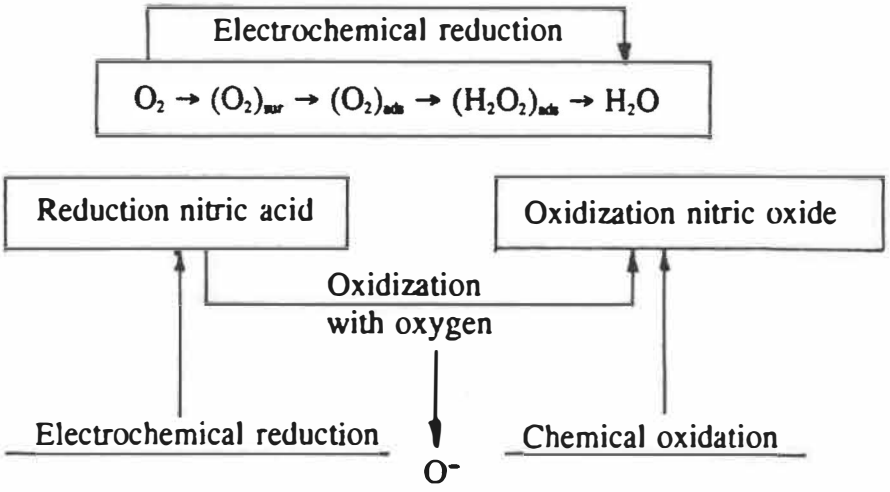

Fig.2-7 An example of the kinetic approach for increasing the rate of the oxygen reduction by introducing a redox system.

2.3.2 Surface modification

Surface modification may be an effective and efficient way to increase the activity of the electrode. This modification can be achieved by changing the surface chemical composition (alloying, doping, deposition and reduction), or oxidizing the surface to form oxides and special surface treatments (plasma and laser techniques).

2.3.2.1 Chemical composition

From the discussion in Section 2.1, it can be seen that transition elements, especially in the form of metal oxides, are the materials most frequently used to construct the oxygen electrode. Alloying nickel with transition metals can improve the activity of the nickel electrodes(29). Tseung(30) studied the OER on the Li-doped NiO in KOH solution. An increased catalytic activity, especially under high current densities, was explained by two factors: (a) an increase in electronic conductivity with the increase in lithium doping; (b) an increase in the Ni^{3+} ion concentration with lithium doping. The Ni^{3+} ion was considered to be the active site for the OER on Li-doped NiO.

2.3.2.2 Reaction nature

Some electrochemical reactions are very sensitive to surface conditions, while others are relatively insensitive (14). Therefore, the electrode reaction type must be studied before considering electrode surface modifications.Boudart(60) has discussed electrode reactions that are "insensitive" or "sensitive" to the surface structure of an electrocatalyst. These concepts are discussed in detail below.

INSENSITIVE--Chlorine evolution proceeds on some of the catalytically active materials with a low overpotential at high current densities. However, for the same electrode

material, this reaction is rather insensitive to surface conditions. Therefore, the chlorine reaction was classified as being "insensitive" to the electrode surface structure. For this reason, a selection of the right type of electrode material may be more important than improvement of electrode activity by surface modifications.

SENSITIVE--In contrast, the OER proceeds on most materials with a high overpotential at low current densities. A large variation in overpotential was observed on different materials. Even on the same material, as a consequence of different surface preparation procedures, varied experimental data are obtained. The OER is defined as a reaction "sensitive" to the electrode surface structures. In other words, optimization of the electrode surface conditions is equally important as the selection of the right catalytically active electrode materials.

Figure 2-8 represents values of the Tafel slopes (b) of oxygen and chlorine evolution reactions as a function of the RuO_2 electrode surface charge q^*(61). The charge q^* was measured by voltammetric technique. It is a charge consumed by the electrode surface charging, such as capacitance, etc., and it relates to the electrode surface defects, oxide thickness, surface annealing and preparation procedures. Therefore, it is a kind of measure of surface morphology. It shows that the

Tafel slope for the OER declined from 55 to 35 mV/dec as charge q^* increased from 0 to 100 mF/cm^2. However, a less than 10 mV decrease in Tafel slope was observed for the chlorine evolution reaction.

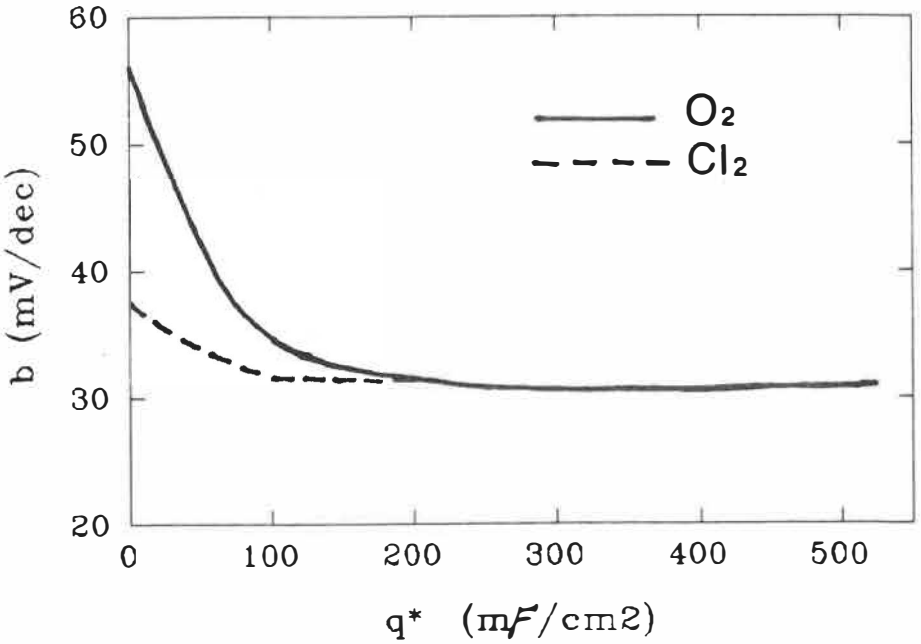

Fig.2-8 Tafel slopes of the oxygen and the chlorine evolution reactions as a function of surface charge (q^*) on the RuO_2 electrode. Adapted from (61).

With an understanding of the relationship between reaction sensitivity and surface conditions, we can improve the catalytic activity by optimizing electrode surface conditions and/or changing electrode morphology towards more favourable electrode kinetic conditions. In the case of the "insensitive" type of reaction, surface modifications and treatments are relatively ineffective in influencing electrode activity. Electrocatalysis research should be concentrated on the appropriate selection of new electrode materials.

2.3.2.3 Physically activated electrodes

Metallic electrodes exist in various surfaces physical states. As a result of some special physical treatments, the electrocatalytic performance for a certain reaction on physically activated electrodes is better than that of untreated electrodes. The chemical composition of physically activated electrode is the same as the untreated electrode. The catalytic characteristics originate from the physical nature of the electrode surface, such as: crystalline or amorphous states, oxide structure, number and position of active sites, and nature of metal atoms. Such activation can be obtained by various methods: e.g., pre-polarization of the electrode to form active surface oxides; electrodeposition of amorphous metals or alloys; *in situ* electro-reductions of formed surface oxides; and mechanical and chemical surface treatments of the electrode.

Physically activated electrodes could have much higher surface areas than inactivated electrodes. This results in a decrease in the real current density and therefore lowers the overpotential at a given apparent current density (based on geometric area).

Pre-anodization or potential cycling is a common practice for the activation and stabilization of the oxide layer(29,30) (e.g., 200 mA/cm^2 for 2 hours to form a stable nickel oxide

film). After anodization, the OER will proceed through the surface oxide phase. The reaction rate on such an activated electrode is much higher than that on a bare metallic electrode. The difference in the constant anodic current oxidation and potential cycling may be found in the electrode surface morphology. At appreciable potential range, potential cycling results in surface oxide formation and reduction. It could therefore result in a surface rougher than that obtained by constant current anodization.

Hall(40) reported that the Ni oxide coating on a Ni screen increased the electrode activity for the OER in alkaline water electrolysis. About 40 μm thick of the Ni powder coating was sintered onto the Ni screen at 760°C for 30 minutes. The η of the OER at i=100 and 200 mA/cm^2 was about 80 mV lower than that on a uncoated nickel screen electrode.

2.3.3 Increasing electrode surface

2.3.3.1 Real surface area

It has been shown(62) that the OER mechanism is not changed if platinum is hot rolled, cold rolled, etched, anodically polished or mechanically polished. However, a higher overpotential was observed on the polished surfaces. Among those platinum electrodes, the major difference in surface conditions is the real surface area. This reflects the real surface area on a catalyst can change the catalytic

activity substantially.

Knowing the real surface area on an electrode is essential to a better understanding of the electrode's catalytic property. Let us consider this from the Tafel equation:

$$\eta = \frac{RT}{\alpha nF} \ln \left(\frac{i}{i_{ex}}\right) \qquad (2\text{-}1)$$

where R is the gas constant; T is temperature in K; α is transfer coefficient; n is electron transferred in reaction; F is a Faradic constant; i_{ex} is exchange current density and i is current density at η overpotential. In Eq.(2-1), the current density is defined as:

$$i = \frac{Total\ \ Current\ \ (I)}{Real\ Surface\ Area\ (S)} \qquad (2\text{-}2)$$

The total current (I) on an electrode is kept constant, the current density (i) will then decrease as the real electrode surface area (S) increases. Consequently, from Eq.(2-1), the overpotential (η) will be lowered. In other words, the reaction rate on the electrode can be increased by deliberately creating a rough surface with a high real surface area. Preparing an electrode with a high real surface area is, therefore, an important part of the technique for fabricating practical electrodes.

2.3.3.2 Techniques

Fabrication of an electrode with a very rough and porous surface is very effective for increasing the electrochemical reaction rate. Large surface areas deliver the a large current at a low apparent current density. Consequently, the overpotential will be low. Electrodeposition of sponge metals, powder deposition and dispersion-deposition with highly rough surfaces are practical techniques known for preparing these electrodes.

Raney-Ni type electrodes represent another method for preparing active Ni electrodes with high real surface areas. Al or Zn metal in Ni-Al or Ni-Zn alloy is leached out in alkaline solution, leaving the remaining Ni with a very porous surface structure. This type of catalyst is widely used in chemical engineering.

2.4. NICKEL AS AN ELECTROCATALYST

2.4.1. Historical review

Nickel was discovered by Cronsyedt(63) in 1751. The first report on the use of nickel as a catalyst was probably Thenard (64) in his studies of decomposition of hydrogen peroxide. He reported: with metallic nickel, the action was "slight", with nickel oxide, it was "mild" and with nickel hydroxide, it was "moderate". Even though this evaluation appears ambiguous, it

still could be understood that nickel hydroxide was the best catalyst among the nickel electrodes tested. The first use of nickel as a commercial catalyst was a nickel electrode in the production of hydrogen from a mixture of carbon monoxide, hydrocarbons and steam in 1888 by Mond and Langer(65).

It has been known for a long time(66) that the oxygen overpotential on nickel and nickel oxide is low, and nickel is quite stable in alkaline media. The oxide on nickel electrodes could be obtained by electrolytic oxidation(67), and later it was found that this oxide was not soluble(66). It was realized then that it was a useful anode material for many electrolytic oxidation processes.

The importance of oxide films on nickel electrodes has attracted attention for a long time. Haber(68) suggested that the actual oxidation was not due to the action of monatomic oxygen, but that it was accomplished by the superficial coating of oxides. Brand and Rambottom(69) found that the oxidation proceeded more satisfactorily with nickel than with iron anodes in laboratory studies. This effect was attributed to the existence of an oxide on the anode surface which acted as an oxygen carrier and promoted the process. Practically, many water electrolysis cells use nickel as the oxygen electrode, and the electrode is in the form of nickel with cladded iron, sintered nickel plaques or screens. It is

reported(70) that nickel oxide prepared by the thermal decomposition method has an electrocatalytic performance superior to nickel in the forms used in water electrolysis. The catalytic activity of nickel prepared by thermal decomposition is comparable to that of the Ni-Co oxide, or of the RuO_2.

2.4.2 Nickel oxides

Nickel possesses several oxides. The most common and stable one is the monoxide, NiO, which has a cubic structure. The higher oxides, Ni_2O_3 and NiO_2, can be produced by anodic oxidation or by the reaction of alkaline with the metals or the salts(66). These higher oxides appear to be stable only as hydrates, e.g., $Ni_2O_3*2H_2O$ and NiO_2*xH_2O(62). NiO_2 is very unstable, and it is expected to lose its O_2 rapidly in aqueous immersion even at room temperature(17). Several Ni suboxides have been reported (e.g., NiO_4; Ni_3O; Ni_3O_2; and Ni_2O), but their existence has not been definitely assured(66). Ni_3O_4 is probably a mixture of NiO and NiO_2 or NiO and Ni_2O_3(66). Mellor(71) and Labat(72) have given extensive reviews of the literature on Ni oxide materials.

According to Glemser and Einerhand(73), various higher oxides of nickel involving Ni^{+3} may be made from a choice of oxidizing agents and nickel salts. An analysis of the X-ray patterns shows that the Ni^{+3} oxide can best be described as

NiOOH. NiOOH exists in three modified forms, which have been designated as α-, ß-, and γ-NiOOH by Glemser and Einerhand (73). X-ray diffraction data and electron micrographs were obtained for these oxides(74). They have hexagonal crystal structures (74). However, only ß-NiOOH has been identified and referred to on the nickel electrode in the discussion of the OER(17,28,75). Information leading to the preparation of α, ß, and γ-NiOOH oxides can be found in reference(72).

2.4.3 OER mechanisms

Milner(76) pointed out that in an analysis of the OER, an unbelievable number of reaction paths was possible when all intermediates were considered. By applying some assumptions, there are still eleven possible mechanisms. Damjanovic(12,77) has analyzed 14 oxygen reaction paths, which are listed in Table (2-6). For a given RDS, two Tafel slopes ($d\eta/dLni$) (low η and high η) are listed on the anodic side.

2.4.4 OER mechanism on Ni electrodes

The OER occurs on an oxidized surface where an average oxidation state of Ni ions is (III)(78). At higher anodic potentials, Ni^{+3} is presumably converted to Ni^{+4}, which is inactive for the OER. Conversion of Ni^{+3} into Ni^{+4} may be the reason for the progressive deactivation of anodes(28,79).

TABLE 2-6
OER PATHS AND ASSOCIATED TAFEL SLOPES(12)

PATH (S IS A SURFACE SITE)	Tafel SLOPE (dη/dLni) ANODIC LOW E	ANODIC HIGH E	CATHODIC
1. The oxide path (80)			
$S + H_2O \rightarrow SOH + H^+ + e^-$	2RT/F		-2RT/F
$2SOH \rightarrow SO + SH_2O$	RT/2F		
$2SO \rightarrow O_2 + 2S$	RT/4F		
2. The electrochemical oxide path (80)			
$S + H_2O \rightarrow SOH + H^+ + e^-$	2RT/F		-2RT/3F
$SOH+S+H_2O \rightarrow SO+SH_2O+H_2 +e^-$	2RT/3F	2RT/F	
$2SO \rightarrow O_2 + 2S$	RT/4F		
3. The hydrogen peroxide path (80)			
$4S + 4H_2O \rightarrow 4SOH + 4H^+ + 4e^-$	2RT/F		-2RT/F
$2SOH \rightarrow SH_2O_2 + S$	RT/2F		-RT/2F
$SH_2O_2 + SOH \rightarrow SOH_2 + SO_2H$	RT/3F		-RT/F
$SO_2H + SOH \rightarrow SH_2O + S + O_2$	RT/3F		
4. The metal peroxide path (80)			
$4S + 4H_2O \rightarrow 4SOH + 4H^+ + 4e^-$	2RT/F		-2RT/F
$SOH \rightarrow SO + SH_2O$	RT/2F		-RT/2F
$SO + SOH \rightarrow S + SHO_2$	RT/3F		-RT/F
$SHO_2 + SOH \rightarrow O_2 + S + SH_2O$	RT/4F		
5. The electrochemical metal peroxide path (80)			
$3S + 3H_2O \rightarrow 3SOH+3H^+ + 3e^-$	2RT/F		-6RT/5F
$2SOH \rightarrow SO + SH_2O$	RT/2F	RT/F	-RT/2F
$SO + H_2O \rightarrow SH_2O + H^+ + e^-$	RT/5F	2RT/F	-2RT/3F
$SH_2O + SOH \rightarrow S + O_2 + SH_2O$	RT/4F		
6. The alkaline path (81)			
$S + H_2O \rightarrow SOH + H^+ + e^-$	2RT/F		-2RT/3F
$SOH + H_2O \rightarrow SH_2O_2 + H^+$	RT/F		-RT/F
$2SH_2O_2 \rightarrow S + SO^{2-} + 2H_2O$	RT/2F	RT/F	-RT/2F
$SO^{2-} \rightarrow S + O_2 + 2e^-$	RT/3F		-RT/F
7. Path suggested by Conway and Bourgault (82)			
$3S + 3H_2O \rightarrow 3SOH + 3H^+ + 3e^-$	2RT/F		-6RT/5F
$SOH \rightarrow SO + H^+ + e^-$	2RT/3F	2RT/F	-2RT/5F
$SO + SOH \rightarrow SHO_2$	RT/3F	RT/F	-RT/F
$SHO_2 + SOH \rightarrow S + O_2 + SH_2O$	RT/4F		

TABLE (2-6) ---contd.

PATH (S IS A SURFACE SITE)	TAFEL SLOPE ANODIC LOW E	ANODIC HIGH E	(dη/dLni) CATHODIC
8. Alternative path of Conway and Bourgault (82)			
$2S + 2H_2O \rightarrow 2SOH + 2H^+ + 2e^-$	2RT/F		-2RT/3F
$SOH \rightarrow SO + H^+ + e^-$	2RT/3F	2RT/F	-2RT/5F
$SO + H_2O \rightarrow SHO_2 + H^+ + e^-$	2RT/5F		-2RT/3F
$SHO_2 + SOH \rightarrow S + O_2 + SH_2O$	RT/4F		
9. Path suggested by Riddiford (83)			
$S + H_2O \rightarrow SOH + H^+ + e^-$	2RT/F		-2RT/3F
$2SOH \rightarrow SO + SH_2O$	RT/2F		-RT/2F
$SO + H_2O \rightarrow SHO_2 + H^+ + e^-$	2RT/5F	2RT/F	-2RT/3F
$SHO_2 + H_2O \rightarrow O_2 + SH_2O + H^+ + e^-$	2RT/7F		-2RT/F
10. Krasilshchikov path (for Ni in alkaline)(75)			
$S + OH^- \rightarrow SOH + e^-$	2RT/F		-2RT/3F
$SOH + OH^- \rightarrow SO^- + H_2O$	RT/F		-RT/F
$SO^- \rightarrow SO + e^-$	2RT/3F	2RT/F	-2RT/F
$2SO \rightarrow O_2 + 2S$	RT/4F		
11. Wade and Hackerman's path (84)			
$2S + 2H_2O \rightarrow SO + SH_2O + 2H^+ + 2e^-$	RT/F		-RT/3F
$SO + 2SOH^- \rightarrow 2S + SH_2O + O_2 + e^-$	RT/3F		-RT/F
12. From reference (12)			
$S + H_2O \rightarrow SOH + H^+ + e^-$	2RT/F		-2RT/7F
$SOH \rightarrow SO + H^+ + e^-$	2RT/3F	RT/F	-2RT/3F
$SO + H_2O \rightarrow SO_2H + H^+ + e^-$	2RT/5F	2RT/F	-2RT/3F
$SO_2H \rightarrow S + O_2 + H^+ + e^-$	2RT/7F		-2RT/F
13. From reference (12)			
$S + H_2O \rightarrow SOH + H^+ + e^-$	2RT/F		-2RT/3F
$SOH + H_2O \rightarrow SO\text{-}H\text{-}OH^- + H^+$	RT/F		-RT/F
$SO\text{-}H\text{-}OH^- \rightarrow SO\text{-}H\text{-}OH + e^-$	2RT/3F	2RT/F	-2RT/F
$SO\text{-}H\text{-}OH \rightarrow SO + H_2O$	RT/2F	RT/F	
$2SO \rightarrow S + O_2$	2RT/F		
14. From reference (12)			
$S + H_2O \rightarrow SOH + H^+ + e^-$	2RT/F		-2RT/7F
$SOH + H_2O \rightarrow SO\text{-}H\text{-}OH^-$	RT/F		-RT/3F
$SO\text{-}H\text{-}OH^- \rightarrow SO\text{-}H\text{-}OH + e^-$	2RT/3F	2RT/F	-2RT/5F
$SO\text{-}H\text{-}OH \rightarrow SO + H_2$	RT/2F	RT/F	-2RT/2F
$SO + H_2O \rightarrow SHO_2 + e^-$	2RT/5F	2RT/3F	-2RT/3F
$SHO_2 \rightarrow S + O_2 + H^+ + e^-$	2RT/7F		-2RT/F

The generally accepted mechanism of the OER on nickel electrodes(17), modified from the Krasilshchikov path (path 10 in Table (2-6))(28,75), consists of the following steps:

$$OH^-(ads) \rightarrow OH(ads) + e^- \quad (2\text{-}3)$$

$$OH(ads) + OH^- \rightarrow O^-(ads) + H_2O \quad (2\text{-}4)$$

$$2\beta\text{-}NiOOH(s) + O^-(ads) \rightarrow 2NiO_2(s) + H_2O + e^- \quad (2\text{-}5)$$

$$2NiO_2(surf) + HO(ads) \rightarrow \beta\text{-}NiOOH(surf) + O(ads) \quad (2\text{-}6)$$

$$O(ads) + O(ads) \rightarrow O_2 \quad (2\text{-}7)$$

Any one of these steps, (Eq.2-3 to 2-7), may be the RDS for the oxygen reaction mechanism. Elina and co-workers(85) suggest that at a low current density the concentration of NiO_2 on the surface would be so low that the rate of spontaneous decomposition of NiO_2 (Eq.2-6) would be slow, and that it, therefore, would become the RDS. At high current densities, however, a relatively large amount of NiO_2 is present, causing a higher NiO_2 decomposition rate. Under this circumstance, the discharge of OH^- ions (Eq.2-3), is the slowest step, and this is in agreement with a Tafel slope of 0.12 V/dec. Lu and Srinivasan (28) studied the Ni oxide film in a 1 N KOH, and their data supported Eq.2-5 as the RDS at low overpotentials. The RDS might be related to the extent of anodized surface(12). The reaction path would depend on the surface oxidization and the current density. It was also suggested that(82) the Tafel slope of about 0.05 V/dec corresponds to the final recombination step (Eq.2-7) at appreciable coverage under activation adsorption conditions.

2.5 EVALUATING ELECTRODE PERFORMANCE

The best electrocatalyst for a given reaction is the one on which current density is the largest at the same applied potential(58). However, it is not so simple to compare the electrocatalytic activity of different electrodes. Even this concept is very straightforward, several factors must be considered before coming to a conclusion for comparison.

In 1818, Thenard(64) used words such as "slight", "mild" and "moderate" etc., to describe the activity of the nickel catalyst. This was too ambiguous. Since then, advances in electrochemistry have resulted in great progress in methods of evaluating electrode performance. Today there are many quantitative or qualitative methods for evaluating electrode catalytic properties. Several essential parameters can be compared for electrode performance, such as current density (i); overpotential (η); exchange current density (i_{ex}); Tafel slope (b) and the transfer coefficient(α). These parameters are basic kinetic parameters and are convenient for carrying out the evaluation.

From a practical point of view, there are other factors such as the real surface area of an electrode, the electrode surface structure or surface morphology, etc.. Long-term service time or corrosion stability of the electrode is the

most important property that must be tested before any practical applications of the electrode. These parameters are discussed in the following sections.

2.5.1 i and i_{ex}

According to Eq.(2-1), between i and η, we have:

$$\eta = \frac{RT}{\alpha nF} \ln \left(\frac{i}{i_{ex}}\right)$$
$$i = i_{ex} \exp\left[\frac{\alpha nF\eta}{RT}\right] \qquad (2\text{-}1)$$

If two electrodes follow an identical reaction mechanism (same paths and RDS), it can reasonably be assumed that the transfer coefficient and the number of electron transferred for the two electrodes are the same, namely $\alpha_1=\alpha_2$ and $n_1=n_2$. The exponential terms in the expression (2-1) are equal at the same overpotential ($\eta_1=\eta_2$). Thus,

$$\frac{i_1}{i_2} = \frac{i_{ex1}}{i_{ex2}} \qquad (2\text{-}8)$$

When comparing i of two electrodes at the same η, we could also compare i_{ex} of the two electrodes instead(22). This could be done by obtaining the linear Tafel regions on the polarization curves, then extrapolating the Tafel lines and intersecting them at the oxygen reversible potential. The current at the intersection is the i_{ex}. Figure 2-9 is a diagram illustrating the determination of the exchange current density and the Tafel slope in the polarization curve.

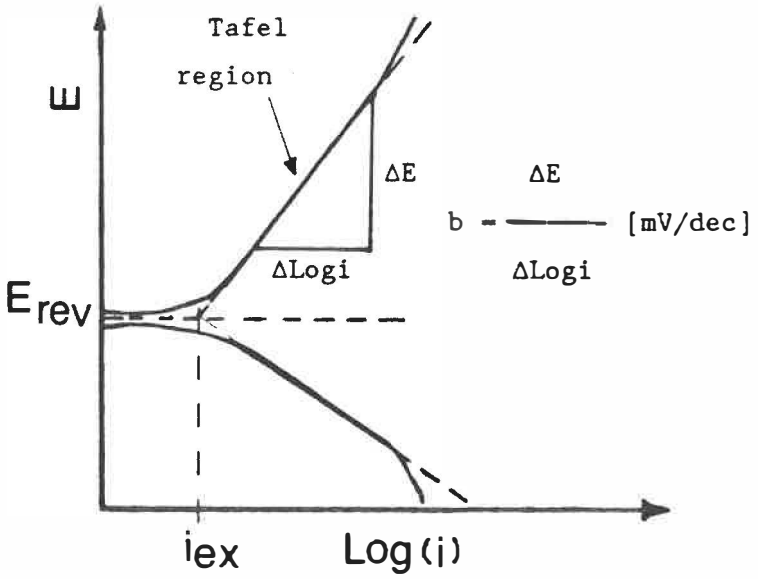

Fig.2-9 A schematic illustration of determination of the exchange current density (i_{ex}) and the Tafel slope (b) in a polarization curve.

When different catalysts are compared in terms of exchange current density (i_{ex}), the mechanisms of the electrode reaction on the two electrodes should be identical. However, this condition is not always secured in the literature. The exact reaction path, RDS and intermediates are sometimes not certain or are difficult to determine.

Unlike the case of the HER, which has a relatively high value of the i_{ex} (10^{-4} to 10^{-6} mA/cm^2), the reported i_{ex} of the OER on most catalytic materials was as low as 10^{-13} to 10^{-7} mA/cm^2. Since the i_{ex} is so small, it is difficult to obtain an accurate measurement. Therefore, the i_{ex} is not a very sensitive and useful measurement for characterization of the electrode performance for the OER.

2.5.2 Tafel Slope

Many previous comparisons of electrocatalysts were based on values of the Tafel slope(14,44,45,86). Table (2-7)(14) gives a comprehensive collection of Tafel slopes (b) and other kinetic parameters of the OER. An electrocatalyst with a low Tafel slope indicates a low rate of increase in current density with an increase in overpotential. The values of the Tafel slope given in Table (2-7) are in the range of 40 to 120 mV/dec. b values are usually obtained from the polarization curves (or very slow scanning rate), but this condition was frequently ignored or neglected. It should be emphasized that determination of the b value must be in the Tafel region (e.g., between 10^{-3} and 10^{1} mA/cm^2 on Pt); otherwise it is not within the limitation of the Tafel equation. In Table (2-7), the Tafel parameters (a) for the OER on several oxide electrodes are also listed. The Tafel parameter (a) might be a better basis for the comparison of electrocatalysts(14), because it combines the b and i_{ex} together as:

$$a = b\,Ln(i_{ex}) \qquad (2\text{-}9)$$

The combination of the b and the i_{ex} could make more sense in electrocatalysis studies, since the best electrocatalyst would be the one with a high i_{ex} but a low b value. However, this parameter is much less frequently used than the Tafel slope and there are no papers emphasizing the importance of this parameter in the field of electrocatalysis.

TABLE 2-7
EXPERIMENTAL KINETIC PARAMETERS OF THE OER (14)

Electrode	Solution	T/°C	b/V		Reaction order		$E^{\neq}$/kJ mol^{-1}	a/V
(Ti)PtO_2	H_2SO_4(0.5)	30	0.113		0		x	
(Ti)PtO_2	KOH(1)	30	0.059	0.114	2	1	x	0.48
Pt	H_2SO_4(1)	80	0.09					0.99
(Ti)PtO_x	KOH(30 wt. %)	80	0.046	?				0.41
(TiN_x)MnO_2	H_2SO_4(1)	20	0.1-0.11				x	
(Pt)MnO_2	H_2SO_4(0.5)	30	0.11		0		x	
	KOH(1)	30	0.11		1		x	
(Ti/RuO_2)MnO_2	H_2SO_4(0.5)	30	0.11				x	
	KOH(1)	30	0.11				x	
β-MnO_2	H_2SO_4(0.5)	30	0.11		0.1	0.1		
	KOH(1)	30			0.9			
β-MnO_2+Mn_2O_3	H_2SO_4(0.5)	30			1	0.1		
	KOH(1)	30			0.9			
Ni	KOH(5-10)	25	0.06	0.12				
Ni	KOH(30 wt. %)	80	0.062					0.41
Ni	KOH(1)	23	0.04					0.46
Ni	H_2SO_4(0.5)		0.110		0			
	KOH(1)		0.055	(0.120)	2.1	0		
NiO_x	KOH(30 wt. %)	80	0.047				34.3	0.34
	KOH(30 wt. %)	80	0.071					0.45
Ir	H_3PO_4(85 wt. %)	25	0.053				67	0.59
Ir	H_2SO_4(1)	25	0.054	0.112(0.126)				0.39
Ir	$HClO_4$(1)	25	0.040	0.120				0.44
	KOH(1)	25	0.040	0.120				0.44
Ir	H_2SO_4(1)	80	0.085					0.58
IrO_x	H_2SO_4(0.5)	25	0.050					
(Ti)IrO_x	KOH(30 wt. %)	80	0.050					0.41
(Ti)IrO_2	H_2SO_4(0.5)	30	0.056		-1			
	KOH(1)	30	0.040		2			
Rh	H_3PO_4(85 wt. %)	25	0.094				58.1	0.98
Rh	$HClO_4$(1)	25	0.060	0.120				0.63
	KOH(1)	25	0.042	0.115				0.47

TABLE 2-7 (contd.)

Electrode	Solution	T/°C	b/V	Reaction order	$E^{\neq}$/kJ mol^{-1}	a/V
(Ti)RhO_x	KOH(30 wt. %)	80	0.067			0.43
Pb	H_2SO_4(3.5)		0.056 0.144			
Pb	KOH(1)	25	0.12			
Pb	NaOH(6.1)	25	0.116	0.8		1.14
PbO_2	H_2SO_4(1)	25	0.118			
PbO_2	H_2SO_4(2.2)	30	0.051(α) 0.121(β)			(α)0.8 (β)1.1
β(?)-PbO_2	NaOH(1-5)	25	0.10-0.12			
(C)PbO_2	H_2SO_4(1)	30	0.134		x	1.18
β-PbO_2	H_2SO_4(0.5)		0.120			1.39
β-PbO_2	H_2SO_4(0.5)	25	0.16		40.6	1.3
$SrFeO_3$	H_2SO_4(0.5)	25	0.065-0.07	0		
	KOH(1)	25	0.065-0.07	2		
$La_xBa_{1-x}CoO_{3-y}$	KOH(6)	25	0.057(x=0.8)-0.059(x=0.5)			0.44
$La_{1-x}Sr_xMnO_3$	KOH(1)	25	0.13-0.14	1		
$NiLa_2O_4$	KOH(1)	25	0.040 0.120	1.85 1.0	x	
Co_3O_4	$HClO_4$(1)	25	0.060			
	KOH(1)	25	0.065			
(Ti)$NiCo_2O_4$	KOH(30 wt. %)	25	0.040		38.5	0.35
$NiCo_2O_4$	KOH(5)	25	0.033 0.107			0.50
$Ni_xFe_{3-x}O_4$	KOH(30 wt. %)	25	0.040			
(Ti)RuO_2(300-500°C)	KOH(30 wt. %)	80	0.067			0.37
(Ti)RuO_2(400°C)	KOH(4)	22	0.040	1		0.32
RuO_2(450°C)	$HClO_4$(1)	30	0.040		x	
RuO_2(850°C)	$HClO_4$(1)	30	0.070		x	
(Ti)RuO_2(350°C)	H_2SO_4(0.5)	25	0.040	≈ -1	x	
(SiO_2)RuO_2(CVT)	H_2SO_4(0.5)	25	0.065			0.38
(Ti)RuO_2(350°C)	H_2SO_4(1)	25	0.040-0.045		55.2	
(SiO_2)RuO_2	H_2SO_4(1)		0.045 >0.120			
(Ti)TiO_2+RuO_2	KOH(30 wt. %)	80	0.045		38.5	0.31
(Ti)TiO_2+RuO_2	H_2SO_4(1)	80	0.066			0.52
(Ti)TiO_2+RuO_2(30%)	pH 0.5 to 13	20	0.035-0.050	pH dependent	1.5(OH^-)	

The Tafel slope is a current density dependent parameter, and it is defined as:

$$b = \frac{d\eta}{dLn(i)} \qquad (2\text{-}10)$$

For example, the OER on the Ir metal electrode gives two Tafel regions in acid and alkali solutions(15): b=(2RT/3F) for low current densities and 2RT/F for high current densities(15). The Tafel slope also depends on the surface coverage of the reactant species and the oxide layer. Conway and Bai(5) pointed out that the function of the coverage of adsorption species with potential f(θ) was involved in the Tafel slope, as in the form of:

$$\frac{dLni}{d\eta} = \frac{dLnf(\theta)}{d\eta} + \frac{\alpha nF}{RT} \qquad (2\text{-}11)$$

Since the coverage of the reactant species is not high at low overpotential, the Tafel slope in the low overpotential region may reflect some actual difference in the electrode surface structure and composition of the oxide layer(14). At high overpotentials, the coverage of adsorption on the electrode surface becomes higher, the oxide layer grows thicker and the Tafel slope obtained at this condition may be affected by these factors. Therefore, when we compare electrocatalysts on the basis of the Tafel slope, we should measure the slope of the polarization curve at low overpotentials. This would be more effective in revealing the difference in the structure and the surface composition of the electrode.

On the other hand, the Tafel slope obtained at high overpotentials will reflect the practical performance of the electrode in industrial applications, since in most industrial applications, the current density of the electrode reaction is as high as 100 mA/cm^2. The Tafel slope measured in this region indicates the increase in cell voltage as electrolysis production is raised. In other words, the results obtained by the comparison of b values at high η could be easier to transfer into industrial applications.

It is understood that the Tafel equation is a special case ($i>>i_{ex}$) of the Butler-Volmer equation. The b values should then be measured under conditions required by the Tafel law, that is under a high polarization. The equation (2-1) can not be used under the condition of $i \rightarrow 0$. In fact, when $i \rightarrow 0$, at low current densities we have:

$$\eta = \frac{RTi}{\alpha nFi_{ex}} \qquad (2\text{-}12)$$

The Tafel slope varies according to the value of pH, as shown with the iridium electrode(16). $(dE_{SHE}/dpH)_i$ = -42 mV/dec at low current densities; $(dE_{SHE}/dpH)_i$ = -105 mV/dec at high current densities.

A break in the Tafel line from low to high overpotential has been observed(12). The possible reasons discussed in the literature were: (1) a change in the reaction mechanism;

(2) transition of the adsorption coverage from $\theta=0$ to $\theta=1$, with the same mechanism; (3) a change in the RDS, with the same reaction paths and steps. However, identification of the exact reason for the Tafel slope change in a certain reaction system is very difficult.

In conclusion, all these uncertainties with respect to b values discussed above make it difficult to use b as a sole parameter to evaluate the electrode activity.

2.5.3 Real surface area

It was mentioned in the previous section that comparisons of overpotentials(η) at a constant current density(i), or vice versa, should be made using the same real surface area of the electrode. An electrochemical reaction occurs on the electrode surface, and the surface state is a critical factor in determining the reaction kinetics, especially, the OER is the reaction in which kinetics is very dependent on surface conditions. It is essential to know the surface conditions to evaluate the performance of the electrode. Real surface area, surface oxide and surface treatments represent three aspects of the surface conditions. In this section, measurements of the real surface area on an electrode are discussed.

2.5.3.1 Measuring electrode surface area

Each of the techniques available for measuring the real

surface area of an electrode(87) yields a value that has a specific meaning with respect to the electrode. One measure could indicate the surface available for adsorption, while another could represent the true surface available for a certain electrode reaction, and may therefore be reaction-type dependent.

It is worthwhile to identify the physical meaning of real surface measured by different methods before we can apply it to the study of an electrocatalyst. Unfortunately, no paper of this kind was seen in the literature.

The methods of measuring electrode surface area can be classified(87) as the physico-chemical (e.g.,adsorption), the purely physical, the chemical and the electrochemical methods. They are discussed below.

(1) BET method (Brunauer-Emmet-Teller method)

The BET method is the most frequently used. This is a technique based on the amount of adsorbate (gas or solution) on the unit surface of a solid electrode. The gas adsorption method has been accepted in the past as a prime standard method for measuring the electrode's real surface area(87).

(2) Physical method

Examining the surface morphology and the porosity of the

electrode is the oldest and most direct method among the methods for measuring electrode surface area. The physical method gives rapid, reproducible results, but it does not have the precision that the adsorption and chemical methods have. In most cases, it is necessary to know the value of the average diameter of the particle on the solid electrode, which is very difficult to ascertain. Microscopic, X-ray diffraction and radioisotopes are commonly used physical methods for measuring surface area. These methods usually require expensive equipment for conducting tests.

(3) Chemical method

The chemical method is a technique of measuring a reaction rate on a surface. The dependence of this chemical reaction rate on the surface area is known. Therefore, by measuring the reaction rate, the surface area of the electrode can be derived.

(4) Electrochemical method

This method depends on either the deposition, adsorption or the removal of an adsorbed layer of some chemical species where the fractional surface coverage is known by measurement of the electrical double-layer capacitance. AC impedance(87), the cyclic voltammetric technique(88), the charge curve method(89), and the triangular voltage sweep method(90) are some examples of measuring double-layer capacitance on solid

electrodes. They are *in situ* techniques that can be carried out in true testing environments and conditions.

Another merit of these tests is that they indicate the surface area of the electrode that is available to the electrochemical reaction. The values obtained by this method are the best for comparison of the catalytic properties of similar electrodes in the same electrolyte system.

The double-layer capacitance (C_{dl}) measurement deserves a special mention. The C_{dl} is considered to be proportional to the real surface area on an electrode. It is therefore an indirect measure of the real electrode surface area. It is believed that a mercury liquid surface is the smoothest surface. Its geometric surface is almost the true surface area. The C_{dl} on liquid mercury ranges from 18 to 24 $\mu F/cm^2$ (91,92). This C_{dl} could be considered as a standard capacitance per unit surface. Therefore, the real surface area on an electrode can be derived by measuring the C_{dl} and comparing the value with the standard one.

The surface area measured by this method especially refers to the surface available for the double-layer charging on the electrode, and it is closely related to the real surface available to the faradaic process. From a practical point of view, where the real surface area for the

electrochemical reaction is concerned, this method may be the most practical and effective method. However, when the electrode material itself participates in the reaction, such as the electrode material oxidation/reduction is involved in the OER mechanism, the C_{dl} can not be measured accurately(86).

2.5.3.2 Comparison of methods

A brief comparison of the methods for surface area measurement is given in Table (2-8)(87).

TABLE 2-8
METHODS FOR SURFACE AREA MEASUREMENTS(87)

No.	METHOD	SURFACE RANGE (m^2/g)	TIME/TEST (hour)	REPRODUCI-BILITY*
1	BET(Nitrogen)	1-2000	2-3	2
2	BET(Krypton)	0.001-5	2-3	2
3	Solute ads.	5-100	1-2	3
4	Conden.vapor ads.	10-300	0.5-1	4
5	Heat of wetting	10-100	3-4	1
6	Microscopic	3-10	1-2	5
7	X-Ray diffraction	3-50	1-2	8
8	Radioisotope	3-50	1-2	7
9	D-L capacitance	10-100	0.5-2	6
10	Current density	10-100	1-2	9

*. 1 being the most reproducible and 10 being the least.

Comments and restrictions--Methods 1 & 2 can be used for all electrode materials, but special equipment is necessary; they can be made nondestructive. No.1 needs approximately $5M^2$ of surface area for analysis. No.3 can be carried out with equipment generally available in most chemical laboratories. No.5 needs very special equipment and is the most difficult test to perform. No.7 is not suitable for most electrode

systems. It is usually used in materials which are uniform powders and have unshared X-ray diffraction peaks.

2.5.4 Complications in evaluation of electrodes

2.5.4.1 Reaction selectivity

Electrocatalytic selectivity means that the catalytic activity varies depending on the reaction occurring on the electrode surface. A good electrocatalyst for the chloride evolution is not necessarily a good electrode for the oxygen evolution. The character of catalytic selectivity tells us to compare the performance of electrodes only with the same reaction.

2.5.4.2 Kinetic conditions

Kinetic conditions (such as increasing temperature and stirring in reactor) complicate evaluation and comparison of electrodes. Electrode conditions can be favourable to a certain reaction path or mechanism. Kinetics of the reaction can also change the catalytic activity on an electrode. Moreover, sometimes the gas bubbles on the surface of the electrode cause an error in the electrochemical measurement that makes evaluation and comparison of catalytic electrodes difficult or incorrect.

Figure 2-10 is an example in which kinetic conditions change the electrocatalytic activity of a RuO_2 electrode for

the reaction of chloride and oxygen evolution(14). From the strict thermodynamic point of view, electrolysis of the brine solution on the RuO_2 should lead to oxygen evolution rather than chlorine evolution. However, under the kinetic conditions, we obtain a reversal in the position of the catalytic activity of the RuO_2 electrode at pH=4.

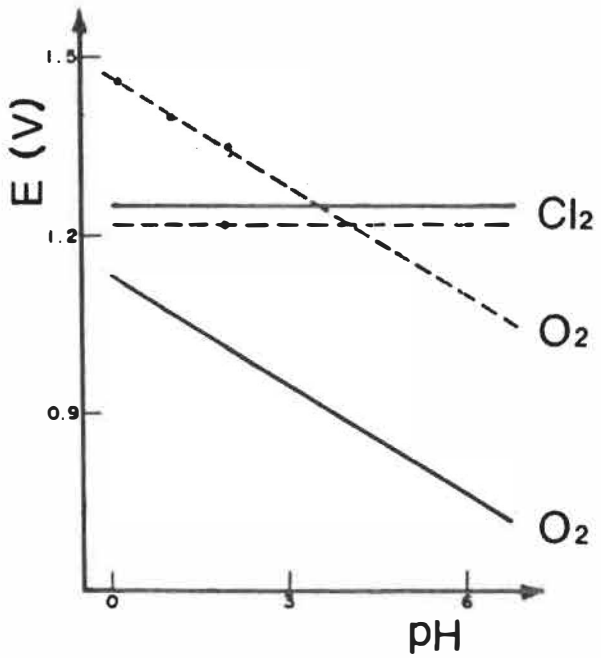

Fig.2-10 An example of kinetic conditions changing the Ruo_2 electrode activity for the O_2 and Cl_2 evolutions. (----) Kinetic and (——) Thermodynamic condition. (a):O_2; (b):Cl_2. From (14).

Comparison of electrocatalysts should then always be made under the same conditions. This sometimes makes it difficult to compare our experimental data with others, especially data in references with unspecified experimental conditions. It is also understood that different electrocatalysts for the same reaction should only be compared if the reactions have the same mechanism (path, Tafel slope, etc.).

2.5.4.3 Potential dependence

At different applied potentials, the activity of an electrocatalyst is not the same. This means that results of comparison of the electrocatalytic activities from different electrodes would not be the same if the applied potentials are not identical. The potential dependence of the electrocatalytic activity introduces uncertainty in comparing electrode performance, which is illustrated by the E-Log(i) plot for the oxidation of ethylene on Pt and a 80Pt-20Ru alloy in Fig.2-11(93). Note that the 80Pt-20Ru alloy electrode is a better catalyst at potentials below 0.45 (V *vs.SHE*), whereas, at high potentials, pure platinum electrode is a better one, based on η.

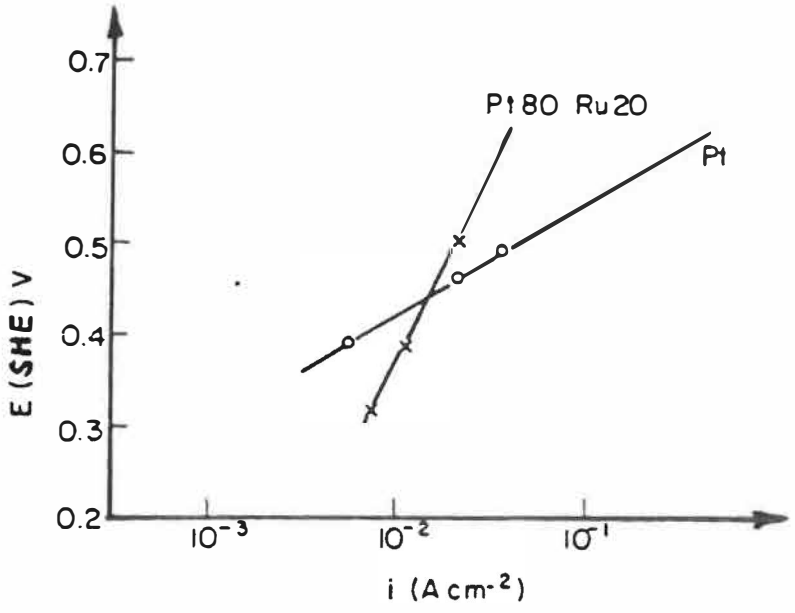

Fig.2-11 Experimental current-density and potential relationship for the oxidation of ethylene on the Pt and the 80%Pt-20%Ru alloy electrode. From (93).

2.5.4.4 Potential of zero charge

At this point, a question should be asked: at what potential should two electrocatalysts be compared? Electrocatalysts have been compared by measurement of the current density generated at different electrodes at the same potential. The η-Log(i) relationship was presented in Eq.(2-1). The potential dependence aspect of the electrode reaction rate appears to be the most important aspect. The potential is based on the electrified interface between electrode and electrolyte. If a zero potential difference across the interface can be found, the catalysts can then be compared at the zero potential without interference of the reaction-accelerating field at the interface. If it were possible to make an experimental arrangement by which the potential difference across various electrode-electrolyte interfaces was zero, the current density at that potential would give a clear comparison of the intrinsic catalytic powers of the various electrodes(58). In this way, the pure catalytic power of an electrocatalyst could be measured and compared.

The potential mentioned above is defined as the potential of zero charge (pzc)(58). In practice, there are several objections against using the pzc as the potential for the comparison of electrocatalysts. First, the experimental values of E_{pzc} are not well established for a majority of metals.

Furthermore, even for the few metals for which the E_{pzc} values are reasonably well-established (as listed in Table 2-9), this potential is nevertheless unsuitable for comparison of the oxygen electrocatalysts. As can be seen, the potential values are well below the E_{rev}(=1.23 V). Therefore, there will be no oxygen reaction at the potential of E_{pze}.

TABLE 2-9
POTENTIAL OF ZERO CHARGE ON SOME METALS(58)

METALS	E_{pzc} (V *vs.SHE*)	METALS	E_{pzc} (V *vs.SHE*)
Hg	-0.19 ± 0.01	Cr	-0.45 ± 0.05
Cu	-0.16 ± 0.05	Au	+0.15 ± 0.05
Fe	-0.37 ± 0.03	Pb	-0.60 ± 0.05
Pt	+0.56 ± 0.03	Ag	-0.44 ± 0.02
Zn	-0.63 ± 0.05	Ni	-0.28 ± 0.03

Another potential at which the rate of a given reaction on various electrocatalysts can be compared is the equilibrium potential (E_{rev}). At E_{rev}, the reaction rate is the exchange current density (i_{ex}), which has been discussed before.

2.5.4.5 Parameter dependence

For comparison of different catalytic materials, the different parameters (i, i_{ex}, η, b and a) might give a varied activity order. Some electrodes may be poor electrocatalysts in terms of exchange current density but good electrocatalysts in terms of the Tafel slope. Figure 2-12 gives an illustration of the case. In the figure, it can be seen that electrode 1 is a better catalyst in terms of i_{ex}, but electrode 2 will be a better one by comparing values of b.

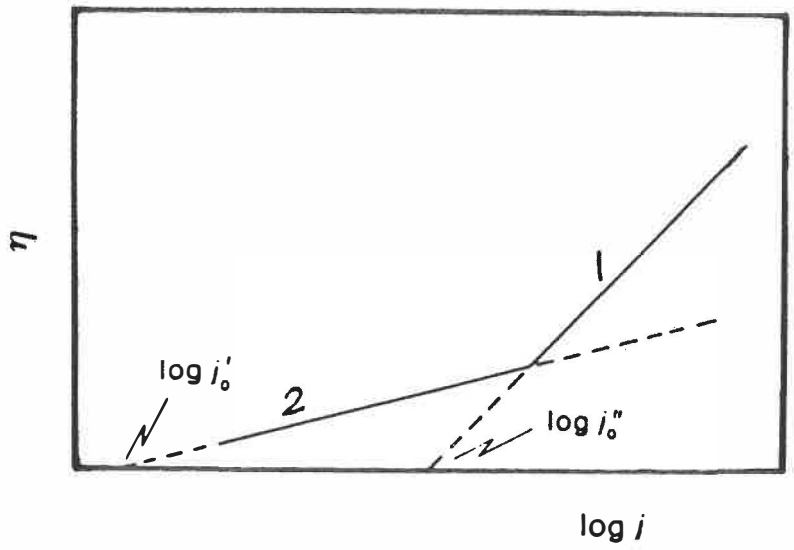

Fig.2-12 The dependence of the electrode catalytic activity on kinetic parameters used for evaluating the electrode performance.

2.5.5 Summary and comments

The electrode performance can be evaluated by comparing several kinetic parameters, such as i, η, i_{ex}, b and α, and other factors such as the real surface area, the surface structure or surface morphology, etc. The corrosion stability of the electrode is also an important property. Complications in the evaluation of electrode performance by reaction selectivity, kinetic conditions, potential and parameter dependence are the major problem in the research and development of electrocatalysts. Simpler, faster and more practical concepts must be developed for a better evaluation of the electrode performance. This type of study is not reported in the literature. Electrode activity can be increased either by creating catalytically active centers on

the surface or by increasing electrode real surface areas. Both methods are effective, and they may even be combined to achieve maximal improvement. However, the effects of increasing electrode performance by these two concepts should be distinguished. In characterizing the electrode with a rough and porous surface, the BET result is useful for indicating the surface area on an electrode, but it offers no information about the effective surface area on the electrode available to electrochemical reaction. We still need an *in situ* and quantitative method to evaluate the effective surface area on the electrode with a very rough surface.

CHAPTER 3

EXPERIMENTAL

3.1 SELECTION OF TECHNIQUES

The techniques for improving the electrocatalytical activity of the OER electrode are based on two concepts: creating electrocatalytically active centres on the electrode and/or increasing the electrode's real surface area. The first method often requires catalytically active materials such as ruthenium, iridium and platinum, while the second method depends on the effectiveness of the technique for achieving a very rough or porous surface on the electrode. Both methods have been proved very successful in practice. They have been adopted in this study to improve the electrocatalytical performance of Ni-based electrodes for the OER.

It has long been known(17,26-30,66) that the Ni electrode has a low oxygen overpotential, and that Ni is quite stable in alkaline media. Ni electrodes can be prepared conveniently by electro-deposition. Ni can be deposited with a wide variety of micrographic structures and physico-mechanical properties. Many types of deposition baths and a wide range of conditions can be selected for the electrolysis(94). The choice of the bath type and the composition for deposition is primarily based on the properties desired in the deposit.

Electrodeposition of Ni from electrolytes of various anionic compositions was, therefore, investigated first in this study. Deposition bath type and conditions for deposition were evaluated, with a special emphasis on the electrocatalytical activity for the OER.

Although Ni is a well-known material for the OER in alkaline solution(17,26-30,66), its electrocatalytical activity is not as good as transition metal oxides such as RuO_2 and IrO_2 (29). Ni suffers from an unstable potential with increasing service time(14,29). However, the catalytic activity of Ni electrodes has been improved by alloying with Li(14), Fe(38,39), Cr(41), Ti, Ir, Ru and W(29), etc.

RuO_2 and IrO_2 are very good electrocatalysts for the OER, both in acid and in alkaline solutions(37,70,95). The Ni-Ir (25-75wt%), Ni-Ru(25-75wt%) and Ni-W(25-50wt%) alloys were studied as electrocatalysts for the OER in alkaline solution (29). The O_2 overpotential decrease, about 40 and 30 mV at the apparent current density of 20 mA/cm^2, was observed on the alloys of 50Ni-50Ir and 75Ni-25Ru, respectively. It was found that the surface oxide layer played a dominate role in electrode performance. Lu and Srinivasan(29) stated that after prolonged anodization the electrode surface was predominantly composed of Ni oxides, which consequently determined the kinetic parameters of the OER. Even alloys containing over

25wt% of the expensive transition elements can not control the surface oxide catalytic property. It is better and more economical to use a low content of the expensive metals to improve the performance of the Ni electrode for industrial applications. In this study, the oxide electrocatalysts based on Ni and transition metals such as Ru and Ir were prepared by electro-codeposition. The precious transition elements in Ni alloys are limited to below 10 wt%. These alloys and pure Ni were anodically oxidized to obtain the mixed oxide surfaces, and these mixed oxide surfaces were then used to study the OER in a KOH solution. By comparing the performance of the different electrodes and analyzing their electrochemical behaviours, the respective beneficial effect of Ru and Ir elements were evaluated.

Several studies were carried out on Ni-based alloy and amorphous alloy electrodes for alkaline water electrolysis (43,44,96,97). These catalytically active electrodes are prepared either by thermal decomposition or by electro-deposition. One of the limitations of these electrodes is the low real surface area. It is very difficult to obtain an electrode with a highly rough or porous surface, which can significantly amplify the electrode's catalytic activity(44). In searching for new techniques and applications of a suitable technology for producing catalytically active coatings and for fabricating the electrode, we found that composite-deposition

or dispersion-deposition was a promising way of preparing high performance electrodes. Brossard and co-workers(98) studied the Ni-Raney composite-coated electrode for the alkaline water electrolysis. Kunugi and co-workers(99) found that a hydrophobic Ni/PTFE (polytetrafluoro-ethylene) composite-plated Ni electrode had a lower oxygen and hydrogen overpotential over a wide range of current density than an unplated one. Other techniques were also reported, such as plasma-spraying carbonyl-Ni and Raney alloy powder mixtures, sintering catalyst powders in a hydrogen atmosphere(100), or melting Ni-Co powders in a flame arc under an argon atmosphere, to fabricate electrodes for the OER(43). However, all of those processes were very complicated and costly in production. Simple and effective techniques for preparing electrodes with a high performance for the OER are still demanded by industry.

In this study, a new approach, composite-deposition, (also referred to as dispersion-deposition or composite-plating) was investigated for preparing the Ni, Co and Fe composite-coatings. The electrode with the composite-coating was oxidized in alkaline solution by electrochemical oxidation, and then used as the electrode for the OER and the HER. The electrochemical characterizations were performed in 5M KOH solution.

3.2 ELECTRODE PREPARATION

The techniques of preparing electrodes for the OER are established to achieve the following goals:

(1) A highly conductive, corrosion-resistant and low cost material as the electrode support;

(2) A thin coating of an electrocatalytically active material, or dispersion of active materials, to keep cost of the electrode to a minimum and to achieve maximal activity;

(3) A surface structure with high roughness and porosity, which provides a large real surface area effectively available to a gas evolution reaction;

(4) A rapid and easy way of fabricating the electrode.

Techniques used in this study to prepare electrodes include: electrodeposition, composite-deposition and thermal decomposition. The oxidation processes, such as *in situ* anodic polarization, potential cycling and thermal oxidation, were adopted to achieve the maximal electrocatalytical activity on the electrode.

3.2.1 Electrodeposition

Ni electrodes were prepared by electrodeposition from electrolytes of various anionic compositions. The deposition bath types and operating conditions were evaluated in this study, with a special emphasis on the electrocatalytical properties for the OER in KOH solution. The deposition substrate, a stainless steel screen (1.0 cm x 1.0 cm, 48 mesh, ~0.3mm sieve opening, supplied by Firth Brown Inox Ltd.), was electroplated with a 0.03 mm thick Ni layer in a Watts bath under a current density of 50 mA/cm^2 at 50°C. It was then used as the cathode for Ni deposition in baths with different anionic compositions. A current density of 100 mA/cm^2 was employed in Ni deposition from electrolytes of various anionic compositions. Deposition current densities from 35 to 350 mA/cm^2 were investigated in the chloride bath to find the optimum range of the deposition current density. Other deposition conditions are listed in Table 3-1. The Watts and six other deposition baths containing various anionic compositions were prepared with the compositions listed in Table 3-2. All chemicals used were of analytical grade, and electrolytes were prepared using doubly distilled water. The Ni^{+2} ion concentration was 85 g/l in the Watts bath and 60 g/l in all other baths. All baths contained 30 g/l of H_3BO_3, which served as a weak buffer for controlling pH in the bath; 0.3 g/l of dodecylsulfate worked as a wetting agent. The pH value of the bath varied between 0.9 and 5.6 depending on the bath

composition, and it was not adjusted during deposition. Figure 3-1 shows a schematic illustration of the deposition bath and current supply unit for the deposition.

TABLE 3-1
CONDITIONS OF ELECTRODEPOSITION OF NICKEL

ANODE:	2 pieces of pure Ni plate (3 cm x 5 cm).
CATHODE:	Stainless steel screen (48mesh), 1 cm x 1 cm.
CURRENT DENSITY:	35 ~ 350 mA/cm^2 (based on geometric area).
TEMPERATURE:	50 ~ 75°C
TIME:	15 ~ 60 minutes.
AGITATION:	Magnetic agitation, 150-200 RPM.

TABLE 3-2
DEPOSITION BATH COMPOSITION

TYPE	COMPOSITION	CONCENTRATION(g/l)	pH
Watts	$NiCl_2$ $6H_2O$	45	0.9
	$NiSO_4$ $6H_2O$	330	
	HCl (37%)	10ml/l	
Chloride	$NiCl_2$ $6H_2O$	243	4.0
Sulfate	$NiSO_4$ $6H_2O$	269	5.2
Mixture	$NiCl_2$ $6H_2O$	122	4.5
	$NiSO_4$ $6H_2O$	135	
Acetate	$Ni(C_2H_3O_2)_2$ $4H_2O$	254	5.6
Sulfamate	$Ni(H_2NSO_3)_2$ $4H_2O$	330	3.3
Nitrite	$Ni(NO_3)_2$ $6H_2O$	297	1.2

All baths contain H_3BO_3 30 g/l and Dodecylsulfate 0.3 g/l.

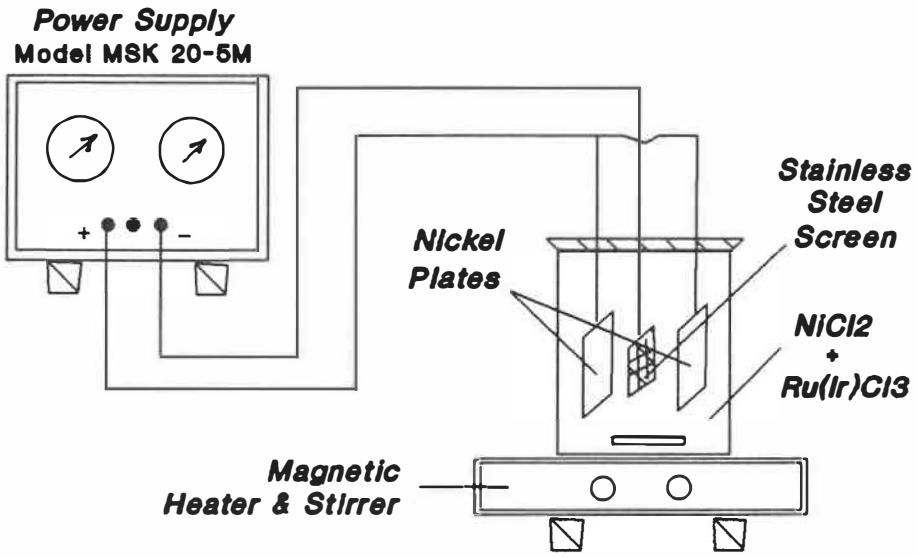

Figure 3-1 A schematic illustration of the electrodeposition bath and control unit.

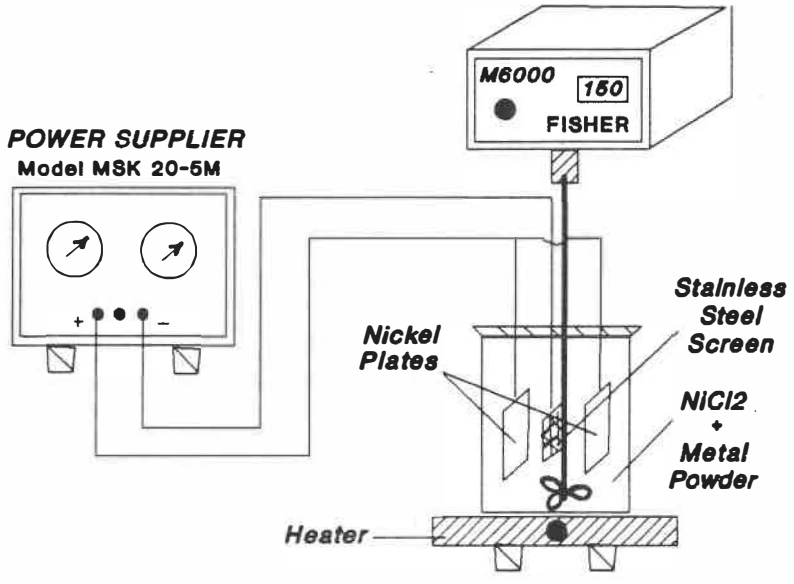

Figure 3-2 A schematic illustration of the composite-deposition bath and control unit.

3.2.2 Codeposition

Ni-Ru and Ni-Ir mixed oxide electrodes were prepared by codeposition of Ni and Ru or Ni and Ir. The quantity of the precious transition elements in Ni deposit was limited to below 10 wt%. Conditions for electro-codeposition were very similar to those for the Ni deposition. The same substrate, a piece of 316 stainless steel gauze, was used. Electrolysis was conducted in a bath of $NiCl_2*6H_2O$ (240 g/l, reagent grade) with the addition of $RuCl_3/IrCl_3$ (0.2-2 g/l, reagent grade) at 55-75°C. The apparent geometric surface area of the cathode was 1.0 cm x 1.0 cm. The electro-codeposition current density was 200 mA/cm^2 (based on geometric area). The deposition amount was about 0.1 g/cm^2 (geometric area).

According to Moffatt(101), the Ni-Ir alloy forms continuous solid solutions in the full range of composition. For Ni-Ru alloys, Manders(102) reported that the solid solution existed at up to about 20 wt% of Ru. However, others (103,104) examined the Ni-Ru alloy by microscope and X-ray diffraction, and their results showed that solubility of Ru in Ni was about 5 wt%. In our case, the electrode with up to 8 wt% of Ru was investigated, but only the Ni-Ru electrode with less than 2.3 wt% was tested extensively. We assumed that the Ni-Ru(2.2wt%) electrode was a solid solution alloy.

The Ni-Ru, Ni-Ir alloys and pure Ni electrodes were

anodically oxidized to obtain the mixed oxide surfaces, and the mixed oxide surfaces were then used as the OER electrode in a 5M KOH solution. By comparing the performance of the different electrodes, respective beneficial effects of Ru and Ir elements were evaluated.

3.2.3 Composite-deposition

The Ni, Co and Fe composite-coating electrodes were prepared by the composite-deposition, followed by an oxidation process in 5M KOH solution to achieve maximal catalytic activity and stability. The substrate for the composite-deposition was the 316 stainless steel gauze, which was initially electroplated with a ~0.25 mm thickness of pure Ni. Electrolysis was carried out in a bath containing $NiCl_2*6H_2O$ (240 g/l, reagent grade) with the addition of either nickel, cobalt or iron powders (total powder: 2 g/l; particle size: -100 mesh; from Aldrich Chemical Co. Inc.), at 50°C for 15 to 40 minutes. Metal powders were suspended in the electrolysis bath by a mechanical agitator. To ensure complete suspension, the mechanical agitator was set at a constant speed of 150 to 250 rpm. Two nickel plates (Ni 99%) were used as anodes in the bath. The composite-deposition bath and its set-up are showed in Fig.3-2. The deposition current density was 100 mA/cm^2 (based on geometric area). The amount of metal deposited was ~100 mg/cm^2 (geometric area). The electrodes thus prepared are referred to as composite-coating electrodes.

3.2.4 Thermal decomposition

RuO_2 and IrO_2 oxide electrodes were prepared by thermal decomposition. Ni and Ti plates (0.8 mm thick with geometric surface area 1.0 cm x 1.0 cm) served as electrode supports. The Ti and Ni plates were polished with water-cooled silicon carbide papers (grit size up to 600) and degreased by acetone, followed by etching either in 20% HCl for 10 minutes or in 48% HF for 5 minutes. They were then washed with double distilled water. The preparation procedure for RuO_2 and IrO_2 oxide coating was similar to that for preparing the DSA^R electrode (105). The dipping procedure was adopted in the coating application. The substrate was dipped into coating solutions and taken out, dried in the dryer at 70-100°C for 10 minutes, then put into an electric furnace at 400°C for 1 hour of firing. The above procedures were repeated 4-6 times for each electrode to achieve the appropriate amount of coating loading. The oxide coating loading was about 12 mg/cm^2. Finally, the electrodes were put into the electric furnace for 4 hours at 400±20°C to achieve complete oxidation.

3.2.5 Oxidation processes

Before electrochemical measurements were made, the activation of the electrodes was performed *in situ* by anodic polarizations at 100 mA/cm^2 for over 30 minutes in 5M KOH solution at room temperature, which produced an oxide layer on the electrode surface. The stable oxidized surface obtained

was verified by the reproducible polarization curves under the same conditions. A thermal oxidation process was adopted for oxidizing the pure RuO_2 and IrO_2 electrode surfaces. The process consisted of placing the electrodes in an electric furnace at 400°C for over 4 hours.

3.3 SURFACE CHARACTERIZATION AND CHEMICAL ANALYSIS

3.3.1 Surface characterization

Morphological analyses of the electrode surfaces were conducted using the scanning electron microscope (SEM) (Model JEOL JSM-840). The Ni electrodes prepared as mentioned above were placed in an air-sealed container, then transferred into the chamber of SEM for the morphological examinations. SEM micrographs were taken with 200x or 1000x magnification.

3.3.2 Chemical composition analysis

Chemical analyses of the electrode surface were conducted by the energy dispersive spectrometer (EDS) which is connected to SEM. The electrode chemical compositions were given by weight per cent. It should be mentioned that compositions given by EDS analysis are semi-quantitative. Chemical composition can be determined more accurately by atomic adsorption or chemical analyses. However, EDS analysis is non-destructive and can be made conveniently with SEM examinations.

3.4 ELECTROCHEMICAL MEASUREMENTS

3.4.1 Electrochemical cell

Characterizations of electrodes were carried out in an electrochemical cell containing 5M KOH solution. N_2 gas was introduced into the electrochemical cell for 15 minutes before each test and was kept constant flowing (~60 bubbles/minute) during measurement. A saturated calomel electrode (*SCE*), as the reference electrode, was inserted into the Luggin capillary, and mounted very close to the anode (<2 mm). The pH value of the 5M KOH solution and the oxygen reversible potential (E_{rev}) at 25°C were calculated using the activity coefficient from Dobos(106). E_{rev} is equal to 0.106 V *vs SCE*. All potentials in this study are referred to *SCE* unless otherwise stated. The system for the electrochemical measurements was shown in Fig.3-3.

3.4.2 Polarization measurements

Polarization curves were measured using the Corrosion Measurement Software (Model 342) with a PAR Model 273 Potentiostat. Potential scanning went from a less noble to a more noble potential direction, with a scan rate of 1 mV/s. The applied potential range was usually within 500 mV. The electrodes were immersed in the electrolyte (5M KOH) for achieving potential stability until three repeatable polarization curves were obtained on the same electrode, and

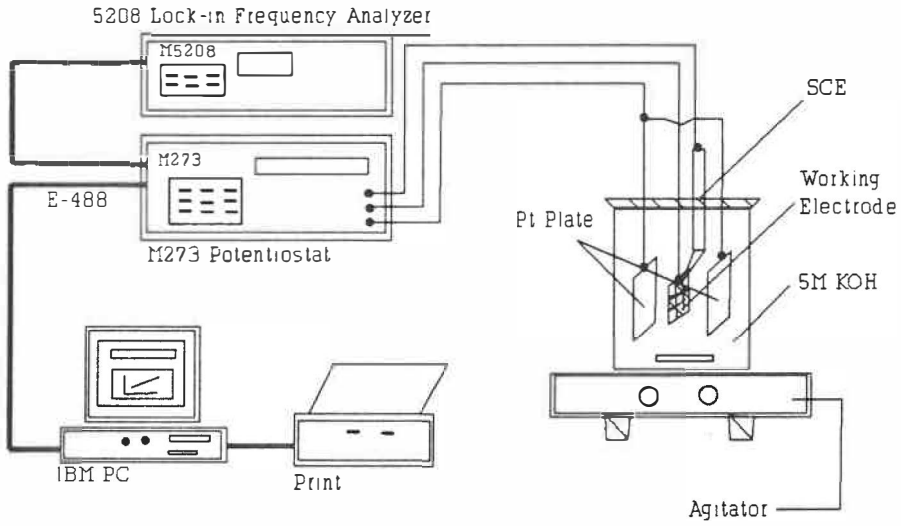

Figure 3-3 A schematic illustration of the system for electrochemical measurements.

then polarization measurements were terminated. The current interruption technique available on the Potentiostat (Model 273) was used to minimize the IR drop in the potential sweep polarization measurements. For constant charging measurements, an oscilloscope was connected to the system to measure the IR drop at 100 ma/cm^2. An evaluation of the IR drop in the electrochemical cell at 100 mA/cm^2 is included in Appendix II. Tafel slopes and exchange current densities were determined by the method discussed in Section 2.5 (see Fig.2-9). The experimental data reported in Chapter 4 are average values for three electrodes. The error range for the kinetic parameters listed in chapter of results was evaluated from the values for these electrodes.

3.4.3 Cyclic voltammetric measurements

Cyclic voltammograms were measured by potentiostat and an IBM microcomputer. The potential scanning proceeded from less noble to more noble potentials, as shown in the figure. The scan rate for the potential was 20 mV/s. The potential pre-cycling was taken more than 10 times. Cyclic voltammograms were recorded until a reproducible cyclic voltammogram was observed. The peak potentials were recorded and compared to the thermodynamically calculated values.

3.4.4 Impedance spectroscopy

The experimental impedance spectra were measured with the

Electrochemical Impedance Software (Model 378) and a PAR Model 273 Potentiostat connected to a PAR Model 5208 lock-in amplifier. A 10 mV peak-to-peak ac potential was superimposed on an applied *dc* potential in the range of the Tafel region. Moreover, magnetic agitation (150 rpm) was adopted to avoid a diffusion impedance element in the spectra. Solution resistance (R_s) was subtracted from the impedance experimental data before the curve fitting was made. The Electrochemical Impedance Software controls the combination of the Lock-in amplifier (5 to 10 kHz) and Fast Fourier Transform (0.001 to 5 Hz) techniques to perform tests. The results were presented in the form of impedance complex-plane plots (-Z" imaginary impedance against Z' real impedance), Bode amplitude plots (log(Z) vs frequency log(f)), and/or Bode phase plots (impedance phase angle (θ) vs frequency log(f)). The points in the plot were experimental data, the continuous lines were fitting generated from the Complex Nonlinear Least Squares Immittance Fitting Program (CNLS), provided by Macdonald (107), with an equivalent circuit of the constant phase element (CPE) and the charge transfer resistance (R_{ct}).

CHAPTER 4

RESULTS

4.1 INTRODUCTION

The experimental results in this section are organized into four groups: 1) Electrodeposition of nickel in electrolytes of various anionic compositions; 2) Ni-transition mixed oxide electrode for the OER; 3) Composite-coating electrodes for the OER; and 4) Composite-coating electrodes for the HER. These results and the contents of discussions in Chapter 5 were adapted from four publications resulted from this study. However, a general discussion on the different types of electrodes is added in Chapter 5. The titles of our papers are: "Electrodeposition of Catalytically Active Nickel for the OER-Effect of Anionic Composition" (published in "the Canadian Journal of Chemical Engineering", Vol.71, 1993); "Electrodeposition of Ni-Transition Alloys for the OER" ("Journal of Applied Electrochemistry", 21, (1991) 55-59); "Composite-Coating Electrodes for the HER", (the Journal of International Society of Electrochemistry, "Electrochimica Acta", 38, (1993) 1079-1085) and "Electrochemical Characteristics of Composite-Coating Electrodes for the OER in Alkaline Solution", (submitted to "Electrochimica Acta").

4.2 EFFECTS OF DEPOSITION CONDITIONS

4.2.1 Deposition bath

4.2.1.1 Surface morphology examination

Figure 4-1 shows the SEM micrographs of Ni deposited from (a) Watts; (b) chloride; (c) sulfate; (d) chloride-sulfate mixture; (e) sulfamate; and (f) acetate baths. The surface of the Ni deposited from bath (a) appears to be relatively homogeneous, with fine-grain structures and no cracks. This surface offered a relatively uniform substrate for Ni deposition in electrolytes with various anionic compositions. Due to a high deposition current density (100 mA/cm^2), a surface with coarse structures was obtained on Ni deposited from electrolytes of various anionic compositions as a common morphological feature. Some nodular clusters were found on Ni deposited from the chloride, the sulfate, the chloride-sulfate, and the sulfamate baths. Microcracks around grain-like particles were found on all surfaces of the Ni deposited from the chloride baths. Some sporadic microcracks were observed on the coating surfaces deposited from the sulfate, chloride-sulfate mixture and acetate baths, but visible cracks on the surface were much less than those on the Ni from the chloride bath. Ni deposited from the nitrate bath was so cracked and coarse that it peeled off from the substrate after deposition. This surface could not be used as an electrode; it was, therefore, not tested electrochemically.

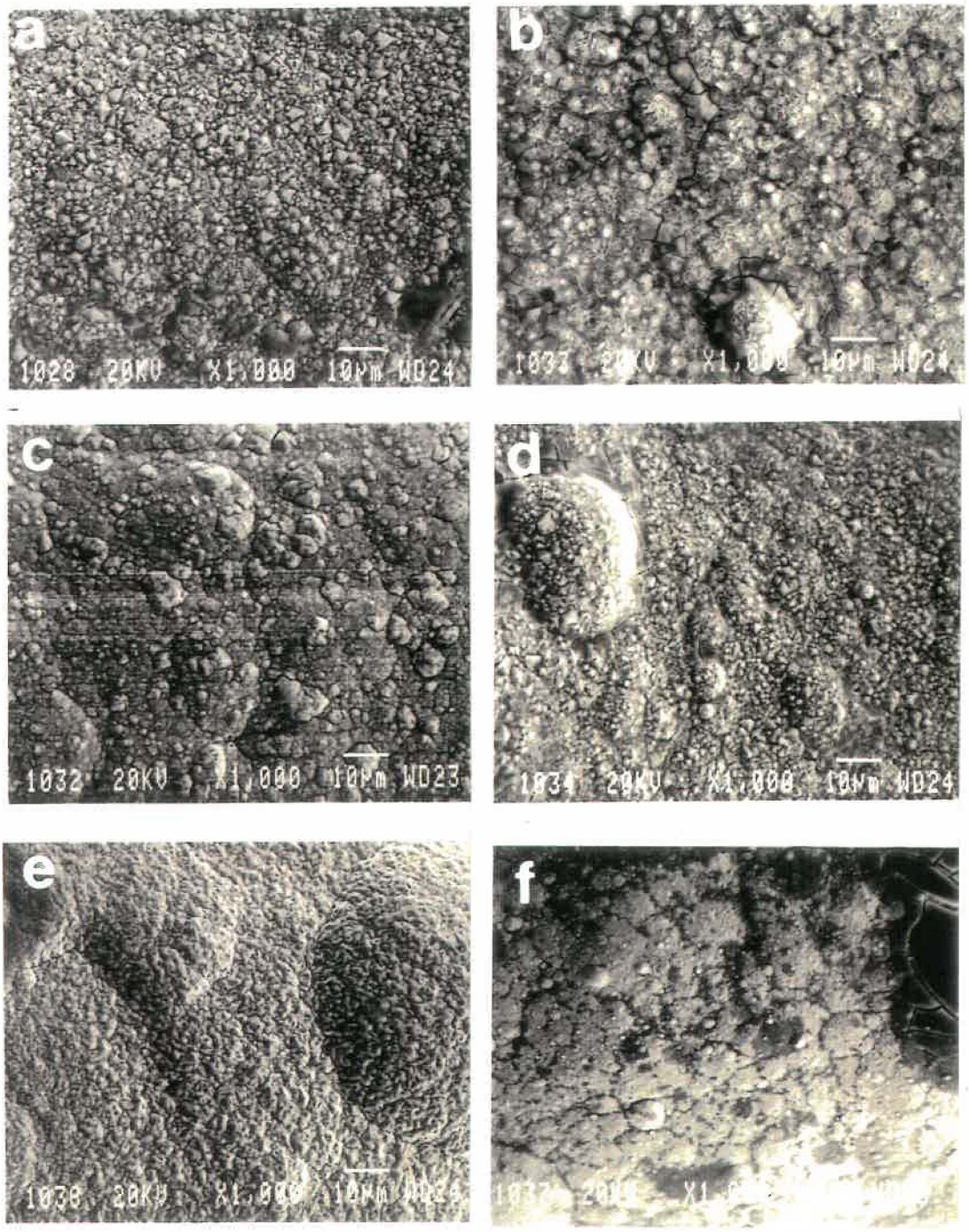

Figure 4-1 SEM micrographs of the Ni deposited from: (a)Watts; (b)chloride; (c)sulfate; (d)chloride-sulfate mixture; (e) sulfamate; and (f) acetate bath. Magnification: 1000x.

4.2.1.2 Polarization measurements

Figure 4-2 shows anodic polarization curves of the Ni electrodes prepared from electrolytes of various anionic compositions. All curves showed a similar polarization behaviour. The electrode surface was oxidized first, followed by the electrochemical reaction (OER) as a principal process on the electrode. At high current densities (> 50 mA/cm^2), the slope is increased significantly due to the interference of reactant diffusions and the oxygen bubbling effect on the electrode, which was observed during the experiment. This type of polarization behaviour was well documented by Hoare(17). Two Tafel slopes (b) (low & high i) and exchange current densities (i_{ex}) were determined from polarization curves. Values are presented in Table 4-1. The lowest b_l (at low i), 50 mV/dec, was found on the Ni deposited from the chloride bath, while the highest b_l, 83 mV/dec, was obtained on Ni deposited from the sulfate and the sulfamate baths. Ni deposited from the bath of the chloride-sulfate salt mixture (50:50 wt%) shows a value of 66 mV/dec, which was near the median between 50 and 83. At high current densities, the Tafel slope b_h (at high i) tended to increase to more than 200 mV/dec, but the highest, 306 mV/dec, was displayed on the Ni electrode deposited from the sulfamate bath. The Tafel slope indicates the rate of increase in overpotential as the current density increases ($b = d\eta/d\log i$). An electrode with a low Tafel slope implies that with increasing current density, the

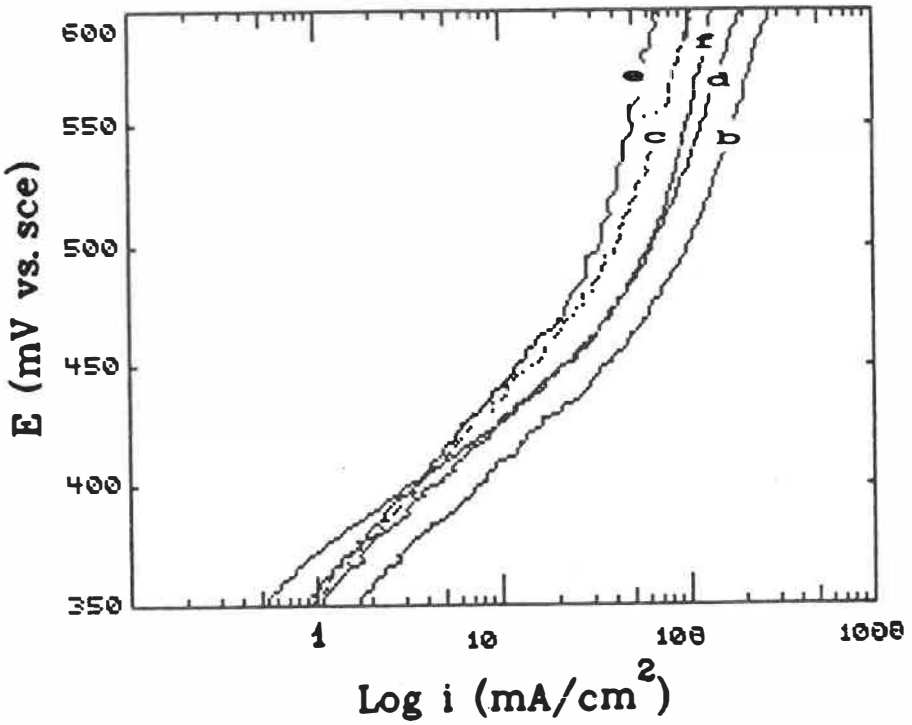

Figure 4-2 Anodic polarization curves for the OER on Ni electrodes prepared from: (b)chloride; (c) sulfate; (d) chloride-sulfate mixture; (e) sulfamate; and (f) acetate bath.

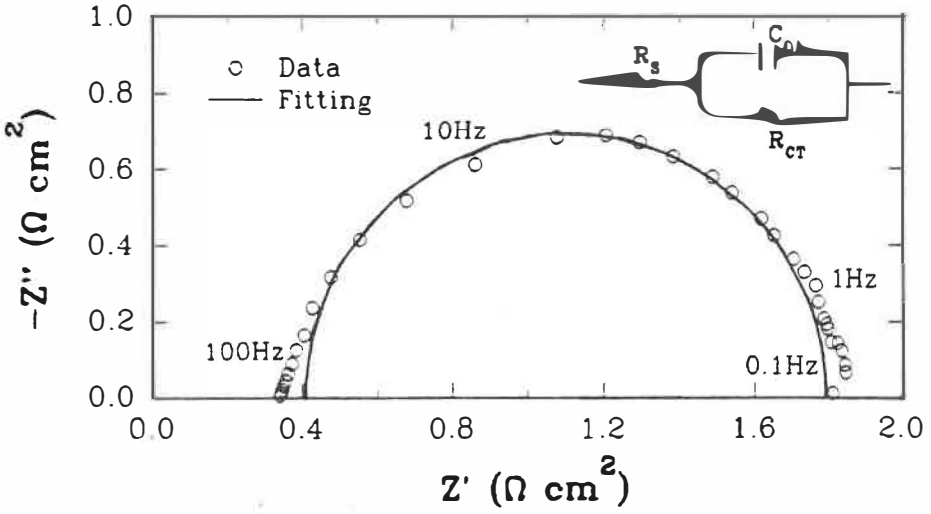

Figure 4-3 The typical impedance complex-plane plot of Ni electrode prepared from the chloride bath.

increase in the overpotential will be lower, which is important for a high performance electrode. The i_{ex} ranged from $1.0x10^{-5}$ to $1.0x10^{-3}$ mA/cm^2, depending on Ni deposited from the different baths.

Electrode activity should be evaluated, as in industry, by comparing overpotential at the same current density. The OER overpotentials (η_{100}) at 100 mA/cm^2 on Ni electrodes were then derived from polarization curves and listed in Table 4-1. Evidently Ni deposited from the chloride bath had the lowest overpotential, 396 mV. The η_{100} on Ni electrodes deposited from various baths increased in the following order:
Chloride < Chloride-sulfate < Acetate < Sulfate < Sulfamate

TABLE 4-1
KINETIC PARAMETERS OF THE OER ON Ni ELECTRODES PREPARED FROM VARIOUS BATHS

Ni FROM BATH	b_L(low i) mV/dec	b_H(high i) mV/dec	iex mA/cm^2	η100 mV
CHLORIDE	50±4	250±10	$1.0x10^{-5}$	396±5
SULFATE	83±5	235±10	$1.0x10^{-3}$	490±5
MIXTURE	66±5	218±5	$6.0x10^{-4}$	430±5
ACETATE	52±2	279±10	$5.0x10^{-5}$	450±5
SULFAMATE	83±5	306±10	$1.0x10^{-3}$	504±5

4.2.1.3 Impedance measurements

The impedance diagrams of Z" (imaginary impedance) vs Z' (real impedance) were established in 5M KOH solution at 25°C with an applied potential of 450 mV vs SCE. A typical complex-plane plot of Ni deposited from the chloride bath is shown in

Fig.4-3. A semi-circular arc, which is the characteristic of simple R-C circuit behaviour(108), was obtained on all electrodes. The depressed angle of the semi-circle remained negligible, and it was not taken into account. The equivalent circuit used to fit experimental data consists of a charge transfer resistance (R_{ct}) in parallel with a double layer capacitance (C_{dl}), connecting with a solution resistance (R_s) in series. The experimental data and the fitting from the equivalent circuit corresponded very well in the frequency range from 1,000 to 0.1 Hz (see Fig.4-3). The R_{ct} was measured directly from the complex-plane plots, and the C_{dl} was calculated by the equation $C_{dl} = 1/(R_{ct}\omega_c)$ (108), where ω_c is the frequency corresponding to the summit of the semi-circular arc. Results are listed in Table 4-2. The lowest R_{ct}, 1.7 $\Omega \cdot cm^2$, and the highest C_{dl}, 29 mF/cm^2, were observed on Ni deposited from the chloride bath. The highest R_{ct}, 7.0 $\Omega \cdot cm^2$, was obtained on Ni deposited from the sulfate bath, and the lowest C_{dl}, 5.4 mF/cm^2, on Ni from the sulfamate bath.

TABLE 4-2
RESULTS OF IMPEDANCE MEASUREMENTS
ON Ni ELECTRODES PREPARED FROM VARIOUS BATHS

Ni FROM BATH	Rct $\Omega \cdot cm^2$	Cdl mF/cm^2
CHLORIDE	1.7	29
SULFATE	7.0	14
MIXTURE	3.4	16
ACETATE	2.5	6.3
SULFAMATE	2.9	5.4

4.2.2 Deposition current density

4.2.2.1 Polarization measurements

Figure 4-4 represents the cathodic polarization curve of Ni deposition in the chloride bath. The open-circuit potential of Ni in 240 g/l $NiCl_2*6H_2O$ at 25°C was -0.45 V *vs SCE*. The standard potential of Ni is -0.25 V *vs SHE* (or -0.49 V *vs SCE*) (109); it is deposited with a 40 mV polarization. The limiting current density (i_L) for Ni deposition in the chloride bath was determined from the polarization curve as 900 mA/cm^2 (see Fig.4-4). The Tafel region for the Ni deposition was observed in the current density range from 5 to 100 mA/cm^2. The current density employed for Ni deposition (i_{dp}) from electrolytes of various anionic compositions, 100 mA/cm^2, was at the high limit of the Tafel region. Under a high i_{dp}(>100 mA/cm^2), gas bubbles were observed on the deposit during deposition. It was evident that a high i_{dp} stimulated the hydrogen evolution reaction, which is the secondary cathodic reaction on the deposit. The hydrogen bubbles thus generated interfere with the normal Ni deposition process. Therefore, the current efficiency for the Ni deposition was decreased. The combination of the release of hydrogen bubbles and Ni deposition made a deposit with a poor bonding to the substrate. To verify this, the i_L for the Ni deposition in the chloride bath was measured at various agitation speeds. It was found that almost the same value of the i_L (900 mA/cm^2) was essentially obtained at various

agitation speeds, suggesting that in the solution near the deposit surface there is strong agitation caused by release of hydrogen bubbles. The impact of the varied agitation speeds provided by the magnetic stirrer in the bath was then relatively ineffective in changing the i_L. A high i_{dp} (more than 350mA/cm^2) is, therefore, not suitable for Ni deposition in the chloride bath.

Ni electrodes deposited in the chloride bath with varied i_{dp} values were characterized for the OER. b and i_{ex} for the OER are presented in Table 4-3. It was noted that those kinetic parameters of the OER on Ni electrode were affected by i_{dp}. The b remained constant at 50 mV/dec within the range of i_{dp}=250 mA/cm^2. A value of 46 mV/dec was obtained at 35 mA/cm^2, but it also had a low i_{ex}. On the other hand, when the i_{dp} passed over 300 mA/cm^2, b values increased 12 mV and reached 62 mV/dec at i_{dp}=350 mA/cm^2. The i_{ex} for the OER increased with increasing i_{dp}.

TABLE 4-3
KINETIC PARAMETERS OF THE OER ON Ni ELECTRODES PREPARED FROM THE CHLORIDE BATH

idp mA/cm^2	b mV/dec	iex mA/cm^2	Cdl mF/cm^2
35	46±5	$1.5\pm1\times10^{-6}$	15±5
70	50±4	$1.0\pm1\times10^{-5}$	31±5
100	50±4	$1.0\pm1\times10^{-5}$	29±5
140	50±4	$3.0\pm2\times10^{-5}$	28±5
200	50±4	$5.0\pm2\times10^{-5}$	85±10
280	54±5	$1.0\pm0.1\times10^{-4}$	90±10
350	62±5	$5.0\pm0.5\times10^{-4}$	200±30

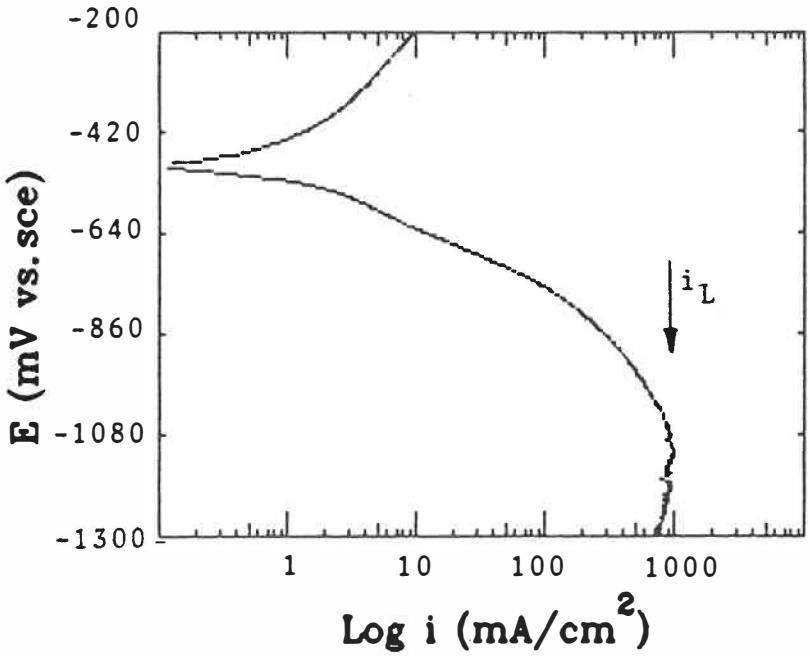

Figure 4-4 The cathodic polarization curve for the Ni deposition in the chloride bath.

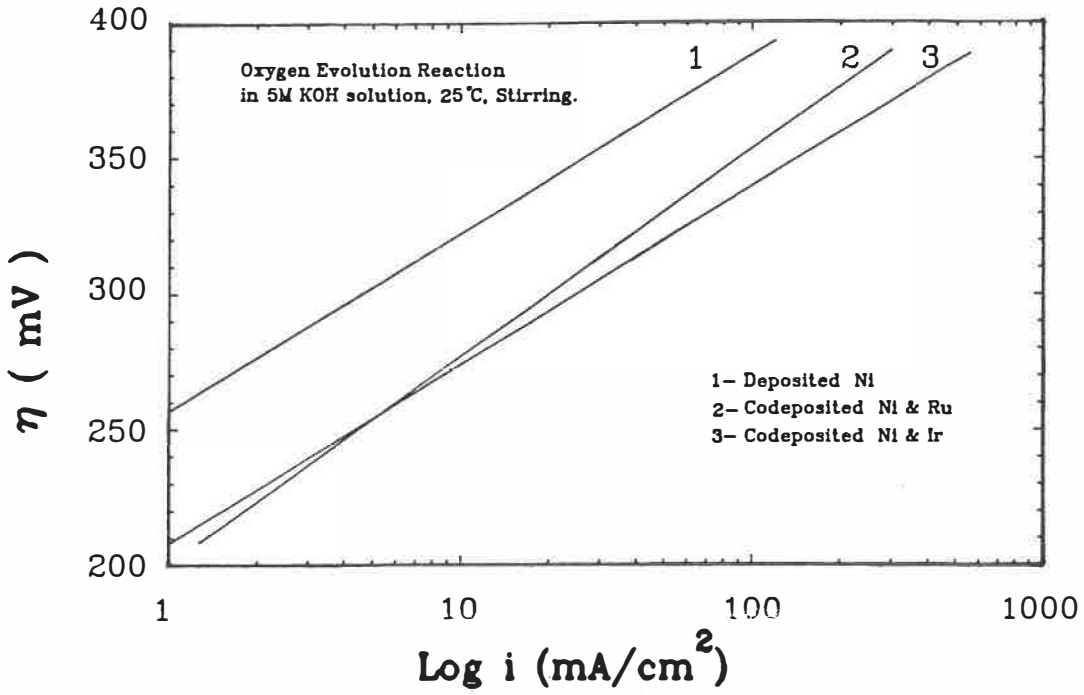

Figure 4-5 Anodic polarization curves of the Ni, Ni-Ru and Ni-Ir electrodes in 5M KOH solution at 25°C.

4.2.2.2 Impedance measurements

The C_{dl} of Ni electrodes, obtained from the complex-plane plots under a potential of 450 mV vs SCE, are included in Table 4-3. Evidently the C_{dl} on Ni electrodes increased with the deposition current density i_{dp}. So, it was found in the test that both i_{ex} and C_{dl} on Ni electrodes increased with increasing i_{dp}.

4.3 Ni-TRANSITION METAL OXIDE ELECTRODES

4.3.1 Polarization measurements

Figure 4-5 are the anodic polarization curves of the Ni, Ni-Ru and Ni-Ir electrodes. The Tafel slopes of the Ni-based electrodes are about 50 mV/dec at current densities between 1 and 100 mA/cm^2. The Tafel slope tends to increase on all electrodes at current densities higher than 100 mA/cm^2. It is understandable that the Ni, Ni-Ru(2.2 wt%) and Ni-Ir(2.3 wt%) alloy electrodes have almost the same Tafel slope, because the predominance of the Ni oxide on electrodes surfaces resulted in the same RDS for the OER mechanism. The exchange current densities (i_{ex}) were determined from the polarization curves, and it ranged from 10^{-4} to 10^{-5} mA/cm^2. The results showed that the Tafel slopes and exchange current densities were not sensitive enough to reveal the difference in electrocatalysis among the Ni-based electrodes in this case.

It has been reported(110) that the electrowinning of Zn from alkaline solution under a high current density resulted in energy-saving and high productivity compared with the classical sulfate electrowinning process. This is also very true for water electrolysis. If the current densities chosen in the range of industrial application were compared under the same η, the difference would have a direct significance for practical applications. Figure 4-6 plots the OER rate (current densities) at an overpotential of 0.4 V as a function of the Ru or Ir content in the Ni alloy electrodes. As can be seen, for both Ni-Ru and Ni-Ir electrodes, the beneficial effects in improving activity for the OER, obtained by the presence of the additional elements, are more significant for the first 1 wt% of the transition elements. With further additions, Ir increased the OER rate to a small extent; in the case of Ru, an adverse effect was observed. Measurement of the current density at a 0.4 V overpotential showed that 6 wt% of Ir increased the OER rate by 6-times, while the best result for the Ni-Ru electrode was obtained at 1 wt% Ru, for an increase of 4-times compared with the value of the OER rate on the Ni electrode.

4.3.2 Cyclic Voltammograms

Cyclic voltammograms for the Ni, Ni-Ru and Ni-Ir electrodes are presented in Fig.4-7. The conditions for measurement were stated in Section 3.4.3. As can be seen in

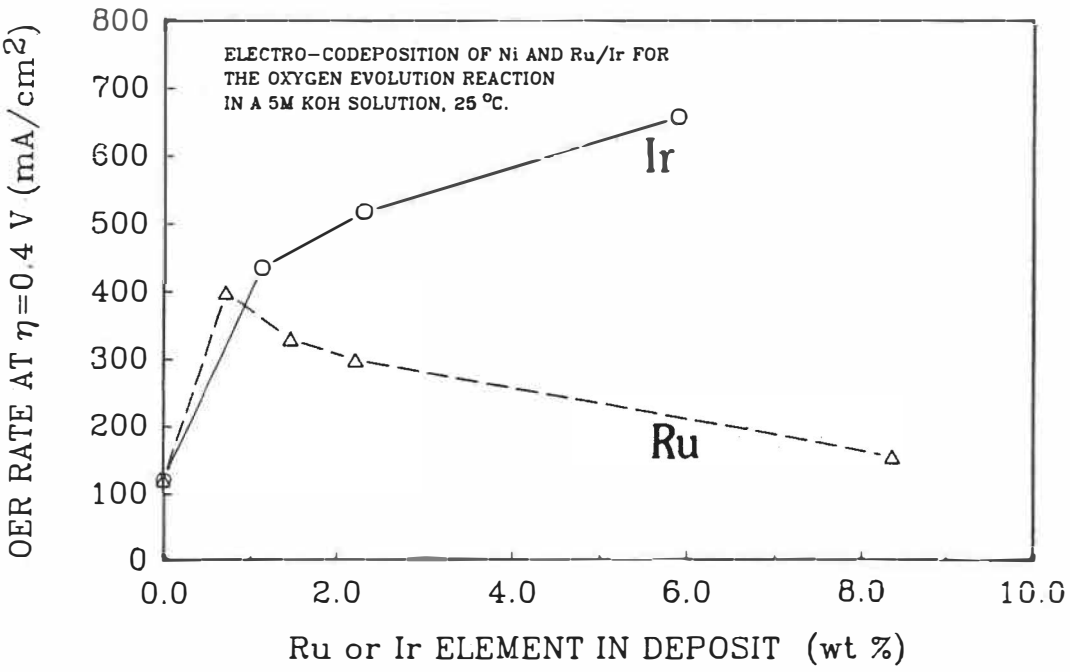

Figure 4-6 The OER current densities (η=0.4 V) as a function of the Ru or Ir content in Ni-based electrodes.

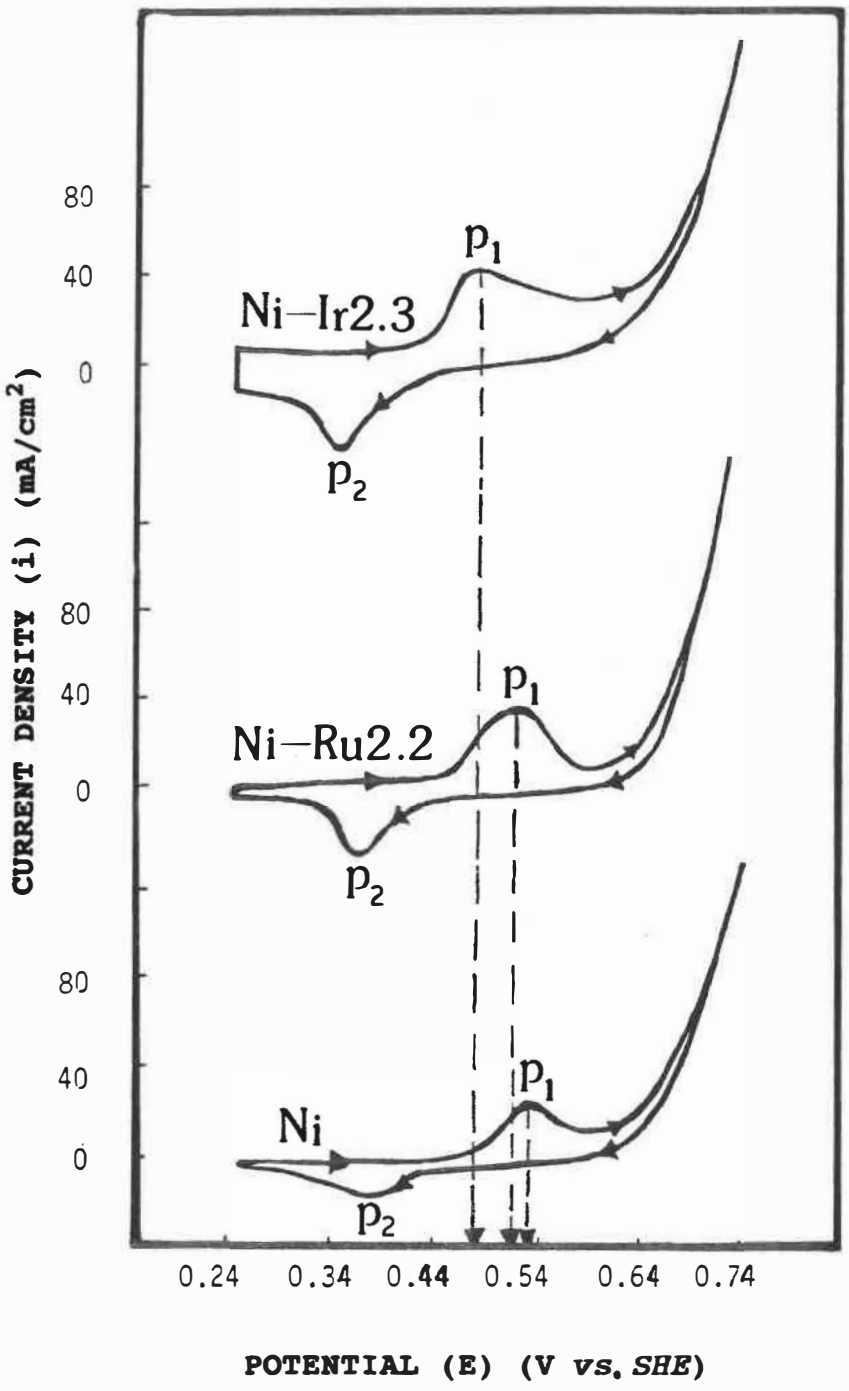

Figure 4-7 Cyclic voltammograms of the Ni, Ni-Ru and Ni-Ir alloy electrodes in 5M KOH solution, 25°C. Potential scanning rate: 20 mV/s.

the figure, all three curves show an oxidation peak (P_1) before the OER on the initial anodic direction. These peak potentials are shifted to less noble values by adding Ru and Ir to the Ni electrodes. The peak potential of the Ni-Ir alloy appears 56 mV before that of Ni, while the difference between peak potentials of Ni and Ni-Ru electrodes is only 10 mV. On the return direction, the observed potential value of peak (P_2) is more active than that of P_1. The P_2 peaks on all three curves have nearly the same values. The overpotentials (η) measured at 20 mA/cm^2 are lowered by 30 and 40 mV, respectively, with the presence of Ru and Ir. Table 4-4 is a summary of the results from the cyclic voltammograms.

TABLE 4-4
SUMMARIZED RESULTS FROM CYCLIC VOLTAMMOGRAMS

DEPOSIT CONTENT(wt%)	E_{P1} V *vs.SHE*	Shift mV	η mV	$\Delta\eta$ mV
Ni99.7	0.534	--	310	--
Ni97.8Ru2.2	0.524	-10	280	-30
Ni96.6Ir2.3	0.478	-56	270	-40

P_1: The oxidation peak potential.
η: Overpotential under 20 mA/cm^2.
$\Delta\eta$: Decrease in overpotential compared with the Ni electrode.

Pure RuO_2 and IrO_2 oxide electrodes were prepared and tested for comparison with the Ni oxide data. Table 4-5 shows the value of the thermodynamically calculated and measured oxidation peak potentials for the Ni oxide, RuO_2 and IrO_2 electrodes in 5M KOH solution at 25°C. The equation for the thermodynamic potentials of oxidation (E_c) for Ni^{3+}/Ni^{4+}, Ru^{4+}/Ru^{8+} and Ir^{4+}/Ir^{6+} were given by Pourbaix(111). The pH

value was 14.93, as calculated using the mean activity coefficients from reference(106). It shows that the maximal difference between these two values is within 15 mV; they correspond very well. The highest measured peak potential (E_{ox}) is 0.534 V on nickel oxide, while ruthenium and iridium oxides show peak potentials of 0.490 V (Ru^{4+}/Ru^{8+}) and 0.300 V (Ir^{4+}/Ir^{6+}), respectively.

TABLE 4-5
OXIDATION POTENTIALS OF Ni, Ru AND Ir OXIDES

ELECTRODE	OXIDES	E_c/V *vs.SHE*	E_{ox}/V *vs.SHE*
Ni oxide	Ni^{3+}/Ni^{4+}	0.538	0.534
Ru oxide	Ru^{4+}/Ru^{8+}	0.505	0.490
Ir oxide	Ir^{4+}/Ir^{6+}	0.290	0.300

E_c=Thermodynamically calculated(111) at pH=14.93 and 25°C.
E_{ox}=Peak potential, measured in a 5M KOH solution, 25°C.

4.3.3 Stability tests

Stability of the mixed oxide electrodes in alkaline solution is of critical importance. It was observed that selective corrosion of the Ru oxide on the electrode caused a loss in electrocatalytical property. As the Ru content increased, an increase in corrosion was observed in our test conditions. The uncoloured solution turned to yellow after a 30-minute polarization of the Ni-Ru electrode at a current density of 100 mA/cm^2. The surface chemical analysis by EDS showed no Ru on the electrode surface after testing (Fig.4-8). After being immersed in the 5M KOH solution for more than 30 minutes, the Ni-Ru oxide containing 2% or more of the Ru

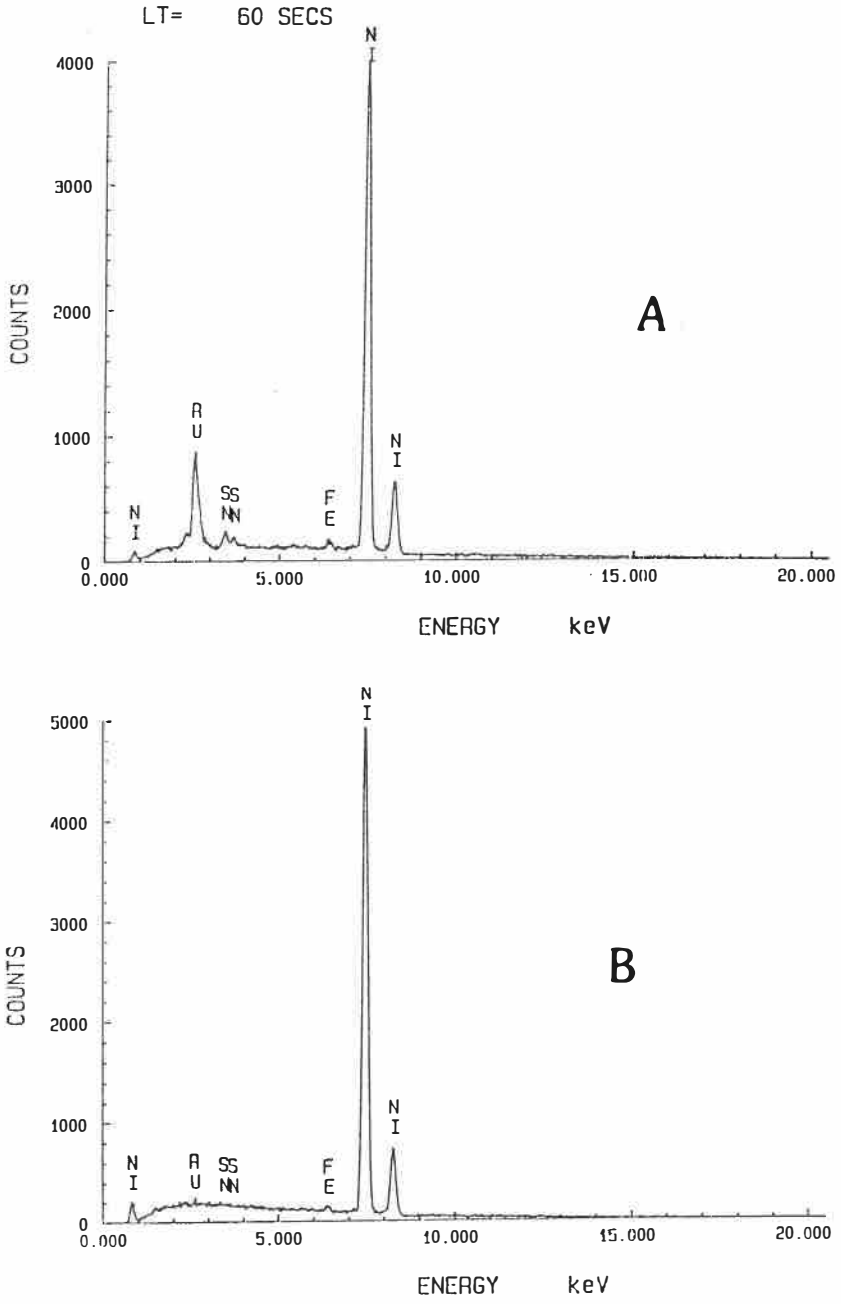

Figure 4-8 EDS spectra for the Ni-Ru electrode surface analysis. (A) before testing; (B) after testing.

showed almost the same current density as the pure Ni oxide. By comparison, the Ni-Ir oxide electrodes showed an increase in electrode activity as Ir content increased from 1 to 6 wt%.

4.4 COMPOSITE-COATING ELECTRODES FOR THE OER

4.4.1 Surface morphology

The electrode surface structures were examined by the SEM; micrographic photos are shown in Fig.4-9. These micrographs provide evidence of the surface inhomogeneity distribution over the electrode surface which could not be obtained by other electrochemical techniques. They were taken after surface oxidation and electrochemical measurements. On the Ni electrode surface (Fig.4-9a), a solid surface with some nodular structures is observed, but no pore structures on the surface can be seen from the photo. The Ni composite-coating (Fig.4-9b) reveals a rough surface with many fine pore structures. When nickel powders were replaced by cobalt or iron powders in the deposition bath, the roughness of composite-coatings increased significantly; the fine structure on the surface became coarser. The dimensions of the surface structure of the Fe composite-coating (Fig.4-9d) appeared much larger than that of the Ni and Co composite-coating electrodes (Fig.4-9b&c). Approximately 20, 50 and 70 μm of the surface structure on the Ni, Co and Fe composite-coating electrodes, respectively, can be evaluated from SEM micrographs.

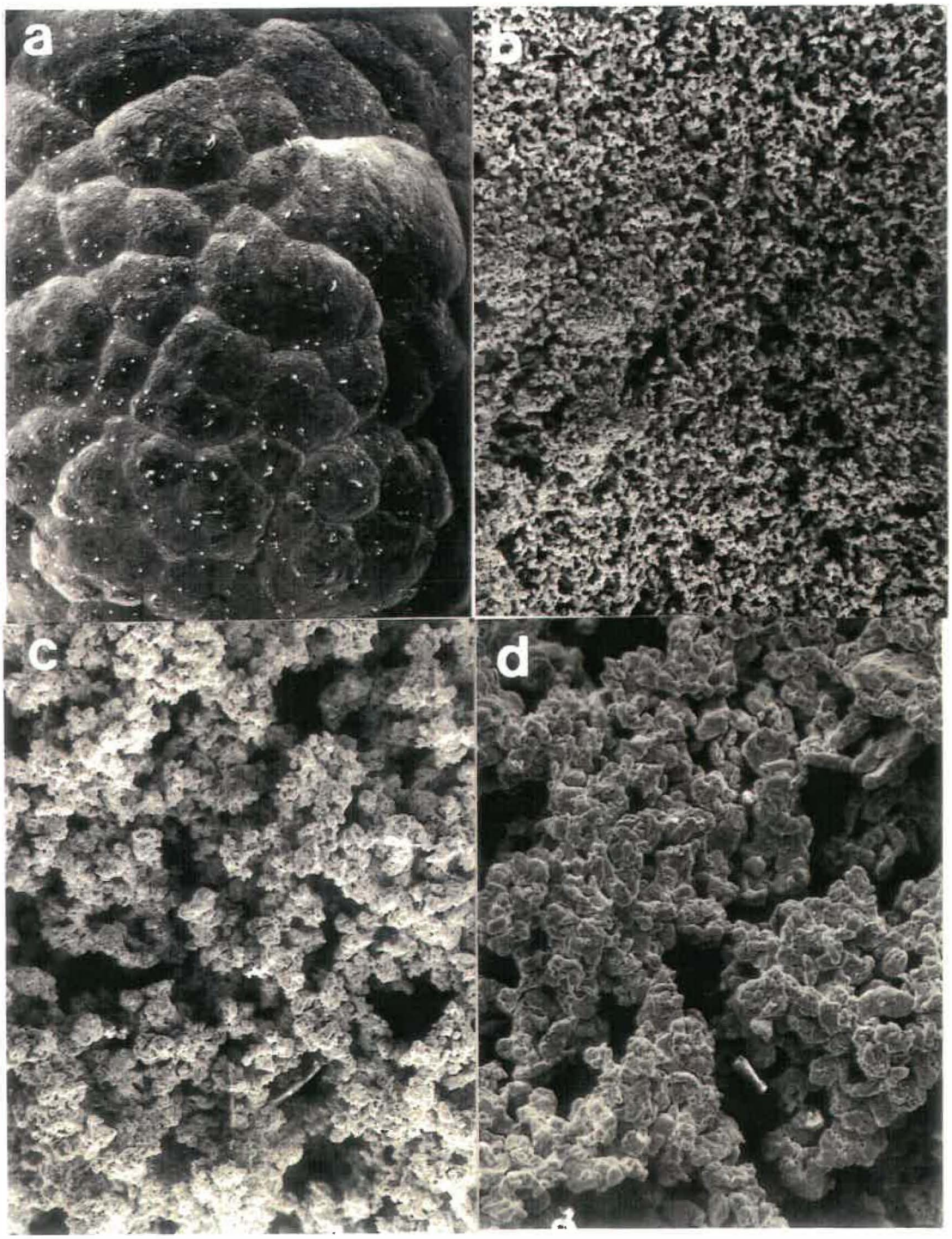

Figure 4-9 SEM micrographs of (a) Ni electrode; (b) Ni composite; (c) Co composite and (d) Fe composite coating electrode. Magnification: 200X.

4.4.2 Chemical composition

Chemical analyses of the composite-coating electrode surfaces were conducted by the energy dispersive spectrometer (EDS), which is combined with the SEM. The electrode chemical compositions are given in Table 4-6 by wt%. As can be seen, Cl (0.5 to 1.5 wt%) was present as an impurity on the surfaces. Co powders were co-deposited with Ni^{+2} with less difficulty than Fe powders; more than 56 wt% of Co was detected on the Co composite-coating electrode.

TABLE 4-6
SURFACE COMPOSITION OF COMPOSITE-COATING ELECTRODES

ELECTRODE	Ni	Co	Fe	Cl(wt%)
Ni Electrode	99.5±5	---	---	0.5±1
Ni Composite	97.5±5	1.0±1	---	1.5±2
Co Composite	42.5±5	56.5±3	---	1.0±1
Fe Composite	75.0±5	---	23.5±5	1.5±2

4.4.3 Polarization measurements

The composite-coatings were oxidized electrochemically in 5M KOH solution before the electrochemical characterizations. Figure 4-10 shows the potentials *vs.* time under a constant current (100 mA/cm^2) charging condition on the electrodes for the first 30 minutes in 5M KOH solution at 25°C. A similar charging behaviour on all the electrodes was observed: an initial potential rise (within 100s), followed by a gradual increase, and finally approaching potential stability (after 600s). The lowest stable potential value under 100 mA/cm^2 current density, 225 mV (IR corrected, same as following), was

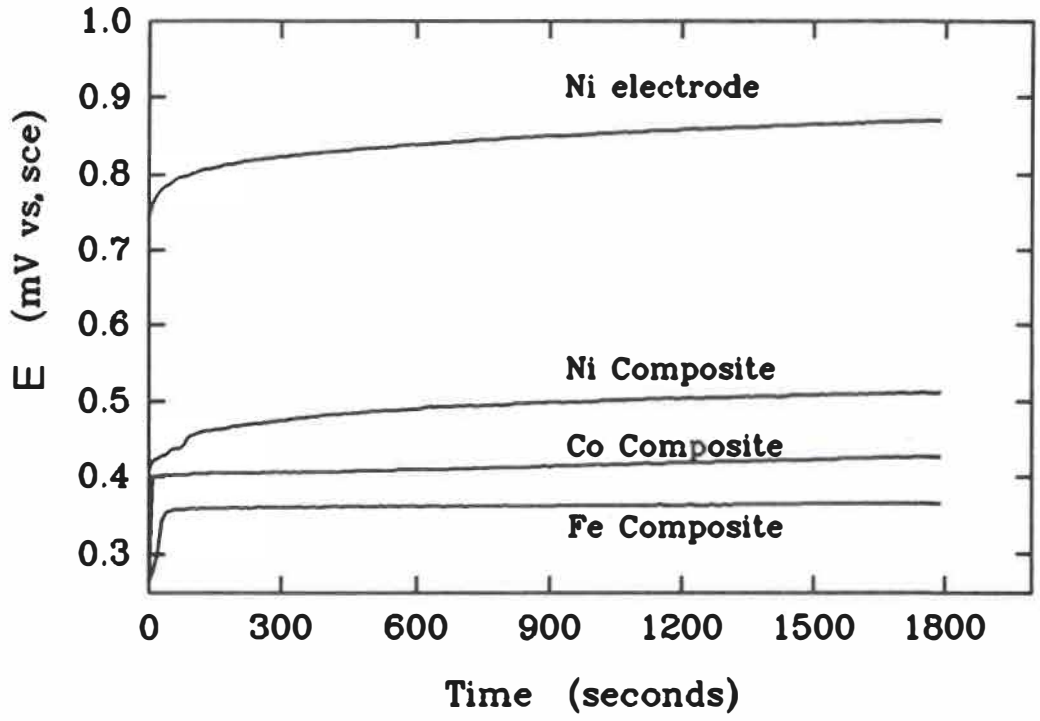

Figure 4-10 Potential versus time under a constant current charging (100 mA/cm^2) for the first 30 minutes for the Ni electrode, Ni, Co and Fe composite-coating electrodes in 5M KOH solution at 25°C.

obtained on the Fe composite-coatingelectrode, while the Co and Ni composite-coating electrodes presented a potential of 287 and 372 mV, respectively. The highest potential, 730 mV, appeared on the Ni electrode. The IR drop, measured by the current interruption technique, was ~140 mV at 100 mA/cm^2.

Figure 4-11 shows the anodic polarization curves (IR compensated) of the electrodes for the OER. The scan rate of potential for polarization was 1 mV/s. The Tafel range was identified between 5 and 500 mA/cm^2, depending on the electrode. The Tafel slopes (b) are over 50 mV/dec on Ni and Ni composite-coating electrodes, and about 40 mV/dec on Co and Fe composite-coatings (see Table 4-7). Electrode performance is evaluated by comparing current densities (i) under an overpotential (η) and *vice versa*. The overpotential on the Fe composite-coating electrode, obtained under 100 mA/cm^2 (η_{100}), was 246 mV, compared with 396 mV on an electroplated Ni electrode. The decrease in η_{100} was 34, 97 and 150 mV on the Ni, Co and Fe composite-coatings, respectively. The current density under an overpotential of 300 mV (i_{300}) on the Ni electrode was 1.5 mA/cm^2, and a 10 times higher value (15 mA/cm^2) of the i_{300} was observed on the Ni composite-coating. By substituting cobalt or iron powder for nickel in deposition of the composite-coatings, we obtained an i_{300} of 109 and 625 mA/cm^2 on the Co and the Fe composite-coating electrodes, respectively. Electrode activities, based on the η_{100} and i_{300},

indicate that composite-coatings are more active than the Ni electrode; and that the Fe composite-coating electrode is the most active one among the electrodes. The highest i_{ex}, $4.0X10^{-4}$ mA/cm^2, was on the Ni composite-coating, while the Co and the Fe composite-coatings had an i_{ex} in the order of 10^{-5} mA/cm^2,. However, the lowest i_{ex} was on the Ni electrode: $1.0X10^{-6}$ mA/cm^2. Table 4-7 is a summary of the results from Fig.4-11.

TABLE 4-7
KINETIC PARAMETERS OF THE OER FROM POLARIZATION MEASUREMENTS ON COMPOSITE-COATING ELECTRODES

ELECTRODE	b mV/dec	i_{ex} mA/cm^2	i_{300} mA/cm^2	η_{100} mV
Ni Electrode	54±4	$1.0\pm1X10^{-6}$	1.5±3	396±10
Ni Composite	58±2	$4.0\pm0.1X10^{-4}$	15±5	362±10
Co Composite	42±2	$7.0\pm1X10^{-5}$	109±25	299±15
Fe Composite	38±4	$1.4\pm1X10^{-5}$	625±60	246±12

4.4.4 Impedance measurements

Impedance spectra were collected on the electrodes under an applied potential range from 200 to 300 mV. An agitation (about 150 rpm) was applied to mitigate diffusion and to enhance the electrode charge transfer process. The solution resistance was subtracted from the impedance experimental data. The impedance complex-plane plot (Fig.4-12), Bode amplitude plots (Fig.4-13) and Bode phase plots (Fig.4-14), measured with an applied overpotential of 300 mV, are presented here. In the figures, the points are experimental data and the continuous lines represent fittings generated by the CNLS program (Complex nonlinear least squares immittance

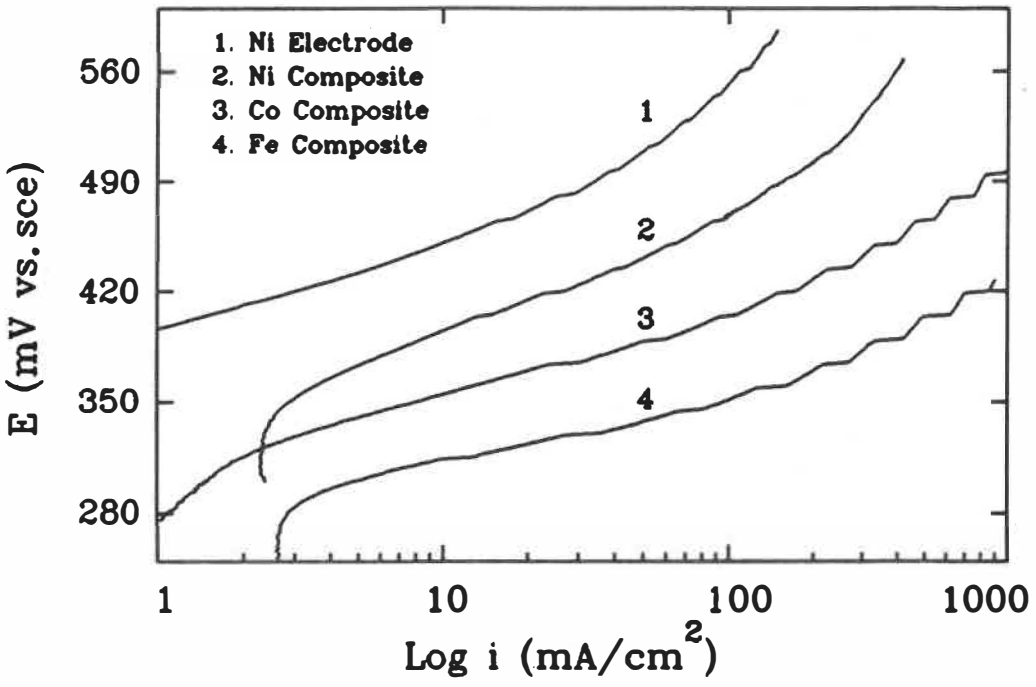

Figure 4-11 Anodic polarization curves for the Ni electrode, Ni, Co and Fe composite-coating electrodes in 5M KOH solution at 25°C. Potential sweep rate: 1 mV/s.

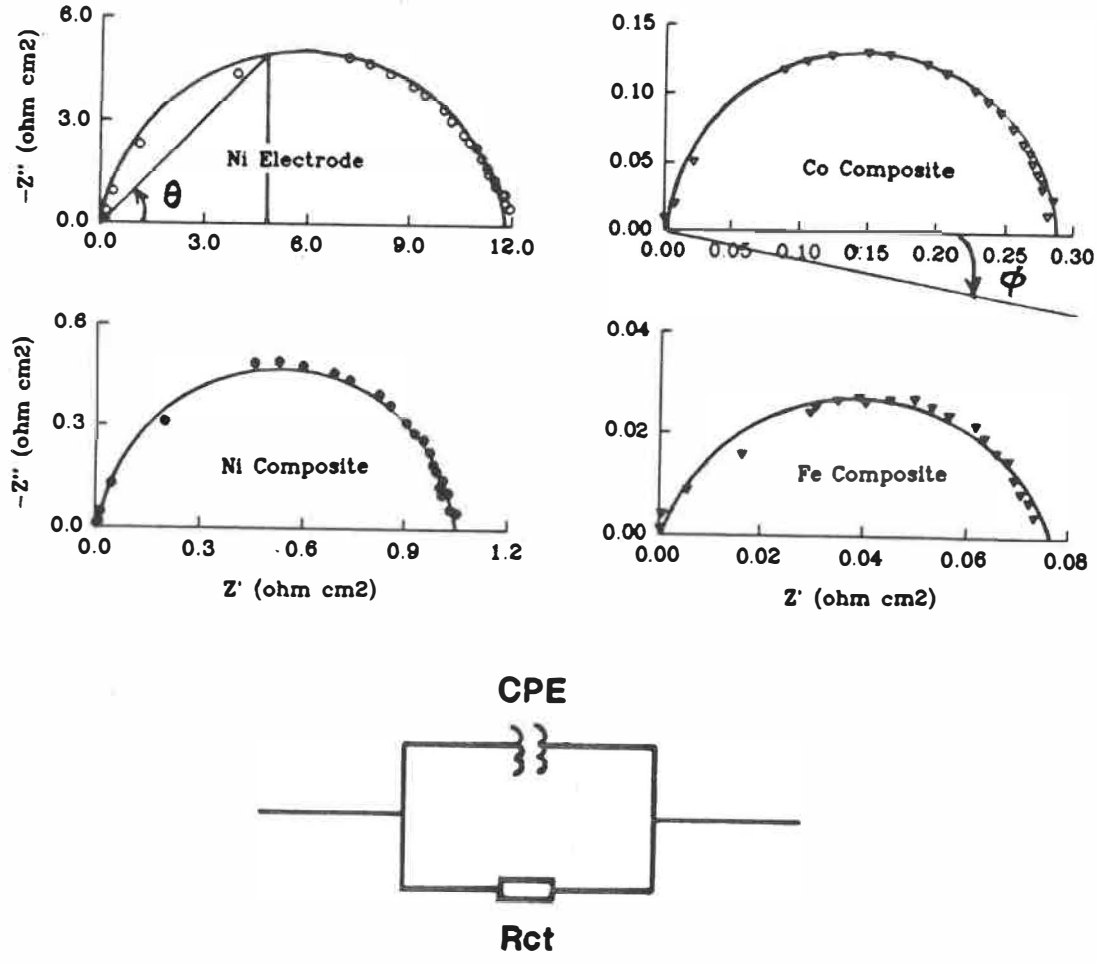

Figure 4-12 Impedance spectra in complex-plane plots on: (1) Ni electrode; (2) Ni composite; (3) Co composite and (4) Fe composite-coating electrode in 5M KOH at 25°C with an overpotential of 300 mV. Points are experimental data; curves are fitting with the equivalent circuit as shown in the figure.

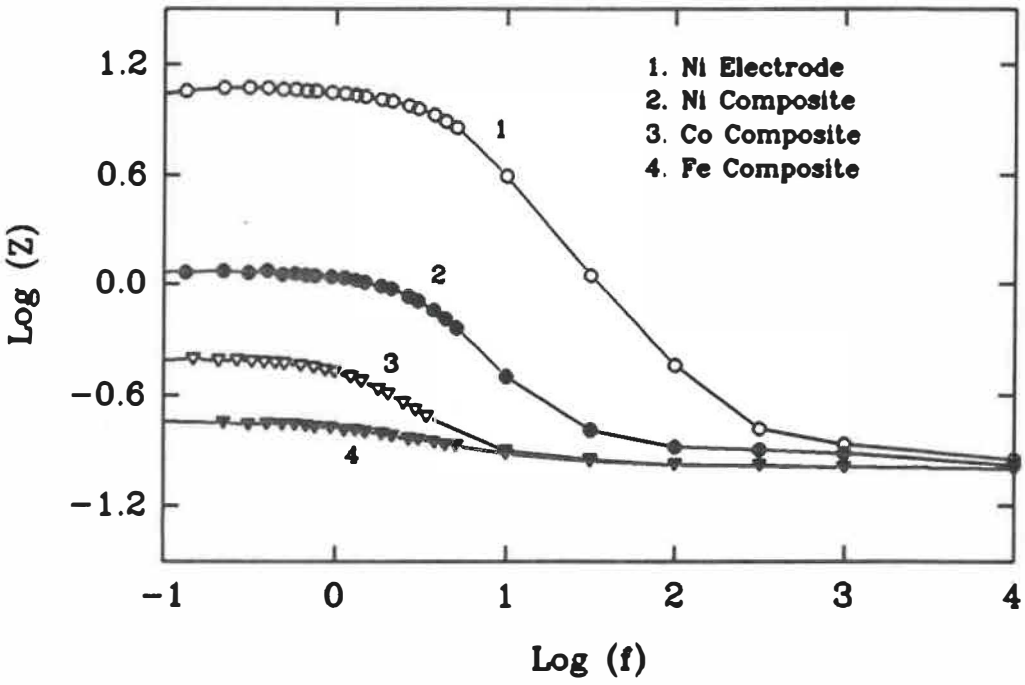

Figure 4-13 Impedance spectra of composite-coating electrodes in Bode amplitude plots.

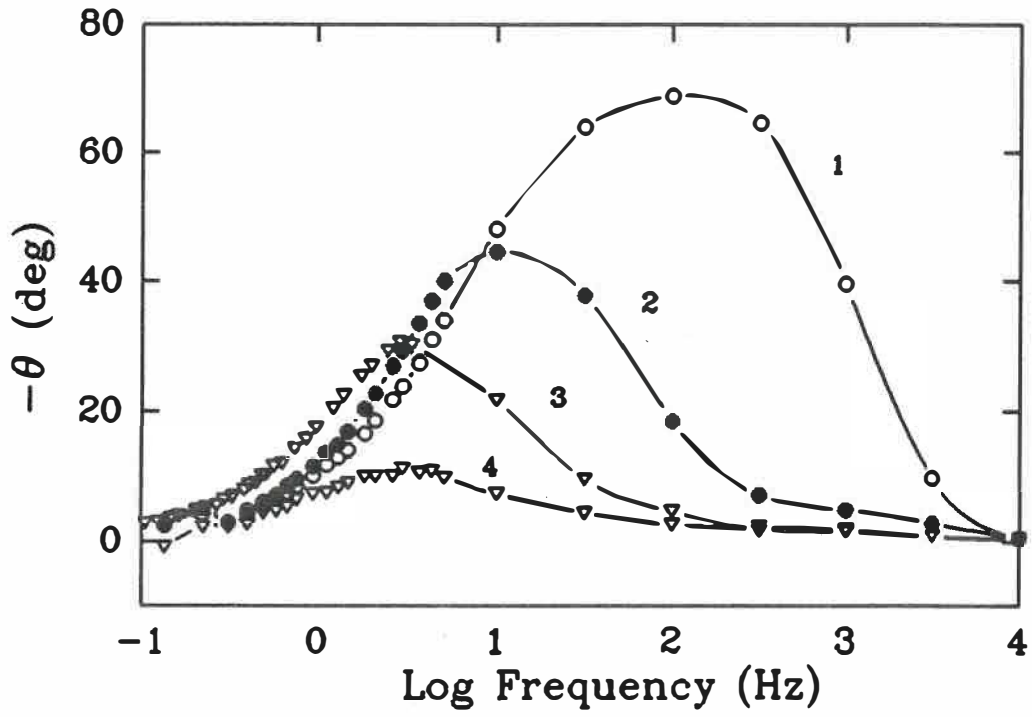

Figure 4-14 Impedance spectra of composite-coating electrode in Bode phase plots.

fitting program) with an equivalent circuit shown in Fig.4-12. Table 4-8 gives the summarized results from impedance spectra fittings and calculations. Surface roughness factors (S), defined as the ratio $C_{dl}/20(\mu F/cm^2)$, are also listed in the table.

TABLE 4-8
SUMMARIZED RESULTS FROM IMPEDANCE MEASUREMENTS FOR THE OER ON COMPOSITE-COATING ELECTRODES

ELECTRODE	E mV	R_{ct} Ω cm^2	C_{dl} mF/cm^2	S $C_{dl}/20$
Ni Electrode	410	11.500±2	1±0.2	50±10
Ni Composite	310	65.000±5	40±5	
	360	4.500±1	40±5	
	410	1.020±0.2	35±5	$1.75X10^3$±250
Co Composite	310	20.300±5	$3.2x10^2$±20	
	360	1.200±0.5	$3.2x10^2$±20	
	410	0.272±0.1	$3.2x10^2$±20	$1.6X10^4$±10^3
Fe Composite	310	1.560±0.5	$1.1x10^3$±20	
	335	0.900±0.2	$1.1x10^3$±20	
	360	0.155±0.1	$1.1x10^3$±20	
	385	0.100±0.1	$1.1x10^3$±20	
	410	0.056±0.1	$1.1x10^3$±20	$5.5X10^4$±10^3

* C_{dl} calculated from the equation in reference(112).
** Surface roughness factor obtained by $C_{dl}/20$ ($\mu F/cm^2$).

As can be seen in Fig.4-12, single semi-circular arcs with a depressed angle (ϕ) are exposed in the frequency range from 10^{-3} to 10^5 Hz. The value of ϕ varied depending on the electrode: 2 ~ 5° on the Ni electrode, 10 ~ 12° on the Ni and Co composite-coating electrodes and 13 ~ 15° on the Fe composite-coating electrode. It is obvious that these impedance spectra can no longer be represented by a simple R-C equivalent circuit. Therefore, a new type of equivalent circuit, R_{ct} and constant phase element (CPE), was used in the curve fitting. The results showed clearly that experimental

impedance data and the approximation from the equivalent circuit fitted very well. The charge transfer resistance (R_{ct}) and the double-layer capacitance (C_{dl}), calculated with the CNLS programme and the equation from reference(112), are listed in Table 4-8. It was found that both R_{ct} and C_{dl} varied depending on the composite-coatings in the selected applied potential range. A low R_{ct} and a high C_{dl} were observed on the Fe composite-coating electrode.

A difference in R_{ct} between electrodes is revealed by the real part of the impedance at the low frequency end. The high frequency (>10^3 Hz) end approached the uncompensated solution resistance (R_s) between the working and the reference electrode (R_s). Fig.4-14 presents the impedance phase angle (θ) ($tg\theta=Z''/Z'$) *vs.*log(f/Hz). All electrodes showed a one-peak behaviour, with the high-frequency end converging to a 0° phase angle, indicating that the solution resistance was dominant; the low frequency end had a phase angle of 0°, indicating that the charge transfer was the principal reaction. The maximal phase angle appeared in the frequency region of 3 to 100 Hz, depending on the electrodes. The Ni electrode had the highest phase angle peak (70°), while the Fe composite-coating exhibited the lowest one (11°). The log(f) values corresponding to the maximum phase angle were 2.2, 1.0, 0.6 and 0.5 on the Ni electrode and Ni, Co and Fe composite-coating electrodes, respectively.

Figure 4-15 shows the impedance complex-plane plots of the Ni, Co and Fe composite-coating electrodes under no applied potential. Without applied potential, the OER are not proceeded. Therefore, on the electrode surface, it was assumed that no Faradaic process was taking place, and that only the rough surface was responding to the *ac* potential perturbing signals. The figure shows straight lines inclined from the -Z" axis, with a rotated angle (ϕ), as predicted by the Eq.(5-3). Although the conditions for *ac* impedance measurement were the same for the Ni, Co and Fe composite-coating electrodes, (e.g., same solution, T, E and f), the rotated angle ϕ varied with the electrode: a lower rotation angle was on the Ni composite-coating electrode and a higher rotation on the Fe composite-coating electrode (see Fig.4-15).

Figure 4-16 shows the potential dependence of the impedance spectra on the Fe composite-coating in the overpotential range from 200 to 300 mV. Ni and Co composite-coating electrodes had a similar behaviour over the same potential range. As η increased from 200 to 300 mV, the R_{ct} declined from 1.6 to 0.07 Ω cm^2, and the C_{dl} kept about constant while the depression angle (ϕ) of the complex-plane plot increased from 3.43 to 14.78 degrees. In figure 4-17, the change of the ϕ as a function of the OER overpotential for the Fe composite-coating electrode is presented.

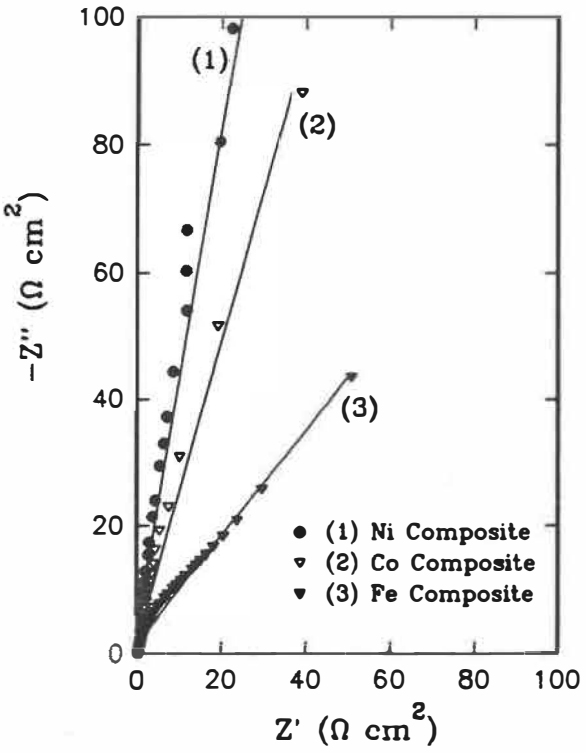

Figure 4-15 Impedance spectra in complex-plane plots, on Ni, Co and Fe composite-coating electrodes in 5M KOH at 25°C with 0V applied potential.

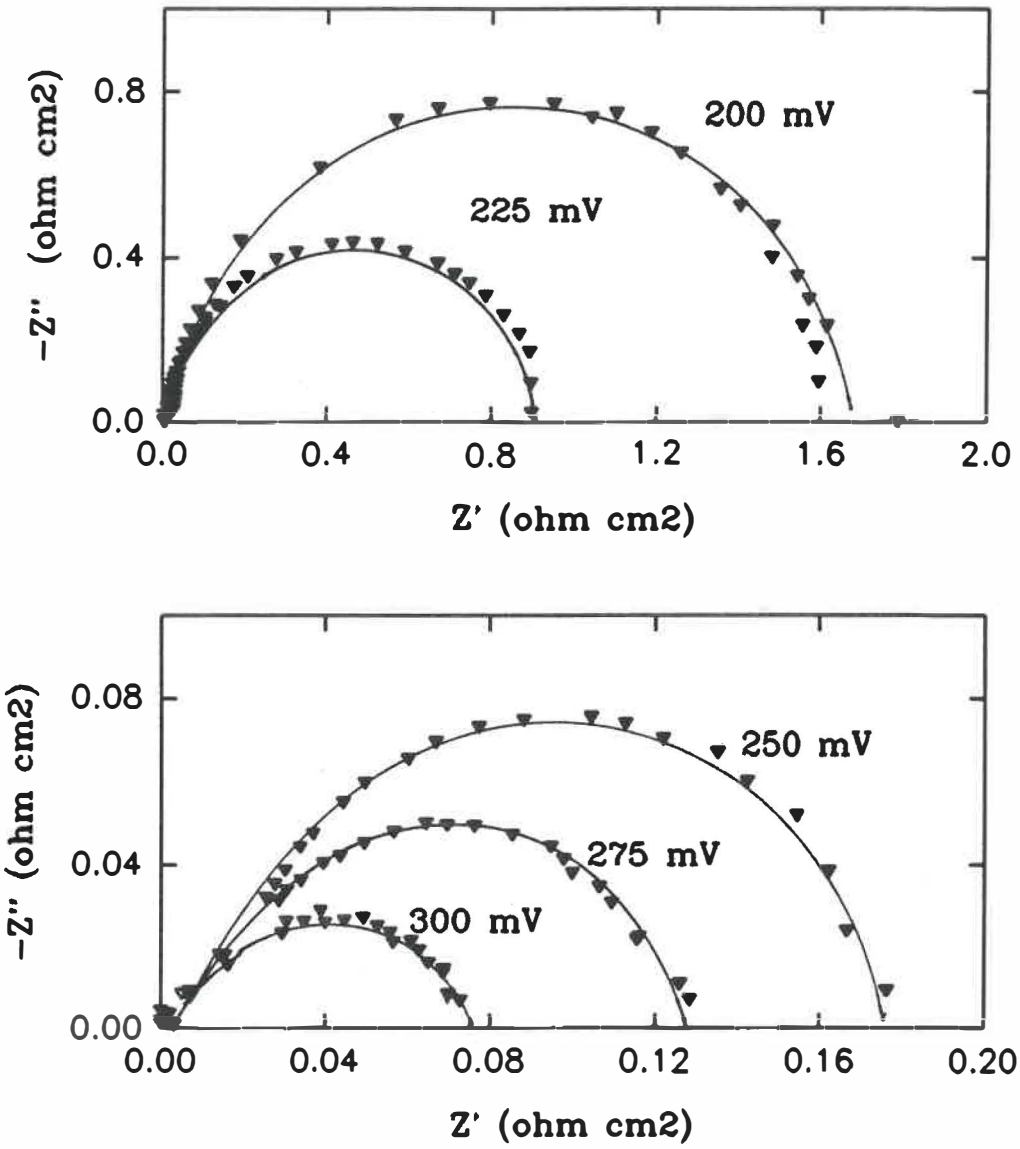

Figure 4-16 Potential dependence of impedance spectra of the Fe composite-coating electrode. Overpotential: 200 to 300 mV.

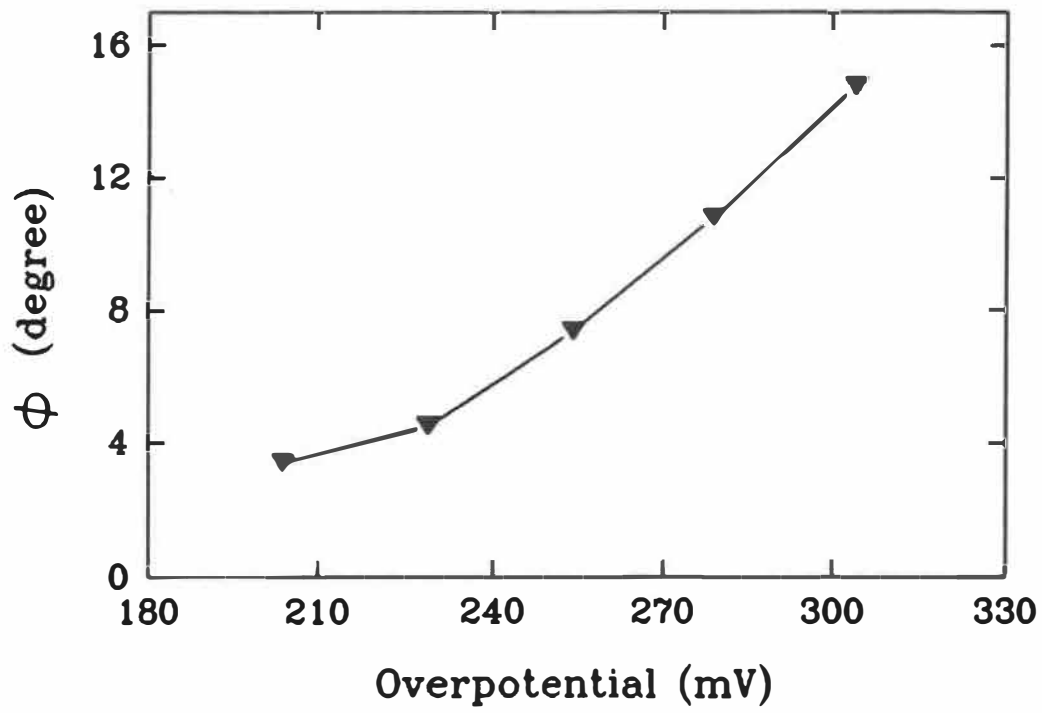

Figure 4-17 Depression angle of the Fe composite-coating electrode as a function of the overpotential.

4.5 COMPOSITE-COATING ELECTRODES FOR THE HER

4.5.1 Polarization measurements

Figure 4-18 shows the polarization curves for the HER in 5M KOH at 25°C. The Tafel slopes (b) were 120 mV/dec on the Ni electrode, 96,90 and 78 mV/dec on the Ni, Co and Fe composite-coating electrodes, respectively. The i_{ex} was in the range from $1.5x10^{-2}$ to $7.4x10^{-2}$ mA/cm^2, depending on the electrodes. The overpotential observed on the Ni electrode was relatively high (500 mV at i=100 mA/cm^2), while a lower value of the η was observed on the composite-coating electrodes. The decreased overpotentials (η_{100}), compared to that on the Ni electrode, were 200, 210 and 250 mV on the Ni, Co and Fe composite-coating electrodes. Improved performance for the HER on the composite-coating electrode was also evaluated on the current densities at an overpotential of -200 mV. Increases in the i_{-200} by 6 to 20 times were displayed on the Ni, Co or Fe composite-coating electrodes, compared to that on the Ni electrode. At high current densities (>50 mA/cm^2), the potential oscillation in a regular small wave form was observed on the composite-coating electrodes (Fig.4-18); however, this phenomenon was not detected on the Ni electrode. Results of the polarization measurements at 25°C are summarized in Table 4-9.

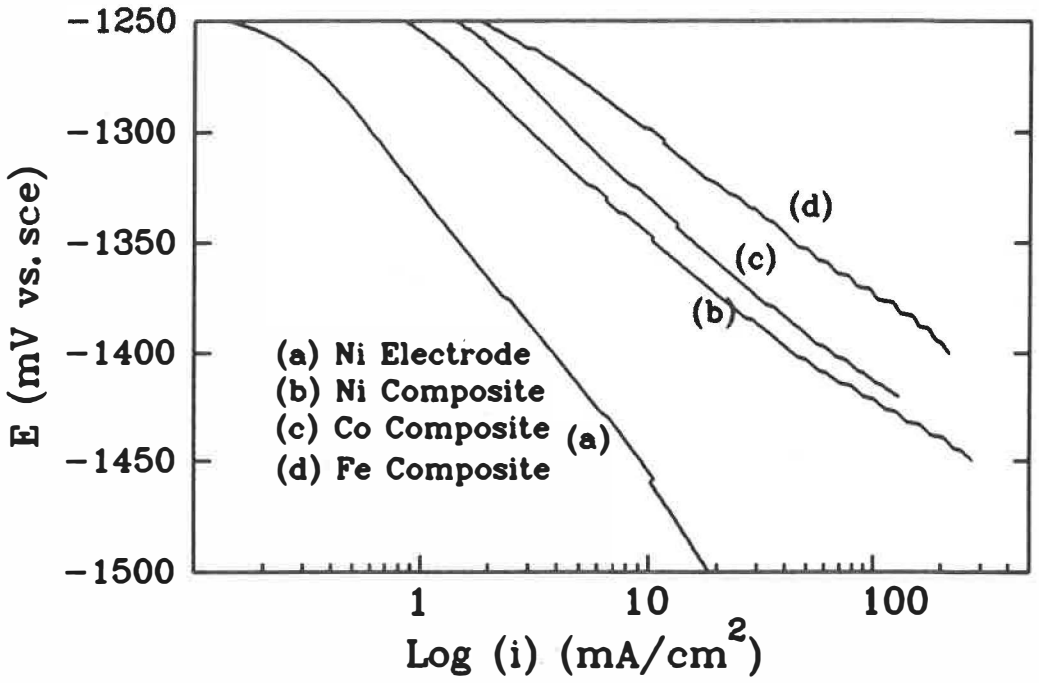

Figure 4-18 Cathodic polarization curves of the Ni and composite-coating electrodes for the HER in 5M KOH solution at 25°C. Potential scanning rate: 1 mV/s.

TABLE 4-9
KINETIC PARAMETERS OF THE HER FROM POLARIZATION MEASUREMENTS ON COMPOSITE-COATING ELECTRODES

ELECTRODE	b mV/dec	i_{ex} mA/cm^2	i_{-200} mA/cm^2	η_{100} mV
Ni Electrode	120±5	1.5±1X10^{-2}	0.93±0.1	500±10
Ni Composite	96±5	4.0±1X10^{-2}	5.45±0.5	300±5
Co Composite	90±5	7.4±1X10^{-2}	8.31±0.5	290±5
Fe Composite	78±5	5.0±1X10^{-2}	20.30±1	250±5

Figure 4-19 shows the HER current density at η=-200 mV on the mixed composite-coating of Ni-Fe (prepared in the bath with both Ni and Fe powders) as a function of the Fe concentration. The figure demonstrates that the HER current density depends on the iron powder concentration in the deposition bath. The Fe composite-coating electrode, prepared in the bath only with iron powder, represents the highest current density, 20.3 mA/cm^2. This series of experiments was initiated to verify if the tiny grained structures on the Ni composite-coating could interact synergetically with the electrocatalytical activity of the Fe composite-coating, and produce a surface with a better catalytic property.

4.5.2 Energy of activation

The apparent energies of activation (ΔH) for the HER on composite-coating electrodes were calculated from the temperature dependence of Log(i_{ex}), using the equation:

$$\Delta H = -2.303R\left[\frac{dLog(i_{ex})}{d(1/T)}\right] \qquad (4\text{-}1)$$

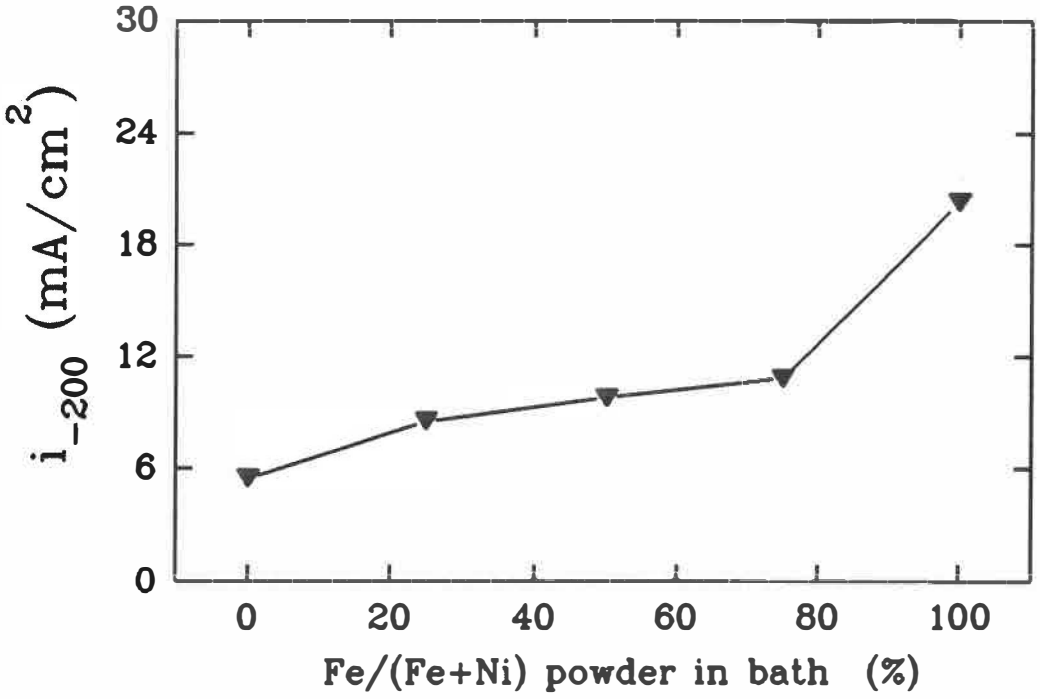

Figure 4-19 Current densities for the HER on Ni-Fe composite-coating electrodes at an overpotential of -200 mV as a function of the metallic powder weight ratio Fe/(Fe+Ni) in the deposition bath. The total metallic powders in the bath: 2 g/L.

Figure 4-20 gives Arrhenius plots for the HER on composite-coating electrodes. The exchange current densities were obtained from polarization curves measured at temperatures ranging from 298 to 348 K. The apparent energies of activation for composite-coating electrodes are listed in Table 4-10. The values of ΔH shown here are in the same range as those obtained on Ni alloy electrodes (113). The highest ΔH obtained on the Fe composite-coating electrode, 74 kJ/mol, indicates that activation of the HER on this electrode is more difficult than that on the Ni electrode. Almost the same value of ΔH is obtained on the Ni and Co composite-coating electrodes, suggesting that activation of the HER on these electrode are nearly the same.

TABLE 4-10
APPARENT ENERGY OF ACTIVATION FOR THE HER ON COMPOSITE-COATING ELECTRODES

ELECTRODE	ΔH(kJ/mol)
Ni Electrode	53±2
Ni Composite	62±4
Co Composite	64±5
Fe Composite	74±5

It was found that the Tafel slope varied depending on the temperature. On the Ni electrode, b remained about 120 mV/dec from 298 to 348 K; on the Ni and Co composite-coating electrodes, b increased slightly (from 96 to 108 for the Ni composite and 90 to 93 mV/dec for Co composite). The Fe composite-coating electrode showed a considerable increase of the Tafel slope (from 78 to 134 mV/dec.).

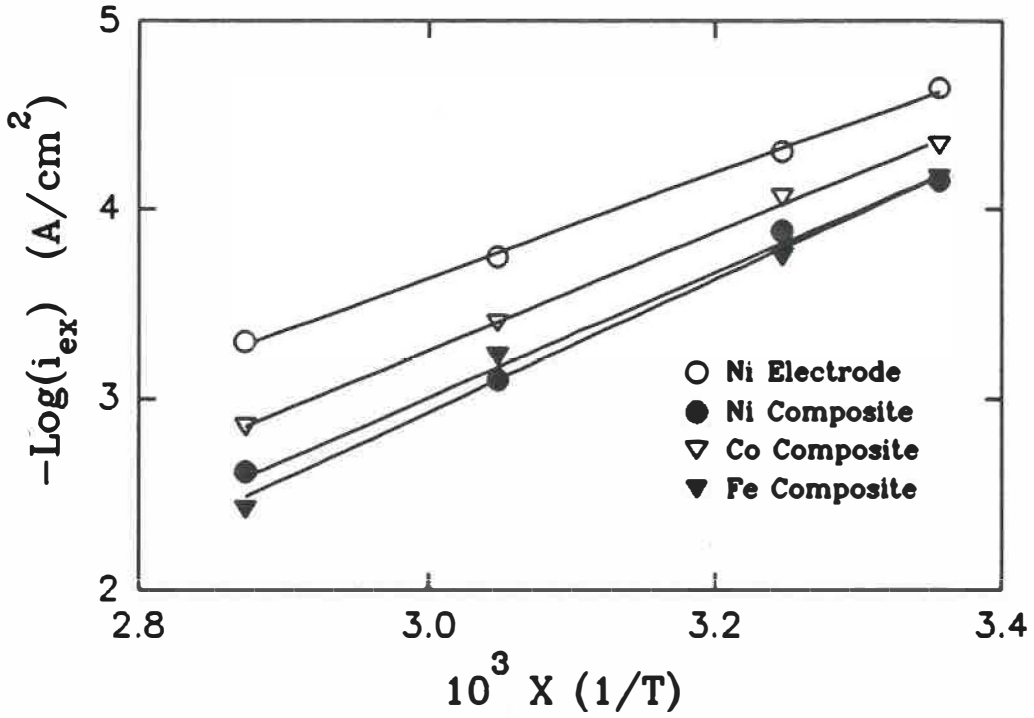

Figure 4-20 Arrhenius plots of the composite-coating electrodes for the HER.

4.5.3 Impedance measurements

Impedance measurements were carried out on composite-coating electrodes in 5M KOH solution at 25°C for the HER. The overpotential applied on the electrode was in the range of -50 to -250 mV. The typical complex-plane plots, -Z" imaginary impedance against Z' real impedance, measured at η = -100 mV on the composite-coating electrodes, are shown in Fig.4-21. The R_s was compensated before the fitting, and it is not shown in the figure. Points are the experimental data and lines are curve fitting using the programm of CNLS with the same equivalent circuit as for the OER. Table 4-11 gives the value of parameters obtained from the impedance spectra fitting and calculation. In general, one semi-circle with a depressed angle was found on all electrodes over the applied potential and frequency ranges. The lowest R_{ct}, 13.3 Ω cm^2, was found on the Fe composite-coating electrode, while twice this value was obtained on the Ni composite electrode. The decrease in the R_{ct} from the Ni to Co, and to Fe composite-coatings was consistent with the increase of the current density obtained by polarization measurements (Table 4-9). It was found that the ϕ varied depending on the composite-coatings and overpotential. The highest ϕ value, 18.8 degrees, was obtained on the Fe composite-coating electrode, while the lowest, 2.0, was on the Ni electrode (see Table 4-11). The order of the increase in the depressed angle of the semi-circular arc is consistent with the order of the current density increase on

the composite-coating electrodes, and they agree with SEM examinations on the composite-coating electrode surfaces (Fig.4-9).

TABLE 4-11
KINETIC PARAMETERS FROM IMPEDANCE SPECTROSCOPY FITTING FOR THE HER ON COMPOSITE-COATING ELECTRODES

ELECTRODES	R_{ct} $\Omega\ cm^2$	C_{dl} $\mu F/cm^2$	ϕ degree	S*
Ni Electrode	65.6	$4.2X10^1$	2.0	2.1
Ni Composite	26.6	$1.4X10^3$	12.9	70.0
Co Composite	22.0	$1.2X10^3$	15.8	60.0
Fe Composite	13.3	$4.0X10^3$	18.8	200.0

Impedance measurements were made at -100 mV overpotential.
* Surface roughness factor, obtained by $C_{dl}/20$ ($\mu F/cm^2$).

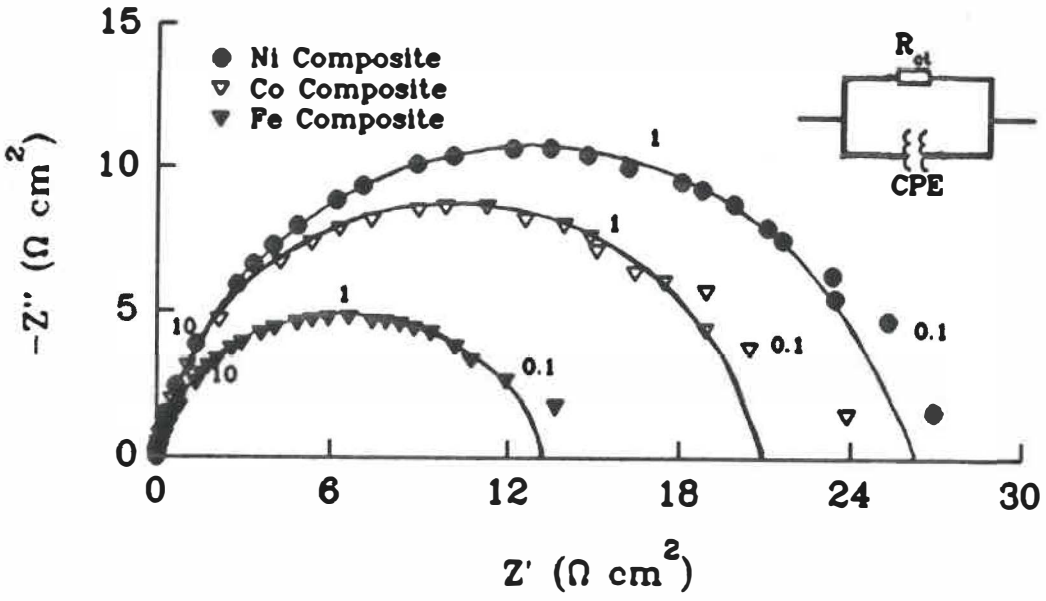

Figure 4-21 The complex-plane plots (R_s compensated) of composite-coating electrodes, measured under an overpotential of -100 mV in 5M KOH at 25°C. Numbers in the figure show frequency; points are experimental data; continuous lines are the CNLS fitting.

CHAPTER 5

DISCUSSION

5.1 METHODS FOR IMPROVING ELECTRODE ACTIVITY

As discussed in Section 2.3, a high electrocatalytical activity on an electrode can be achieved in three ways: i) the kinetic approach - changing the reaction path and accelerating the RDS rate; ii) surface modifications - introducing more active sites on the surface; and iii) surface modifications - enlarging the real surface area on the electrode to deliver a larger current at a lower overpotential. Approach i) involves designing a new reaction system or path; and approaches ii) and iii) focus on techniques for improving electrode activity, which are based on two concepts: using highly catalytically active materials and/or making the electrode surface highly rough and porous with a larger real surface area. The first method requires expensive materials such as ruthenium, iridium and platinum, while the second method depends on adopting practical techniques to produce a highly rough and porous surface and to make this surface available to the electrochemical reaction. These two techniques have been adopted in this study to improve the catalytic performance of the Ni-based electrode. Both of them have been very successful in practice. The remaining questions are: a) How do these techniques improve electrode activity? b) How effective are

these techniques for increasing activity? c) What is the limit in applying these techniques? The following discussions are attempts to search answers for these questions.

5.2 DEPOSITION CONDITIONS VS. ELECTRODE ACTIVITY

There are many types of deposition baths, and a wide range of conditions can be selected for electrodeposition(94). The choice of bath type and composition for deposition in this study is primarily based on the electrocatalytical properties for the OER. Electrodeposition of nickel powders from a variety of baths have been investigated by many authors (114,115,116,117), but these powders were produced as chemical catalysts, and not as electrodes for electrochemical reactions such as the OER. On the solid Ni deposit, studies of the effect of anion compositions on the electrocatalytical property for the OER are not available. On the basis of this, research was therefore initiated here to study of effects of the electrodeposition bath type and conditions on the electrode activity.

5.2.1 Electrode activities

Kinetic parameters such as the b, the η and i_{ex} are valuable parameters traditionally used for evaluating electrode performance. From Table 4-1, clearly, the Ni electrode prepared from the chloride bath has a low Tafel

slope (b_L=50mV/dec) and overpotential (η_{100}=396mV). It is the most electrocatalytically active electrode for the OER among the Ni electrodes prepared in various baths. However, an evaluation based on the i_{ex} (Table 4-1) shows that the Ni electrodes prepared from the sulfate and sulfamate baths have a higher exchange current density ($i_{ex}=10^{-3}$ mA/cm^2), and are, therefore, more active than the others. The i_{ex} is a current density at no polarization potential; it represents the catalytic activity under no applied potential. As the i_{dp} increases, an increase in the i_{ex} was observed on the Ni electrode prepared in the chloride bath (Table 4-3). It is suggested that the increase in the i_{ex} results from the electrode surface roughness. As the surface roughness increases, a part of it will be actively available to the OER, resulting in a high apparent i_{ex} value (based on geometric surface area). In Sections 5.4.3.6 and 5.6.4, the surface roughness factor on composite-coatings and their effectiveness are discussed.

It should be noted that the i_{ex} is measured from the polarization curves at high polarization, and that the Tafel equation (η=a + blogi) is a special case ($i>>i_{ex}$) of the Butler-Volmer equation(58). At low current density, the relationship of η and i_{ex} is linear, as expressed by Eq.(2-12) in Section 2.5.2: $\eta = RTi/(\alpha nFiex)$. Therefore, the accuracy of the i_{ex} obtained under high polarization (by extrapolating the

Tafel lines) is in question. Nevertheless, unlike the case of the HER, the value of i_{ex} for the OER is very small (10^{-9} to 10^{-3} mA/cm^2)(14), and it is difficult to have an accurate value of i_{ex} by extrapolating the Tafel line to the reversible potential. In other words, the i_{ex} is not a very sensitive measure for comparing two electrocatalysts for the OER.

Due to the difference in reaction mechanisms among Ni electrodes deposited in various baths, a divergence in i_{ex} values was expected. As explained in Section 2.5.1, to evaluate two electrodes' performance by comparing current densities at the same η, we could obtain the same evaluation by comparing the i_{ex} on the two electrodes. It should be certain that the mechanisms of the two electrode reactions are identical. As we have seen in Table 4-1, the Tafel slopes on Ni electrodes prepared from the various baths were different. It is not certain that the OER mechanisms on those electrodes are the same. It is then not appropriate to use the i_{ex} as the parameter for evaluating electrode activity in this case.

5.2.2 Surface conditions

Among the Ni electrodes prepared from different baths, the electrode deposited from the $NiCl_2$ bath showed outstanding electrocatalytical properties based on the b, η_{100} and C_{dl}. It is interesting to know what makes the difference in the Ni electrode activity. Since the chemical compositions of the Ni

electrodes prepared in various baths (Ni > 98 wt% by EDS analysis) were nearly the same, the difference in electrode performance must result from the electrode surface morphology.

According to Brown and co-workers(94), the chloride bath produces a deposit with a hard, fine-grained and highly stressed surface. Residual stress is in the range of 2800 to 3500 kg/cm^2, which is the highest value among Ni deposits from all kinds of baths(94). According to Pinkerton and Carlin (118), the stress on Ni deposits from various baths was tensile stress. High stress can cause spontaneous cracking during deposition(94,118), and in fact, the SEM micrographs illustrated the existence of microcracks on the Ni deposits. These cracks may result in an increase in real surface area. Since the sulfate bath has a greater tendency to form a nodule and tree structure than the chloride or the Watts bath, the high internal stresses in the deposit cause a sporadic cracking(94), which can be seen in Fig.4-1(c). The degree of the cracking was, however, much less than that on the Ni deposited from the chloride bath. The real surface area may be lower than that on Ni deposited from the chloride bath; therefore, the electrode performance for the OER was poor. By mixing sulfate and chloride salts in the deposition bath, we obtained a Ni electrode with a better electrocatalytical property for the OER (on the basis of η_{100}) than the electrode deposited from the sulfate bath. Decreases in the b and R_{ct}

were also observed (see Table 4-1&2). The sulfamate bath gave a deposit with low stress and good ductility, (reported residual stress was 35 kg/cm^2), and it was the lowest value for nickel deposited from any bath(94). In electrocatalysis, which is favoured by a larger real surface area, cracks can not be induced on a low-stressed deposit surface; therefore, a Ni deposit surface was obtained as seen in Fig.4-1(e), without any surface cracks or nodule structures. Although a few highly stressed spots with cracks existed on the surface of Ni from the acetate bath, the majority of the surface was still covered by a relatively smooth compact deposit.

If the surface internal stress is responsible for the spontaneous cracking of the deposit, however, measurement of the internal stress level would be difficult. When measuring the residual stress on the deposit, what we measured would be the result of the cracking, and not the stress that caused the cracking, because cracking releases the stresses. Therefore, attempts to measure the stress values in deposits were not considered, and efforts were focused on catalytic activity by electrochemical measurement.

Since C_{dl} indicates the real surface area on the electrode, it is reasonable to assume that the C_{dl} would be high on Ni electrode prepared from a chloride solution. The close relationship between R_{ct} and C_{dl} was given in(108) as:

$$R_{ct} = \frac{1}{(\omega_c C_{dl})} \qquad (5\text{-}1)$$

where ω_c is the angular frequency at maximal impedance phase angle, located at the summit of the arc. Assuming a constant ω_c, the higher the value of C_{dl}, the lower the R_{ct} would be. This explains why a low R_{ct} appears on the Ni deposited from the chloride solution.

It has been reported that the catalytic activity of the RuO_2 oxide electrode is dependent on the crystal face(119). The study of the RuO_2 indicated that the value of the Tafel slope is face-specific as a result of difference in crystal orientation. For example, the Tafel slope on the (010), (110) and (011) face of the RuO_2 electrode was 75, 105 and 140 mV/dec, respectively(119). It was suggested that the crystal structure of the oxide was of key importance for the properties of DSA electrodes(14,119).

The Ni deposited from electrolytes of various anionic compositions has a polycrystalline surface with different preferred orientations(120). The electrocatalytical activity on nickel powder(115) and Co(121), deposited from various baths, was related to the preferred orientations. X-ray diffraction studies proved that the preferred orientation on Ni was {110} (from chloride bath) and {210} (from sulfate bath)(120). The preferred orientation was found again to be

{110} on Ni deposited from the chloride-sulfate mixture bath. A good electrocatalytical performance for the OER was obtained on the Ni from the chloride and an improved performance on the one from the chloride-sulfate bath (see Table 4-1). Since the Ni electrode from these two baths shared the same orientation {110}, and it was suggested that the preferred orientation {110} plane could then be the one favouring the OER. This is another reason why a good electrocatalytical performance is obtained on Ni deposited from the chloride bath, and an improved catalytic property is found on Ni deposited from the chloride-sulfate mixture bath.

5.2.3 Selection of deposition baths

Based on evaluation of the electrocatalytical activity, the chloride bath is a favourable choice for the deposition bath for preparing Ni electrodes. There are also other advantages of the chloride bath. A high deposition current density can be employed in the chloride bath, as chloride solutions have a high conductivity. The presence of Cl^- ions in the deposition bath will also improve the anode dissolution by reducing polarization (94). Nickel chloride is a chemical salt which is relatively cheap and readily available; sulfamate and acetate salts are more expensive. Although sulfate salt is the most popular compound used in electroplating on an industrial scale, the Ni deposited from this bath offers a relatively poor electrocatalytical

performance for the OER.

5.3 OXIDATION POTENTIAL VS. ELECTRODE ACTIVITY AND STABILITY

5.3.1 OER overpotential

The presence of Ru or Ir in the Ni-based electrode decreased the OER overpotential by 30 and 40 mV, respectively (Table 4-4). This indicates an even better result for Ir than for Ru in improving the Ni-based oxide electrode performance for the OER in KOH solution. This improvement of performance on the electrode for the OER has been attributed to the surface concentration of active sites on the oxide layer(15), although the exact nature and location of these sites have not been determined experimentally. All the discussions in the literature were tentative deductions. In this study, the Ru or the Ir element was detected on the electrodes by the EDS. The improved electrocatalytical performance should be attributed to the modification of the Ni electrode surface. Therefore, the presence of small amounts of Ru or Ir species in the oxide layer must favour the formation of such special sites and increase the electrocatalytical effect. How would those special sites function in promoting the OER? Since we did not get the answer to this question from microscopic examinations, we turned to electrochemical methods.

As observed in the cyclic voltammograms (Fig.4-7), forward

potential scanning on the Ni-based electrodes showed a potential peak (P1 in Fig.4-7) before the OER. This peak represents surface oxidation. It is well established (15,17) that oxide layers are formed before the oxygen evolution takes place. Some studies(15,28,122,123) of the OER have suggested that the oxidation process of the metal on the electrode surface was involved in the OER process, or that it became one of the progressive steps in the OER mechanism.

We can take another approach to this phenomenon. Let us divide the overall overpotential for the OER into two parts (see Fig.5-1):

$$\eta = \Delta E_{ox} + \Delta E_{O2} \qquad (5\text{-}2)$$

where ΔE_{ox} is a polarization potential between the reversible oxygen potential (1.23 V *vs.SHE*) and the electrode surface oxidation potential (P1); and ΔE_{O2} is the potential difference between the OER (i=20 mA/cm_2) and the peak (P1) potential. Table 5-1 shows the overall oxygen overpotential and its divided values in terms of ΔE_{ox} and ΔE_{O2}. The lowest ΔE_{ox} value corresponds to the Ni-Ir oxide electrode, and the highest to the Ni oxide electrode. In the case of ΔE_{O2}, the position is different. The lowest ΔE_{O2} value belongs to the Ni-Ru oxide electrode and the highest ΔE_{O2} value appears on the Ni-Ir oxide electrode. The Ni oxide is in the middle. We will discuss the ΔE_{ox} and the ΔE_{O2} in greater detail in the following section.

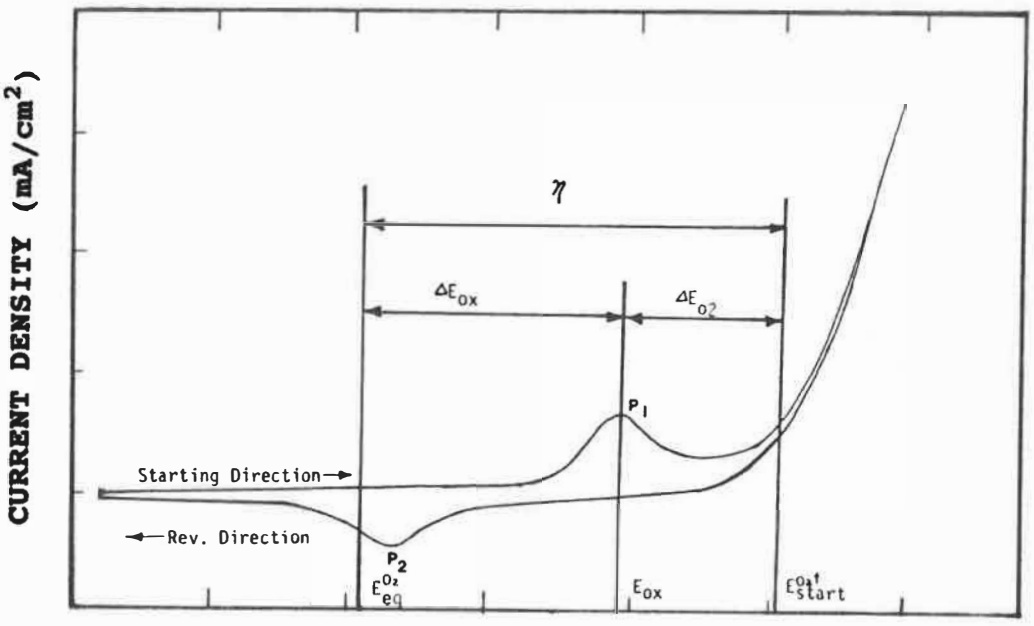

Figure 5-1 An illustration of division of the total oxygen overpotential into two parts: $\eta = \Delta E_{ox} + \Delta E_{O2}$.

TABLE 5-1
DIVIDED OER OVERPOTENTIAL VALUES AT 20 mA/cm^2
ON THE Ni-Ru AND Ni-Ir ELECTRODES

ELECTRODE	ΔE_{ox}/mV	ΔE_{O2}/mV	η/mV
Ni	188	122	310
Ni-Ru(2.2%)	178	102	280
Ni-Ir(2.3%)	132	138	270

5.3.2 Peak potential

The oxidation potential peaks were observed both on the pure metal oxide (RuO_2 and IrO_2) and on the mixed oxide (Ni-Ru and Ni-Ir) electrodes. In the case of the pure metal oxide, the peak potential was observed at a value very close to the thermodynamic potential calculated for transforming the oxide Ni^{3+}/Ni^{4+}, Ru^{4+}/Ru^{8+} and Ir^{4+}/Ir^{6+} (comparing E_c & E_{ox} in Table 4-5). It can be seen that the peak potential for the Ru oxide is rather close to that of the Ni oxide; it appears only 44 mV before the Ni oxide peak (see E_{ox} in Table 4-5). The Ir oxide peak is observed at a much less noble value, and it appears at some 234 mV before the Ni oxide peak.

Although the Ni oxide dominates the surface oxidation reaction, the Ir in the Ni oxide results in a displacement of the Ni^{3+}/Ni^{4+} peak position to a lower value, and this decreases the ΔE_{ox} value on the Ni-Ir electrode (ΔE_{ox}=132mV). Since the OER takes place on the oxide formed at the peak potential, it is possible to say that the catalytic oxide layer formed by oxidation of Ni^{3+}/Ni^{4+} is produced more easily on the Ni-Ir oxide than on the Ni-Ru oxide.

5.3.3 ΔE_{O2}

The second part of the overpotential, ΔE_{O2}, represents the effectiveness of the electrocatalysis on the mixed oxide surface, because the OER always takes place on an oxidized surface. Table 5-1 shows that the Ni-Ru oxide has the lowest ΔE_{O2} value and corresponds to a better and more effective mixed oxide surface for the OER. A larger value of the ΔE_{O2} on the Ni-Ir oxide (see Table 5-1) indicates that this mixed oxide layer is less electrocatalytically active. However, the total overpotential of the Ni-Ir oxide remained at the same level as that of the Ni-Ru oxides. This is because of the lower value of ΔE_{ox} on the Ni-Ir oxide. The lower value of ΔE_{ox} compensated for the higher value of the ΔE_{O2} when the total overpotential η was counted. It should be noted that in studying various oxide coatings for the OER in acidic solution by cyclic voltammograms, the different anodic charge behaviours were found on RuO_2-TiO_2 and IrO_2-TiO_2 oxide systems(124). The reason was not elucidated in the literature, but we suggest that it might be explained by the difference in the oxidation behaviours in the RuO_2 and IrO_2 oxide systems.

5.3.4 Corrosion behaviour

Although the overall overpotential is rather similar for both mixed oxides, their stability in alkaline solution is not the same. Corrosion of the Ru on the oxide layer resulted in

a loss of electrocatalytical property. Makarychev and co-workers (125) reported that the higher the Ru content, the more rapidly the electrode corroded. This is why the Ni-Ru oxide containing 2% or more Ru showed almost the same catalytic effect as the pure Ni oxide after immersion of the electrode in a 5M KOH solution for more than 30 minutes. By comparison, the Ni-Ir mixed oxide electrode in this study was much more stable, and it retained its good electrocatalytical activity for more than 24 hours at a current density of 100 mA/cm^2.

5.4 COMPOSITE-COATING ELECTRODE WITH A VERY ROUGH SURFACE

5.4.1 Effective surface areas

It was believed (17) that the oxygen evolution takes place on oxidized surfaces. When the metallic electrode surface undergoes an oxidation process, the surface will be oxidized before the OER occurs. It has been reported(28) that the top oxide layers on the Ni electrode determine the kinetics of the OER. Oxidation can be achieved *via* different processes and routes. Electrochemical oxidation is performed *in situ* before electrochemical characterization. After activation, a hydrous oxide or hydroxide is formed on the Ni electrode surface(28), which favours the electrode kinetics and increases the surface stability and its catalytic activity.

On the basis of overpotential, the composite-coating electrode is more active for the OER than the Ni electrode. We suggest that the improved catalytic properties of the composite-coating could come from the surface activation and/or utilization of very rough and porous surfaces. It was found in this study that improvement of the performance for the OER on the Ni electrode (η from 730 to 396, see Section 4.4.3) was more significant than that achieved on the Ni composite-coating electrode (η from 372 to 362) by electrochemical oxidation. Lu and Srinivasan(28) stated that the improvement of electrocatalytical activity for the OER on the pre-anodized Ni electrode was associated with the formation of the "right type of oxide", namely β-NiOOH, which provided active sites, such as Ni^{+3} ions, for the OER. The active site here is defined as a special spot on the electrode surface, where the activation energy of the RDS for the electrochemical reaction is lower than other places on the electrode. Bockris and Otagawa(126) gave an example of this: when the OH^- desorption step is the RDS for the OER mechanism on the mixed oxides of Ni-Fe, and when nickelate has a lower adsorption energy for OH^- than ferrite does, then a lower activation energy for the RDS will be on the nickelate, and the nickelate will be the active site on the electrode. In our case, less improvement in the activity on the composite-coating electrodes by oxidation may suggest that significant active sites have not been formed on the surface.

Another possibility is that the conditions used for electrochemical oxidation of the composite-coating surface may be improper for achieving complete oxidation, due to a very high real surface area and low true current density on the composite-coating. We therefore tried a higher current with a prolonged time for the oxidation of composite-coatings. However, no beneficial effect was observed at the end of the tests. Thus, it appears that improvement in the catalytical property on the Ni composite-coating electrode is limited by the technique of surface activation. Much efforts should therefore be devoted towards increasing the surface area on the composite-coating electrodes.

The most significant difference observed by SEM between the conventionally deposited Ni and the Ni composite-coating is the surface roughness, as shown in the micrographs in Fig.4-9. Based on this, Co and Fe composite-coatings were prepared with the hope of achieving a rougher surface with a larger real surface area available to the reaction. The availability of the electrode surface for the reaction is very important. To acquire this information, it is necessary to measure the real surface area on the electrode and to evaluate its availability for the electrochemical reaction.

5.4.2 Estimation of real surface area

As discussed in Section 2.3.3, kinetic parameters such as

the i_{ex}, b and η are valuable parameters for evaluating electrode performance. An evaluation based on information given by these parameters is, however, not complete unless information related to the electrode surface is provided. The surface area and structure are critical factors in determining the reaction kinetics. Moreover, the real surface area of the electrode can strongly affect electrode performance. If this information is missing, evaluation of the electrode performance becomes vague.

Evaluation of the real surface area of a solid electrode is traditionally made by the Brunauer-Emmett-Teller (BET) method (127), which has been accepted as a standard method of measuring real surface area. However, it should be mentioned that values of the real surface areas obtained by this method depend on the hypothesis of monolayer coverage of the adsorbate. This assumption can not always be made, because the gas adsorbate (such as Ar_2, Kr_2, N_2 and CO_2) used for the BET measurement is not necessarily always adsorbed in a monolayer on the surfaces. Some special sites, such as grain boundaries, dislocation lines, surface defects, etc., which have a lower adsorption energy, can attract more adsorption. The calculation of the BET surface area is based on the estimated value of the cross-sectional area of an adsorbed gas molecule, which is not a highly accurate value. The different gases selected for the BET test will give different values of

the surface area. We should consider these uncertainties before we accept the BET surface area.

Accessibility of the pore to the adsorbate and the structure size on materials measured are other uncertainties for the BET measurement. For example, a porous Australian brown coal(128) has a BET area in the range of 1-5 m^2/g by N_2 at -196°C, 200-300 m^2/g by CO_2 adsorption at -78°C, and more than 200 m^2/g by water adsorption at ambient temperature. Brunauer(129) pointed out that the "absolute" surface area values determined for certain adsorbents were in error by as much as 20%. The surface area given by this method is only meaningful for pure gas adsorption.

It should be remembered that electrochemical reactions occur in aqueous media, and the active surface accessed by gas adsorption is not the one available for an electrochemical reaction in solutions. The double-layer capacitance, on the contrary, is measured at the electrode/electrolyte interface by electrochemical techniques, and it is frequently used as an indication of the electrode surface area. This gives an indirect measure of the electrode surface area with an emphasis on the electrode/electrolyte interface.

Table 5-2 gives the real surface area values on solid Pt electrodes, reported by Brodd and Hacherman(130). It shows

that the BET surface area by Kr adsorption varied from 23.9 to 615 cm^2 among six electrodes prepared under identical conditions. The reproducibility was poor among the electrodes. The double-layer capacities measured by the electrochemical polarization method were, however, consistent, and the difference among the electrodes was much smaller. It is also possible to say, on the other hand, that the BET measurement is too sensitive to microporosity on the surface. However, this microporosity on the surface is not necessarily actively available to the electrochemical reaction in a solution. This also proves that the capacitance could serve as a better indicator of the active real surface area available to the electrochemical reaction in a solution.

TABLE 5-2
SURFACE AREA AND DOUBLE LAYER CAPACITY OF Pt ELECTRODES(130)

ELECTRODE	BET SURFACE AREA cm^2	CAPACITY $\mu F/cm^2$
1	56.7	21.4
2	271	21.8
3	615	17.3
4	407	21.5
5	80.3	18.2
6	23.9	20.7
AVERAGE	242.3	20.1

5.4.3 Impedance characterization

It has long been known that surface roughness can influence the impedance frequency dispersion of an electrode (131,132,133). In this study, it was seen in Fig.4-12 that the complex-plane plots were not perfect semi-circular

arcs, but depressed ones. The simple R-C equivalent circuit cannot fit these plots. We consider that this represents an advantage to be used for characterizing the rough surface. To deal with this problem, we must first find a suitable equivalent circuit to fit the impedance responses from the rough surface. Second, the parameters of the equivalent circuit should be related to the surface geometric conditions of that electrode. The roughness of the electrode surface can then be evaluated.

The OER was investigated by the impedance technique (134,135,136). Those results were limited to providing an impedance diagram or using double-layer capacitance to evaluate the surface. No fractal dimension of surface roughness evaluation was reported for an oxygen electrode. Our study is the first report of the impedance characterization of the oxygen electrode with a very rough surface.

5.4.3.1 Impedance responses on the rough surface

The first attempt to calculate the effect of surface roughness on impedance was made by De Levie(133). For an infinitely long and thin pore, in the absence of the faradaic process, De Levie determined that the admittance of an electrode with a rough surface was $Y=1/Z=(j\omega C)^{0.5}$, where an exponent 0.5 was introduced by the surface geometric factor. Later, on the ideally polarizable rough electrode, Nyikos and

Pajkossy(137) used an empirical relationship to describe the impedance over a wide range of frequencies:

$$Y=1/Z = \delta(j\omega)^{\beta} \qquad (5-3)$$

where Z is impedance; $j=\sqrt{-1}$; δ is a frequency independent real constant; and β is an exponent with a value between 0.5 and 1 (132). In the complex-plane plot, the equation is represented by a line rotated clockwise through an angle ϕ. The impedance data can be fitted by this equation over a wide range of frequencies. Since those works were based on an empirical relationship, a direct link between impedance responses and the surface geometric conditions cannot be established.

Let us consider the impedance responses on some of the equivalent circuits that represent the electrode system. Figure 5-2a is the equivalent circuit of the electrode system without faradaic or diffusion processes on the interface (which could be simulated on the real electrode under no polarization and strong agitation). The ac impedance response on this type of electrode system with a perfectly homogenous smooth surface is in the form of a vertical line in the complex-plane plot (Fig.5-2b). The impedance response is expressed as:

$$Z = R_s + 1/j\omega C_{dl} = (j\omega R_s C_{dl} + 1)/j\omega C_{dl} \qquad (5-4)$$

The impedance response of this type of electrode system with a rough surface is found again to be a straight line, but it is rotated clockwise through some angle ϕ (112,137,138).

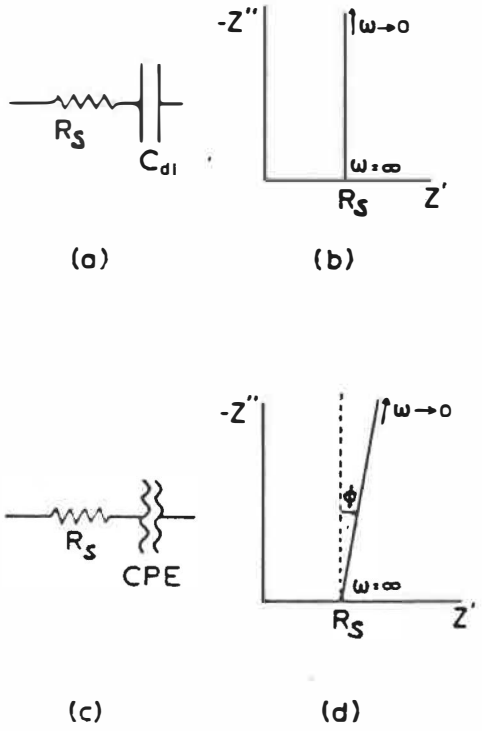

Figure 5-2 Equivalent circuits for solid electrodes and their impedance responses under the condition of no Faradaic and diffusion processes.

(Fig.5-2d). This phenomenon is also described over a limited range of frequency by the constant phase element (CPE) (108,112,137,138,148); the equivalent circuit for this electrode system is presented in Fig.5-2c, and the impedance responses can be approximated by Eq.(5-3).

An irreversible electrode reaction takes place on the surface when a polarization is applied. On a perfectly smooth homogeneous electrode surface, the system is represented by an equivalent circuit consisting of R-C and a solution resistance (R_s)(Fig.5-3a). The impedance response of this equivalent circuit follows the equation:

$$Z(\omega) = Z'(\omega) + jZ''(\omega) = R_s + R_{ct}\frac{(1 - j\omega R_{ct}C_{dl})}{1 + (\omega R_{ct}C_{dl})^2} \qquad (5\text{-}5)$$

In the complex plane, the result of this equation would be a semi-circle with a diameter R_{ct}, with the left end on the real axis with a value of R_s and the right end on the real axis with a value of R_s+R_{ct}. (Fig.5-3b).

For a rough solid electrode, a simple R-C equivalent circuit will be replaced by a distribution of similar branches parallel to the R-C branch (Fig.5-3c). The impedance response is a clockwise rotation of an "ideal" impedance diagram over some angle (ϕ), shown in Fig.5-3d, and the angle (ϕ) is referred to as the depressed angle of the semi-circular arc of the complex-plane plot. On the other hand, the rotated semi-

circular complex-plane plot suggests a lack of homogeneity on the electrode surface. This behaviour can be theoretically modelled with an equivalent circuit (Fig.5-3e), which consists of a charge transfer resistance (R_{ct}) and the (CPE). The C_{dl} in the equivalent circuit of Fig.5-3a is replaced by the CPE in Fig.5-3e. In the case of the electrode with an irreversible reaction, the presence of the CPE causes a rotation of the complex-plane axis by an angle ϕ, and the impedance of the CPE is defined in a form very similar to Eq.(5-3)(148):

$$Z_{CPE} = \frac{1}{C(j\omega)^{1-\alpha}} \qquad (5\text{-}6)$$

where Z_{CPE} is the impedance of the CPE, $\Omega\ cm^2$; C is a constant related to the electrode capacitance; ω is angular frequency, rad/s; $j = \sqrt{-1}$; and α ($=1-\beta$) is a parameter corresponding to a depression angle, which is equal to $\phi = \alpha*\pi/2$. When $\alpha=0$, $\phi=0$, C corresponds to the electrode capacitance; when $\alpha=1/2$, $\phi=45°$, C is a resistance, such as the Warburg impedance. In a limited frequency range, the depressed angle of the complex-plane plot represents the roughness on electrode surface.

With these equivalent circuits, we used the CNLS program for the curve fitting, as seen in Fig.4-12 and Fig.4-21. Is it then possible to link the parameter in the equivalent circuit to geometrical roughness on the surface? In the following section, we will see whether this kind of bridge can be established by the fractal concept.

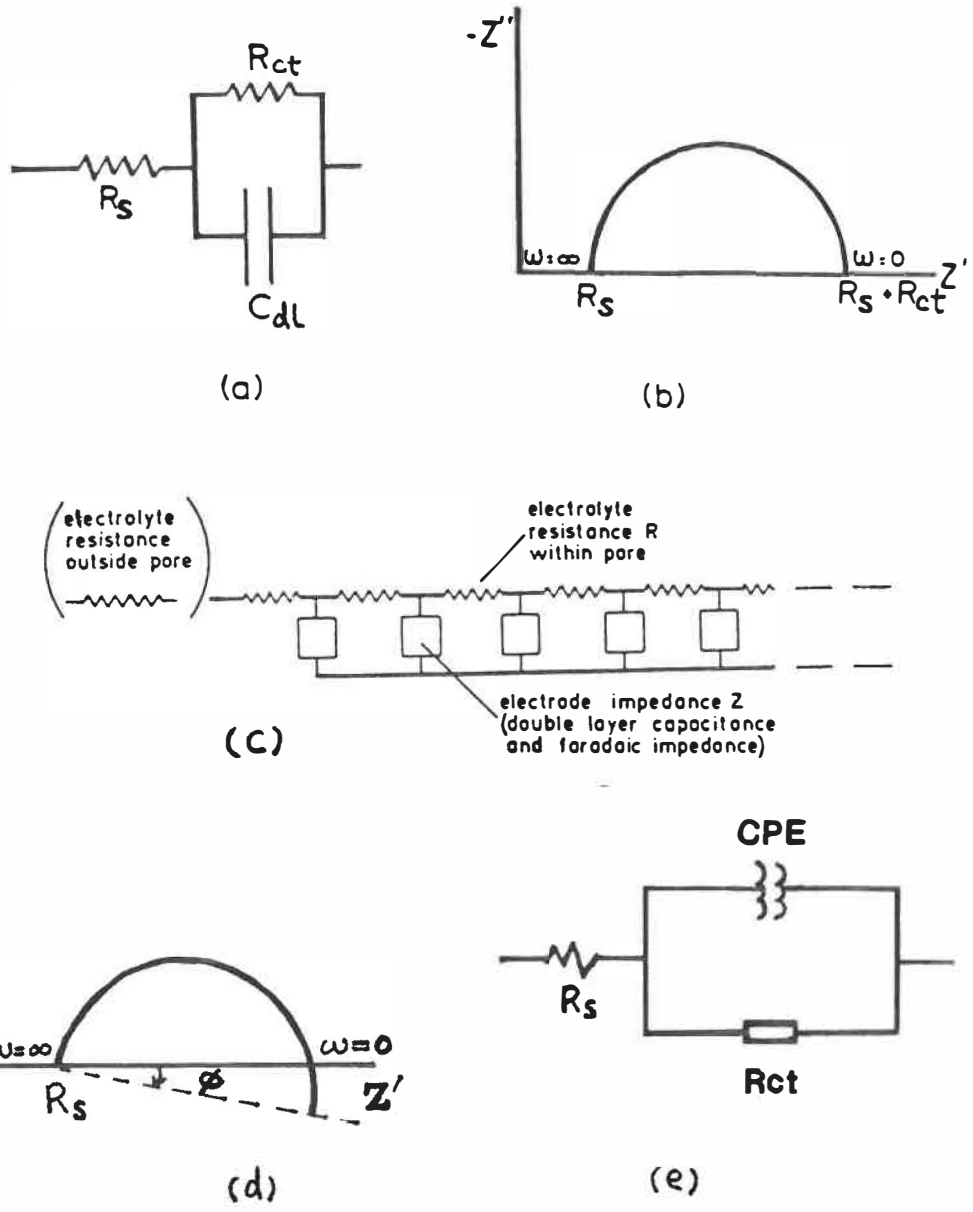

Figure 5-3 Equivalent circuit for solid electrodes and their impedance responses under polarization conditions.

5.4.3.2 Fractal magnification

It is almost impossible to relate the surface roughness to an impedance parameter by classical mathematical analysis (such as the Laplace Equation). Characterizing the random roughness without requiring a detailed description was also very difficult. The situation changed drastically recently after Mandelbrot(139) introduced the concept of the fractal magnification to description of the electrode with rough surface.

The fractal concept means that the magnification of an irregular surface has self-scaling characteristics. Figure 5-4 shows two types of magnification methods. In (b), the conventional simple method, every part in (a) is magnified, and no new structures are generated; if the magnification factor is r, a measure after magnification will be r times its original, or A'=rA; in (c), the fractal magnification not only increases the image of the original profile, but also generates new structures according to the pattern in the original profile. According to this concept, the magnification factor is r^D, where D is the fractal dimension. A measure after magnification will be $A'=r^DA$. This type of self-scaling feature is also a general form in many systems (139,140,141). Description of the surface roughness by the fractal concept gives us the essential and general image of the roughness without detailed geometrical information. This concept was

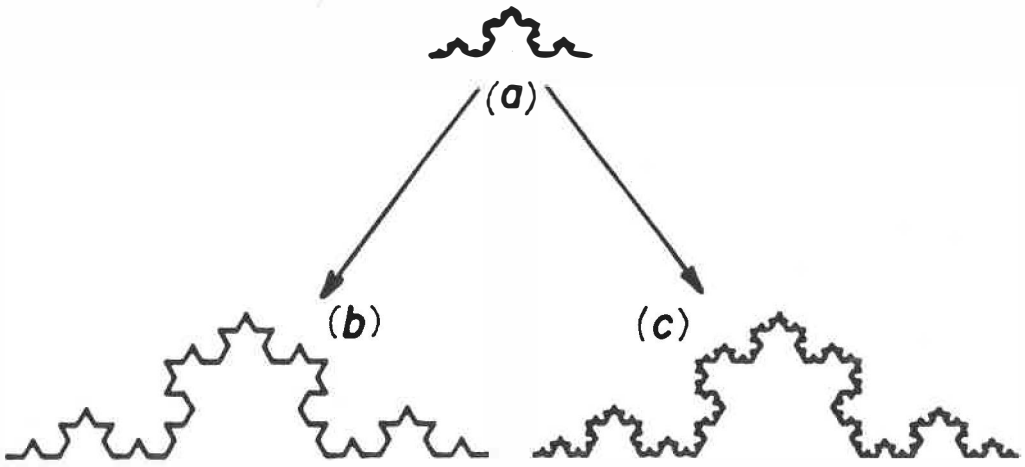

Figure 5-4 Electrode surface magnification methods: (a) rough surface profile; (b) conventional simple magnification; (c) fractal magnification.

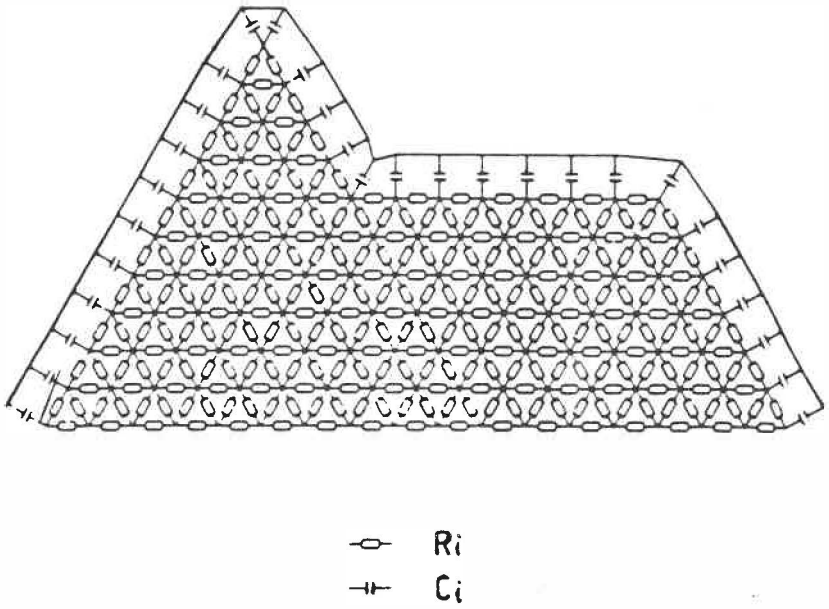

Figure 5-5 An illustration of division of the irregular surface of an electrode into small segments by the finite-difference procedure.

first applied to electrochemical problems by Le Méhauté and co-workers(140). Only recently, the fractal model of rough surface and its relation to impedance measurements have been gradually developed. The fractal model was the subject of several papers, but there have been few experimental results to confirm or verify the concept in a real electrode system with a very rough surface.

It has been found that the electrode with a rough surface has similar self-scaling characteristics (141): the surface area measured by adsorption techniques has yielded different values for different adsorbents with varied molecule sizes. Smaller adsorbents are sensitive to the fine details of the rough surface, and the apparent area thus increases. The impedance response is also closely related to the geometry, namely pore size and texture of the porous surface(142). This unique feature provides a useful measure for estimating the porosity and roughness of an electrode surface. Examples of this are given by Candy and co-workers for gold powder (143) and Raney-nickel electrodes(144).

Let us consider Eq.(5-6), $Y = 1/Z = C(j\omega)^{1-\alpha}$. At a different frequency $k\omega$, we have:

$$\frac{Y(k\omega)}{Y(\omega)} = \frac{C(jk\omega)^{1-\alpha}}{C(j\omega)^{1-\alpha}} = k^{1-\alpha} \qquad (5-7)$$

This states clearly that the ratio of the complex admittances

at frequencies ω and kω is a real number $k^{1-\alpha}$ for any scale factor. This real number is only related to the difference in frequency and the parameter corresponding to a depression angle. We assume that the electrode can be divided into many small segments by the finite-difference method, as showed in Fig.5-5. The admittance of each small segment of the electrode can be written as $Y_i=j\omega C_i/(1+j\omega R_i C_i)$(Eq.5-4), where R_i and C_i are the resistance and capacitance of the i segment on the electrode. The total admittance of the electrode is:

$$Y = \sum Y_i = \sum \frac{j\omega C_i}{1+j\omega R_i C_i} \qquad (5\text{-}8)$$

Since the interface of the rough electrode has the fractal characteristic, we assume that the rough structures are similarly self-scaling, no matter what kind of actual irregularities there are; that Y, R_i and C_i obey the scaling law, e.g., $A'=r^D A$; and that the electrode is two-dimensional. If the rough structure of the electrode is magnified by a factor of r, Y is, therefore, magnified as:

$$Y(r,\omega) = r^2 Y(\omega) \qquad (5\text{-}9)$$

Because the capacitance is proportional to the area of the electrode, when the area changes by r^D (D is the fractal dimension), the capacitance increases as:

$$C_i(r) = r^D C_i \qquad (5\text{-}10)$$

The resistance is a bulk nature, which scales up as:

$$R_i(r) = r^{-1} R_i \qquad (5\text{-}11)$$

Combining Eq.(5-10), Eq.(5-11) and Eq.(5-8), considering the

fractal magnification, we have:

$$\begin{aligned} Y(r,\omega) &= \sum \frac{j\omega C_i(r)}{1+j\omega R_i(r)C_i(r)} \\ &= \sum \frac{j\omega r^D C_i}{1+j\omega (r^{-1}R_i)(r^D C_i)} \\ &= r \sum \frac{i(r^{D-1}\omega)C_i}{1+j(r^{D-1}\omega)R_i C_i} \\ &= r\, Y(r^{D-1}\omega) \end{aligned} \qquad (5\text{-}12)$$

and we obtain:

$$\frac{Y(r^{D-1}\omega)}{Y(r,\omega)} = \frac{1}{r}$$

Thus, by considering Eq.(5-9), we have:

$$\frac{Y(r^{D-1}\omega)}{Y(\omega)} = r \qquad (5\text{-}13)$$

Comparing Equations (5-13) and (5-6) with $k=r^{D-1}$, we have:

$$r^{(1-\alpha)(D-1)} = r,$$

and therefore, $$(1-\alpha)(D-1) = 1 \qquad (5\text{-}14)$$

where D is the fractal dimension of the rough surface from the topography, and its value is between 2 and 3. As D increases from 2 to 3 (α from 0 to 1/2), the surface roughness increases. D=2 represents the purely capacitive behaviour of a smooth surface, while D=3 represents a porous surface, as demonstrated by De Levie(133). It has been found that the fractal dimension D provides a good indication of surface roughness (137,138,145,146,147,148). The α, which is related to the depressed angle (ϕ) in the complex-plane plot ($\phi=\alpha*\pi/2$), can be obtained from the impedance measurements. It is linked to the geometric parameter of the electrode surface

by Eq.(5-14). Both α and D offer a simple comparison between surfaces with widely different morphologies. This model is apparently obtained when the charge transfer reaction (OER) is not anticipated, and the impedance responses are assumed to reflect the surface inhomogeneity or the fractal geometry without the reaction interference. In this sense, a higher D on the electrode would be a good indication of a very rough surface. Later, Mulder and Sluyters(148) and De Levie(138) developed a model for the electrode with irreversible reactions, that is the depressed angle of the complex-plane plots.

5.4.3.3 Fractal dimension D

Using log(-Z) vs. log(ω) plots (Fig.5-6), the fractal exponent $1-\alpha$ and fractal dimension D can be determined. The results are listed in Table 5-3. The values of D on the Ni, Co and Fe composite-coating electrodes are 2.07, 2.18 and 2.30, respectively, as predicted in Eq.(5-3). The highest D appears on the Fe composite-coating electrode, which is consistent with the results from SEM and polarization characterizations.

TABLE 5-3
FRACTAL DIMENSION FROM IMPEDANCE MEASUREMENTS ON COMPOSITE-COATING ELECTRODES

ELECTRODE	$1-\alpha$	D
Ni Composite	0.931	2.07
Co Composite	0.847	2.18
Fe Composite	0.770	2.30

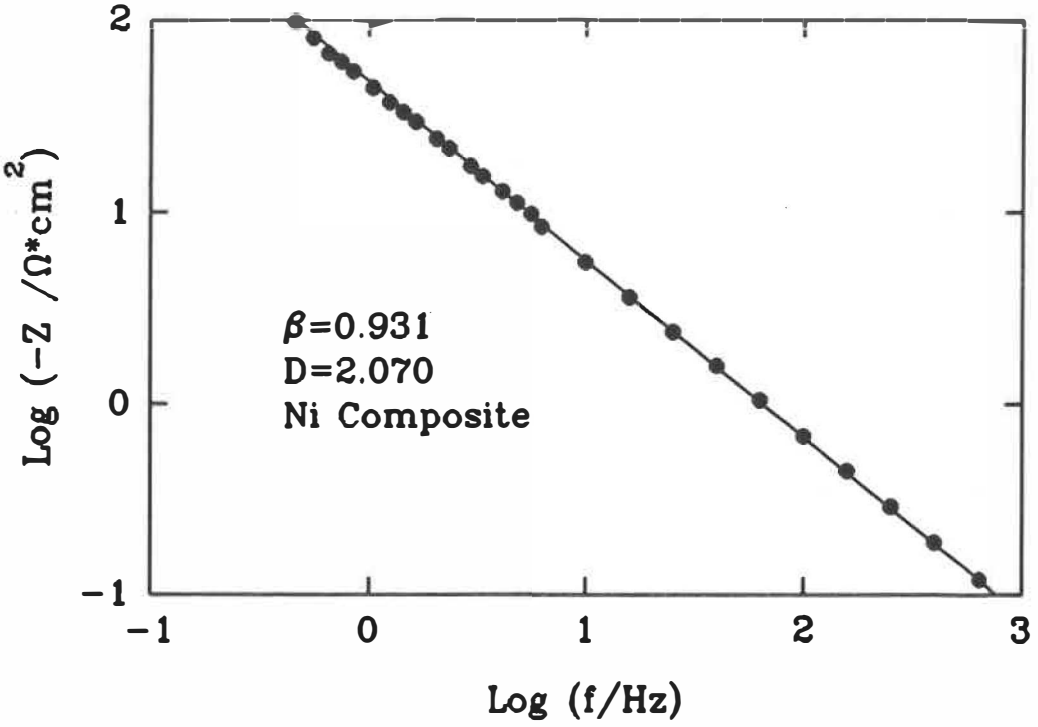

Figure 5-6 Log(-Z) vs log(ω) presentation of the impedance data of the Ni composite-coating electrode.

5.4.3.4 Depression angle ϕ

In the frequency range from 10^{-3} to 10^{5} Hz, only one semi-circle with a depression angle was obtained on all electrodes tested for the OER. The depression angle is the frequency-independent parameter; its value is only related to surface inhomogeneity. The behaviour of the depressed semi-circular arc is an expression of the CPE under limited frequency range(148). It suggests inhomogeneity on the surface. The SEM examinations suggest that roughness constitutes the major surface inhomogeneity on the composite-coatings, which is also responsible for the behaviour of the depressed angle on the complex-plane plot.

An increase in the ϕ as a function of the overpotential from 200 to 300 mV was observed on the composite-coating electrodes. A typical example was presented in Fig.4-17 for the Fe composite-coating. De Levie(138) pointed out that the depressed angle is a characteristic of the interfacial morphology, and that it should therefore be kept constant from one potential to another as long as the interfacial texture does not change. However, in reality, the value of ϕ varies at different potentials. This phenomenon was also reported by Brug and co-workers(112), but without an explanation. A possible explanation for the changes in ϕ is that high polarization (high η) activates the internal surface of small pores for the reaction, thus modifying the total surface

texture available to the reaction. Consequently, there are more fractionally rough surface areas becoming actively available for the reaction, and consequently, an increase in the depressed angle in the complex-plane plot. In this way, the effective surface pore size distribution on the electrode surface can be appraised by the changes in the value of ϕ with respect to the applied potential. Another possibility is that the gas bubble screen effect and the diffusion process become significant at high overpotentials. The release of gas bubbles interferes with the charge transfer process on the electrode, and the impedance responses on the electrode change. The equivalent circuit used for curve fitting should be modified to accommodate the diffusion impedance.

5.4.3.5 Impedance phase angle θ

The impedance phase angle θ is a frequency-dependent parameter; its value is determined by the relation $tg\theta=Z''/Z'$, as shown in Fig.4-12. Although the dependence of impedance on frequency was similar among the tested electrodes (Fig.4-12), the value of the θ at the same frequency varied among the Ni, Co and Fe composite-coating electrodes. This was demonstrated clearly in Fig.4-14. As the surface roughness increased, the position of the frequency corresponding to the maximal θ moved in the direction of low frequencies (about 160 Hz on the Ni electrode, 10, 4 and 3 Hz on the Ni, Co and Fe composite-coatings, respectively. See Fig.4-14). The intensity of the

phase angle peak gradually wore away. This phenomenon is generally observed on the electrode with a rough surface (139, 141,149). In this way, the frequency related to the maximal impedance phase angle can be used to characterize the effective surface area on an electrode.

5.4.3.6 Surface roughness factor S

As discussed in Section 5.4.2, the double-layer capacitance can serve as a relative measure of the effective real surface area on an electrode. For comparison of electrodes tested under the same conditions, it indicates the effective real surface area available for an electrochemical reaction in solutions. A 20 $\mu F/cm^2$(92) capacitance on the liquid Hg was used to calculate the surface roughness factor (S) on the composite-coating electrodes, which is given by the ratio $S=C_{dl}/20$. The values of S were found to be $1.75x10^3$, $1.6x10^4$ and $5.5x10^4$ for the Ni, Co and Fe composite-coating electrodes, respectively. By comparison, the surface roughness factor S, obtained under the same conditions and method, was equal to 50 and 5 on the polished Ni and smooth Pt sheet. It is evident (see Table 4-8) that the Fe composite-coating has the highest surface roughness factor, as much as 10^4 times higher than that on the smooth Pt electrode. This result confirms that a highly rough surface on the composite-coating electrodes is mainly responsible for the improvement of the catalytic activity for the OER.

5.5 OER MECHANISMS

5.5.1 OER mechanism on Ni electrode

A generally accepted mechanism for the OER on the Ni electrode(17) consists of the following steps:

$$OH^- \rightarrow (OH)_{ads} + e^- \quad (5\text{-}15)$$

$$OH(ads) + OH^- \rightarrow (O^-)_{ads} + H_2O \quad (5\text{-}16)$$

$$2\beta\text{-}NiOOH + (O^-)_{ads} \rightarrow 2NiO_2 + H_2O + e^- \quad (5\text{-}17)$$

$$NiO_2 + (OH)_{ads} \rightarrow \beta\text{-}NiOOH + (O)_{ads} \quad (5\text{-}18)$$

$$2(O)_{ads} \rightarrow O_2 \quad (5\text{-}19)$$

Any one of these steps may be the rate-determining step (RDS). Some data(14,28) support the charge transfer step (Eq.5-17) as the RDS, while Conway and co-workers(82) suggest that the b of about 50 mV/dec could correspond to the final oxygen bubble recombination step (Eq.5-19) at appreciable coverage of adsorbates under activation adsorption conditions. However, there is no definitive conclusion on this matter. The chemical composition of Ni deposited from various baths was metallic Ni (Ni>98 wt% by EDS). The OER mechanism on Ni electrodes is identical if the characterization conditions are kept the same. Consequently, b should be the same. However, that is not what we obtained. A Tafel slope of 50 mV/dec was obtained on Ni electrodes deposited in the chloride and the acetate baths. This indicates that the chemical reaction step (Eq.5-16), the second charge transfer step (Eq.5-17) and the oxygen bubble formation step (Eq.5-19) or a combination of these steps in certain circumstances with a surface coverage could be the RDS of the OER. However, a Tafel slope of 70 to

85 mV/dec for Ni deposited in the chloride-sulfate, sulfate and the sulfamate baths could not correspond to any one of the reactions (Eq.5-15 to 5-19) above. The value of b higher than 60 mV/dec may suggest either that the fractional coverage of oxygen on the surface or that the first electron transfer step, the discharge of OH^- ions (Eq.5-15) with b=120 mV/dec, is involved in determining the rate of the OER. It is suggested from our results that the surface microstructure and preferred crystal orientation on the Ni electrode alter the reaction route and path, and that this made the difference in the OER mechanisms on the Ni electrodes deposited from various baths. It should be noted that the Tafel slope on nickel electrodes deposited in the chloride bath was the lowest among the electrodes.

5.5.2 OER mechanism on composite-coating electrodes

The Tafel slopes (see Table 4-7) of the polarization curves are in the range of 50 mV/dec on the Ni electrodes and 40 mV/dec on Co and Fe composite electrodes. This suggested that the RDS on these electrodes could be different. According to Krasil'chikov(75), the suggested OER mechanism and paths in alkaline solution are as follows:

$$OH^-(ads) \rightarrow OH(ads) + e^- \qquad b = 2.3*2RT/F \qquad (5\text{-}20)$$

$$OH(ads) + OH^- \rightarrow O^-(ads) + H_2O \qquad b = 2.3*RT/F \qquad (5\text{-}21)$$

$$O^-(ads) \rightarrow O(ads) + e^- \qquad b = 2.3*2RT/3F \qquad (5\text{-}22)$$

$$2O(ads) \rightarrow O_2 \qquad b = 2.3*RT/4F \qquad (5\text{-}23)$$

where the discharge of OH^-ions step(Eq.5-20) has b=120 mV/dec,

formation of H_2O step (Eq.5-21) b=60 mV/dec, discharge of O^- ions step (Eq.5-22) b=40 mV/dec and oxygen evolving step (Eq.5-23) b=15 mV/dec. The Ni electrode with b=50 mV/dec suggests that the RDS is neither the OH^-discharging(Eq.5-20) nor the O_2 formation step(Eq.5-23). A b=50 mV/dec could also represent the formation of H_2O (Eq.5-21) as the RDS under a slight modification of the Tafel slope caused by the surface roughness. It is understood that adsorption species on electrode surfaces(5) and surface morphology changes(150) affect and modify the slope of the polarization curve. On the Co and Fe composite-coating electrodes, however, with b=40 mV/dec, the RDS could be the discharge of O^- ions (Eq.5-22).

Conditions for deposition of the Ni composite-coating are the same as for the Ni deposit, except for the presence of metallic powders in the bath. The co-deposition of the Ni^{+2} and metallic powders produces a highly rough and porous surface coating. Table 4-7 shows that the i_{300} is 1.5 mA/cm^2 on the Ni electrode and 15 mA/cm^2 on the Ni composite-coating electrode. This improvement was initiated by a highly rough surface, which was prepared with the addition of 2 g/l of Ni powder to the deposition bath in composite-deposition. An increase in the real surface area yields a lower overpotential and higher current density on the electrode. The superior performance was displayed on the composite-coating electrode prepared with Fe powders in the deposition bath: the observed

i_{300} was 625 mA/cm^2 on the Fe composite-coating, which is more than 400 times larger than that on the Ni electrode and 40 times more than on the Ni composite-coating. With respect to reductions in overpotential, 246 mV was registered under 100 mA/cm^2 on the Fe composite-coating electrode, which is about 150 mV lower than that on the Ni electrode and 116 mV lower than that on the Ni composite-coating electrode. It should be noted that the Tafel slope of the Co and Fe composite-coating electrode is in the range of 40 mV/dec, which is lower than for the Ni electrode. The estimated contribution of low b to the reduction of η is around 20 mV ($\Delta\eta=\Delta b*Logi=0.01*Log100=0.02V$). This is still a minor consequence, compared with 150 mV. It may be concluded, therefore, that a highly rough surface on the composite-coating electrode has the most impact in ameliorating electrode performance.

5.6 HER ON COMPOSITE-COATING ELECTRODES

5.6.1 Surface roughness and electrode activity

In general, the composite-coating electrodes are more active for the HER than the conventional electroplated Ni electrode. The overpotential on the composite-coating electrode is lower than that on the Ni electrode. The improvement of the electrocatalytical property should be attributed to modification of the chemical composition of the composite-coating material, namely nickel, cobalt and iron

transition metals, and/or to an enlarged surface area on the electrode. However, the most significant difference between the Ni deposit and the Ni composite-coating, observed by SEM, is in the surface roughness, as shown in Fig.4-9. Results in Table 4-9 show that the i_{-200} was less than 1 mA/cm^2 on the Ni electrode and 5.45 mA/cm^2 on the Ni composite-coating electrode. A more than 20 mA/cm^2 on the Fe composite-coating electrode shows that it is the most active electrode.

An improved electrocatalytical activity for the HER on the Ni electrode has been achieved by coating it with Fe(151). The improvement was attributed to the change in the electrode surface morphology, and consequently, an increase in the electrode real surface area. It was concluded that the enhanced electrocatalytical activity was not due to the introduction of active sites of iron metal(151). In the present study, it was found that iron powders in the deposition bath promoted uneven deposition, making the surface of the Fe composite-coating rougher than the surface of the Ni composite-coating. Fig.4-19 demonstrates that the i_{-200} is related to the coating compositions. As the ratio of Fe/(Fe+Ni) increases, the i_{-200} increases, and the electrode activity increases. The highest i_{-200} was obtained on the electrode prepared in the bath with only iron powder. This confirms that there was no active site effect on the electrode prepared in the bath with nickel and iron powders. The SEM

micrograph examinations proved that the Fe composite-coating electrode had the highest surface roughness among the electrodes prepared with the mixed Ni-Fe powders. Hence, the results support the conclusion that this electrode is the most active among the mixed Ni-Fe composite-coating electrodes. Similar results were obtained on the Co composite-coating electrode, but the Co content on the composite-coating was much higher, due to a stronger phenomenon of anomalous deposition(109). Although the Co powders were co-deposited with Ni^{+2} with less difficulty than the Fe powders, the Fe powders were more effective in creating a highly rough surface. This is why the Fe or the Co composite-coating electrode has a surface with rougher structures than the Ni composite-coating electrode (see Fig.4-9).

5.6.2 Tafel slope

It has been seen that the composite-coating electrodes have a lower b and a higher i_{ex} (Table 4-9) than the Ni electrode. The 120 mV/dec of b obtained on the Ni electrode agrees with the Volmer-Tafel mechanism of the HER, which suggests that the RDS is the Volmer discharge step followed by the electrochemical desorption recombination step(58). However, identification of the reaction mechanism by the Tafel slope is only possible in very limited cases. In most cases, the function of surface coverage of the adsorption species will affect and modify the value of the Tafel slope(5).

Furthermore, due to surface morphology changes leading to modifications in reaction kinetics(150), the Tafel slope on an electrode with an irregular surface will be different from that on the electrode with a flat surface.

The importance of the Tafel slope lies in the fact that it indicates the rate of change in the current density with overpotential. At 25°C, the Tafel slope for the Ni or Co composite-coating electrodes is in the range of 90 mV/dec, and 78 mV/dec for the Fe composite-coating electrode. Since these values are lower than 90, it is apparent that a higher HER rate can be obtained on the composite-coating electrodes without a higher increase in overpotential on the electrode.

Between 25 and 75°C, the highest increase of b was observed on the Fe composite-coating electrode (from 78 to 134mV/dec); b on the Ni electrode remained the same, while there was a slight increase on the Ni composite-coating electrode. Temperature had no effect on the Tafel slope for the Co composite-coating electrode. Different increase in the b on the composite-coating electrodes reflects the difference of activation for the reaction. The highest increase on the Fe composite-coating electrode means activation for the HER is difficult on that electrode. This gives an additional confirmation that the improvement of electrocatalytical activity on the Fe composite-coating electrode is achieved by

high roughness of the surface, and not by the activation.

It should be mentioned that compared with the Ni electrode, improvement in the electrode performance for the OER on the Fe composite-coating electrode is superior to that for the HER on the same electrode. Only a 20-times increase in i_{-200} was observed on the Fe composite-coating for the HER; whereas about 400-times increase in the i_{300} on the Fe composite-coating was achieved for the OER. This confirms that the kinetics of the OER is more dependent on electrode surface conditions than for the HER.

Boudart(60) has discussed electrode reactions which are "insensitive" or "sensitive" to the surface structure of an electrocatalyst. The OER proceeds on most materials with a high overpotential at low current densities. A large variation in overpotential was collected on different materials(14). Even on the same material, as a consequence of different surface preparation procedures, various data were displayed. The OER is defined as a reaction which is "sensitive" to electrode surface structures. In other words, optimization of the electrode surface condition to achieve maximal reactivity for the OER is extremely important.

5.6.3 Surface roughness indicated by depressed angle

The depressed angles are 12.9, 15.8 and 18.8 on the Ni,

Co and Fe composite-coating electrodes, respectively. Values of ϕ up to 15° were previously reported(112), and it was believed that the diffusion of some adsorbing components was not involved. A possible explanation in this particular case is that on a highly rough surface, such as the Co or the Fe composite-coating, diffusion of the reactant in the electrode and the release of hydrogen bubbles outside the pores could be difficult, thus causing some additional rotation of the impedance complex-plane plots. The potential oscillation (see Fig.4-18) at high current densities observed on the composite-coating electrodes could be caused by the release of hydrogen bubbles from the rough electrode surface.

5.6.4 Surface roughness factor under conditions for the HER

In the case of the HER, the surface roughness factor S was estimated, as in the case of the OER. Table 4-11 shows these values to be 2.1 for the Ni electrode, and 70, 60 and 200 for the Ni, Co and Fe composite-coating electrodes, respectively. The exchange current density (based on geometric surface area) divided by the surface roughness factor gives the real exchange current density, which indicates the true electrocatalytical nature of an electrode for the HER. Thus, values of the i_{ex}, based on the unitary real surface area, are 5.7×10^{-7}, 1.2×10^{-6} and 2.5×10^{-7} A/cm^2 on the Ni, Co and Fe composite-coating electrodes, respectively, which are lower than on the Ni electrode, 7.1×10^{-6} A/cm^2. We can therefore

reach the conclusion that an increase in the real surface area may be a primary reason for the improvement of the electrode activity for the HER on the composite-coating electrodes, especially on the Fe composite-coating electrode. Moreover, based on the results of double-layer capacitance, the real surface areas on the Ni, Co and Fe composite-coating electrodes are 70, 60 and 200 times larger than that on the Ni electrode. The i_{-200} (based on the geometric areas) are 6, 9 and 20 times as large as that on the Ni electrode, which is about one-tenth of what would be expected based on the surface roughness factor. It can be assumed that the effective surface areas on the composite-coatings are one-tenth of that revealed by C_{dl}. This could be related to the surface coverage by hydrogen bubbles and/or to the gas diffusion overpotential on the composite-coating electrodes.

It is noteworthy that the S for the HER is much lower than the S for the OER. A different capacitive charging for the OER and HER may result in a different C_{dl}. Therefore, it is not surprising to find out that there are differences among capacitances obtained for different reactions. The questions we should ask are why there should be such a large difference and which C_{dl} (for the OER or the HER) reflects the true interface area? At this moment, it is assumed that the C_{dl} obtained under the OER serves as an indication of the real surface area available for the OER, but not for the HER.

5.7 GENERAL DISCUSSION

5.7.1 Comparison of electrode performance for the OER

Evaluations of the performance of the electrode prepared by various methods were made by comparing several kinetic parameters, such as i, η, i_{ex}, b and α, and other factors such as the effective real surface area and the surface roughness factor of an electrode. Complications in evaluating electrode performance by the kinetic condition, polarization potential, reaction type and parameter dependence made it impossible to have an absolute appraisal of the electrode performance under a wide range of conditions. Only a relative comparison of the activity under certain specified conditions or terms was achieved. The Ni electrode prepared from the chloride bath has a low Tafel slope (b_L=50mV/dec) and overpotential (η_{100}=396mV). It is more active than the electrodes deposited from other baths. However, the evaluation based on the i_{ex} shows that the Ni electrodes prepared from the sulfate and sulfamate baths have a higher exchange current density ($i_{ex}=10^{-3}$ mA/cm^2), and are therefore more active than the others.

In the case of composite-coating electrodes, the values of the surface roughness factor, S, estimated under conditions for the HER was 2.1 for the Ni electrode, 70, 60 and 200 for the Ni, Co and Fe composite-coating electrodes, respectively. They are much lower than ones obtained for the OER (50,

$1.75x10^3$, $1.6x10^4$ and $5.5x10^4$ for the Ni electrode, Ni, Co and Fe composite-coating electrodes, respectively).

It was found that a simple and practical comparison of the electrode performance can be made by comparing current densities (i) under the same overpotential (η) and *vice versa*. Table 5-4 summarizes the performance of the various electrodes for the OER. The overpotential was measured under 100 mA/cm^2, while the apparent current density was obtained under an overpotential of 300 mV.

TABLE 5-4
COMPARISON THE ELECTROCATALYTICAL PERFORMANCE FOR THE OER ON ELECTRODES STUDIED

ELECTRODE	η_{100} (mV)	i_{300} (mA/cm^2)
Ni Electrode	396	1.5
Ni-Ir(6wt%)	330	30
Ni-Ru(2.2wt%)	345	20
Ni Composite	362	15
Co Composite	299	109
Fe Composite	246	625

The lowest η, namely 246 mV, was displayed on the Fe composite-coating electrode, and all other electrodes showed a η_{100} less than that on the Ni electrode, i.e., 400 mV. Looking at the apparent current density, however, a significant increase was observed on the composite-coating electrodes. The highest current density under 300 mV of overpotential, 625 mA/cm^2, was presented by the Fe composite-coating electrode, prepared by composite deposition from the bath containing 2 g/l of iron powders and 240 g/l of

$NiCl_2 \cdot 6H_2O$. This value is about 400-times higher than that on the Ni electrode. The Ni-Ir(6wt%) electrode achieved a current density as high as 30 mA/cm^2 under 300 mV of η, which is 20-times higher than that on the Ni electrode for the OER.

5.7.2 Mechanisms for improving electrode activity

Understanding the mechanism for improving electrode performance would make it easier to fabricate a better electrode for electrochemical reactions. The techniques for increasing electrode activity have been discussed in Section 2.3. Among them, surface modification and the increasing the real surface area have been adopted in this study.

The improvement of the Ni-Ir and Ni-Ru electrode performance for the OER has been related to the increase in the surface concentration of the active site on the oxide layer, reported by Trasatti and O'Grady(15). This study maintained that the shifted oxidation potential was responsible for the increase in catalytic activity effected by introducing Ru or Ir elements to the Ni oxide layer. The active site theory could support the view that inclusion of Ir or Ru may favour the formation of active sites, but it does not indicate how the active site functions in promoting the OER kinetics, since the activation energy level on Ru or Ir site cannot be measured separately.

In this study, the OER overpotential was divided into two parts: $\eta = \Delta E_{ox} + \Delta E_{O2}$ (where ΔE_{ox} is a polarization potential between the reversible oxygen potential (1.23 V) and the electrode surface oxidation potential (P1) and ΔE_{O2} is the difference of the potential between the OER and the peak (P1) potential, (see Fig.5-1). The lowest ΔE_{ox} on the Ni-Ir oxide electrode indicates that the catalytically active oxide layer on the Ni electrode could be developed more easily by mixing with Ir oxide than with Ru oxide. This also means that Ni-Ir oxide may be more stable than Ni-Ru oxide. The lowest ΔE_{O2} on the Ni-Ru oxide electrode means that the OER could proceed on this surface faster, and that its electrocatalytical power is high. These results suggest that although Ru and Ir are both beneficial for improving the catalytic property of the Ni electrode, the mechanism for improving the performance of the Ni electrode with Ir differs from that with Ru: Ir decreases Ni oxidation potential while Ru lowers the OER overpotential on oxidized surface. This constitutes the new contribution to the understanding of transition-metal based oxide electrocatalysts for the OER.

A new process, composite-deposition, for fabrication of electrodes with very rough surfaces, was studied. The improved catalytic properties of the composite-coating could result from surface activation and/or the utilization of highly rough and porous surfaces. SEM examinations showed that the

composite-coating electrode has a visibly rough surface, and the coating roughness was increased when the electrode was prepared with Ni, Co or Fe powders in the bath. Impedance characterizations disclosed that the fractal dimension, the depression angle of complex-plane plot and the surface roughness factor obtained by double-layer capacitance measurement on composite-coatings were much higher than that on the Ni electrode. These measurements suggest that the high real surface areas on the rough electrode surfaces were responsible for the improvement in electrode performance for the OER and the HER. This understanding was confirmed by polarization measurements in our tests. We first reported in this field (152,153) that the value of the depression angle of the complex-plane plot was not a constant as the η changed, and the double-layer capacitance varied depending on the OER and the HER.

5.7.3 Evaluation of methods for electrode preparation

It has been demonstrated that Ir or Ru on the Ni electrode increases electrode activity. As can be seen from Fig.4-6, for both Ni-Ru and Ni-Ir electrodes, the beneficial effects obtained are more significant for the first 1% of addition of the transition elements. With further additions, Ir increases the OER current density to a small extent; in the case of Ru, the selective corrosion of the Ru component in the oxide layer on the surface causes a loss in electrocatalytical

property. The Ni-Ir mixed oxide electrode was much more stable; however, this element is very expensive, and addition of a high percentage of Ir to the Ni electrode is not economically practical. Furthermore, the compact-solid surface on the Ni-Ir electrode with a low real surface area cannot compete with the composite-coating electrode (see comparison in Table 5-4). It should be pointed out that based on the unitary surface area, the electrocatalytical activity on the Ni-transition metal oxide electrode is superior to that on the composite-coating electrode.

The advantages of simplicity, easily controlled conditions and low cost of composite-deposition make the composite-deposition method attractive and effective for fabricating electrodes with very rough surfaces. For the gas-evolving electrode, the effectiveness of the rough surface available to the electrochemical reaction is not satisfactory, as demonstrated by the composite-coating electrodes for the OER and HER (see the discussion in Sections 5.4 & 5.6). It has been estimated that the effective surface area for the HER on the composite-coating electrode is one-tenth of that revealed by the C_{dl}. Surface activation for the OER on the composite-coating electrode by electrochemical oxidation has a limited effect in improving its activity. If the activity on the composite-coating electrode is counted on a unitary basis, a low catalytic activity would be obtained. Increase of the

unitary catalytic activity (pure electrocatalytical activity) and improvements in the effectiveness of the rough and porous surface for electrochemical reactions would further improve the electrocatalytical performance of the composite-coating electrode.

CHAPTER 6

CONCLUSIONS

The Ni electrode can be prepared in electrolytes with various anionic compositions. SEM micrographs showed that the electrodes have coarse surfaces, due to the high deposition current density employed. The surface of Ni deposited from the chloride bath was covered with microcracks. Those microcracks resulted in a larger real surface area on the electrode. Ni deposited from the chloride bath has a {110} preferred orientation, which could favour the OER kinetics.

Electrochemical characterizations in 5M KOH solution at 25°C have showed that the electrode deposited from the chloride bath, with a low Tafel slope (50 mV/dec) and an overpotential of 396 mV at 100 mA/cm^2, is the most electrocatalytically active electrode for the OER. On the basis of the ac impedance measurements, this electrode has the highest real surface area and the lowest charge transfer resistance among Ni electrodes deposited from various baths. The optimized i_{dp} in chloride bath was 100~300 mA/cm^2.

The electrocatalytical activity of the Ni electrode can be improved by alloying the Ni with transition metals. A practical method for preparing the Ni-Ru and Ni-Ir electrodes is by co-deposition. Electrochemical characterizations showed

that the presence of transition metals (Ru or Ir) in the mixed oxide layer of Ni electrodes lowered the overpotential and increased current densities. An overpotential decline of 30 or 40 mV (under 20 mA/cm^2) was observed on Ni-transition electrodes. The current density under an overpotential of 0.4 V on the Ni electrode prepared by co-deposition with Ru or Ir was increased by 3-times with 2.2 wt% Ru and 6-times with 6.0 wt% Ir, respectively.

Cyclic voltammetric studies showed a surface oxidation peak before the OER peak. The OER on Ni-based electrodes in a 5M KOH solution occurs only after oxidation of the electrode surface. The addition of Ru or Ir changed the surface oxidation peak potential, which was determined by the cyclic voltammetric technique and thermodynamic calculations. The OER overpotential may be divided into two parts: $\eta = \Delta E_{ox} + \Delta E_{O2}$. ΔE_{ox}, which characterizes the peak potential, was the lowest in the case of the Ni-Ir mixed oxide; ΔE_{O2}, which represents the potential difference between the peak and the OER, was the lowest in the case of the Ni-Ru mixed oxide. This suggests that the mechanism of improving the performance of the Ni electrode with Ir differs from that with Ru: Ir decreases the Ni oxidation potential, while Ru lowers the overpotential on the oxidized surface. However, the presence of either Ru or Ir is beneficial for improving the catalytic properties of the Ni electrode.

The beneficial effect on electrode activity of the OER was obtained with only a small quantity of Ru (<1 wt%). A large quantity of Ru in the Ni-based electrode resulted in a selective dissolution of Ru on the electrode surface. Increasing the Ru content in the Ni-Ru electrode resulted in an increase in electrode corrosion in the 5M KOH solution. The electrode stability tests showed that the corrosion resistance of the Ni-Ir oxide was high, and it retained its good electrocatalytical property for at least 24 hours in the long-term test.

Electrolytic composite-deposition is an effective and attractive method for fabricating electrodes with a highly rough surface in industries. Electrochemical oxidation had a limited effect in surface activation of the composite-coating for the OER. Electrochemical characterizations, including polarization and impedance measurements, were correlated and they confirmed that Ni, Co and Fe composite-coatings had a very large real surface area. The greatest surface roughness appeared on the Fe composite-coating electrode, and it gave the best performance for the OER and HER in the 5M KOH solution at 25°C.

AC impedance characterizations were carried out on the composite-coating electrodes. The impedance spectra were collected in the frequency range from 10^{-3} to 10^{5} Hz under

conditions for the OER and HER. The electrode impedance behaviour was theoretically modelled with an equivalent circuit consisting of a R_{ct} and the CPE. Experimental data for the OER and HER corresponded very well with the CNLS curve fitting with the equivalent circuit. The results showed that the values of the depression angle of the complex-plane plot were not constant as the overpotential changed; and the double-layer capacitances varied depending on the reaction (OER or HER). It is possible to use the impedance phase angle (frequency-dependent parameter) and the depressed angle of the complex-plane plots (frequency-independent character) for characterizing the electrode with a highly rough surface.

REFERENCES

1. R.L. LeRoy, J. Hydrogen Energy, 8, 401-417 (1983).

2. A. P. Brown, J. H. Melsenhelder and N. P. Yao, Ind. Eng. Chem. Prod. Res. Dev., 22, 263 (1983).

3. R.W. Bartlett and D.E. Malmquist,J. Metals,36, 45 (1984).

4. Battelle Columbus Laboratories, "A Survey of Electrochemical Metal Winning Processes", Argonne National Laboratory Report ANL/OEPM-79-3, Argonne, Illinois, USA (1979).

5. B.E. Conway and L. Bai, in "Proceedings of the 4th Canadian H_2 Workshop", Canadian Hydrogen Association, Nov.1-2, (1989), Toronto Canada.

6. K. Kinoshita, "Electrochemical Oxygen Technology", John Wiley & Sons, Inc., N. Y. (1992).

7. J. St-Pierre and D.L. Piron, J. Appl. Electrochem., 16, 447 (1986).

8. D.L. Piron, in "Electrochimie de Base pour Ingénieurs", Ecole Polytechnique de Montréal, Montréal Canada (1979).

9. D. Pletcher, J. Appl. Electrochem., 14, 403 (1984).

10. A.J. Appleby, in "Electrocatalysis Comprehensive Treatise of Electrochemistry", Vol.7, p.173, Plenum Press, N.Y. (1983).

11. E. Yeager, in "Electrochemistry in Industry", Ed. by U. Landau and E. Yeager, Plenum Press, N. Y. (1982).

12. A. Damjanovic, in "Modern Aspects of Electrochemistry", Vol.5, p.369, Ed. B. E. Conway and J. O'M. Bockris, Plenum Press, N.Y. (1969).

13. S. Trasatti, Electrochim. Acta, 29, 1503 (1984) and 32, 369 (1987).

14. S. Trasatti and G. Lodi, in "Electrode of Conductive Metallic Oxide", Part B, p.521-626, Ed. S. Trasatti, Elsevier Sci. Pub. Co., N. Y. (1981).

15. S. Trasatti and W. E. O'Grady, in "Adv.in Electrochem. and Electrochem. Eng.", Vol.12, p.177, Ed. H. Gerischer and C. W. Tobias, John Wiley & Son, N. Y. (1981).

16. M. R. Tarasevich et al., in "Comprehensive Treatise of Electrochemistry",Vol.7, p.301, Plenum Press, N.Y.(1983).

17. J.P. Hoare, "The Electrochemistry of Oxygen", Intersci. Pub., N. Y. (1968).

18. J.P. Hoare, in "Advance in Electrochemistry and Electrochemical Engineering", Vol.6, Ed. P.Delahay, Intersci. Pub., N. Y. (1967).

19. A.J. Appleby, in "Modern Aspects of Electrochemistry", Vol.9, p.369 Ed. B. E. Conway and J. O'M. Bockris, Plenum Press, N. Y. (1974).

20. J.J. MacDonald and B.E. Conway, Proc. Roy. Soc., London A269, 419 (1962).

21. E.W. Brooman and T.P. Hoar, Platinum Metals Rev.,9, 122 (1965).

22. A. Damjanovic, A. Dey and J. O'M. Bockris, J. Electrochem. Soc., 113, 739 (1966).

23. A. Damjanovic, M. L. B. Rao and M. Genshaw, ASTIA Rept. No. AD 431148, Sept. (1963).

24. R.Kötz and S.Stucki, J.Electrochem.Soc., 132, 103 (1985).

25. M. H. Miles, J. Electroanal. Chem., 60, 89 (1975).

26. J. O'M Bockris and S. Srinivasan, in "Fuel Cells, Their Electrochimstry" Ch.8, McGraw-Hill Book Co., N.Y.(1969).

27. M.H. Mill, G. Kissel, P.W.T. Lu and S. Srinivasan, J. Electrochem. Soc., 123, 332 (1976).

28. P.W.T. Lu and S. Srinivasan, J. Electrochem. Soc., 125, 1416 (1978).

29. P.W.T. Lu and S. Srinivasan, J. Electrochem. Soc., 125, 265 (1978).

30. J.C. Batejue Nadesan and A.C.C. Tseung, J. Electrochem. Soc., 132, 2957 (1985).

31. K. Elbs and J. Korsell, Z. Elektrochem., 8, 760 (1902).

32. J. C. Schumacher, D. R. Stern and P. R. Graham, J. Electrochem. Soc., 105, 151 (1958).

33. A.K. Gorbachev, E.E. Krech and V.I. Shmorgun, Elektrokhimiya, 13, 1046 (1977).

34. D. Cipris and D.Pouli, J.Electroanal.Chem.,73,125 (1976).

35. B.E. Conway, M.A. Sattar and D. Gilroy, Electrochim. Acta, 14, 677 (1969).

36. R.F. Scarr, J. Electrochem. Soc., 116, 1526 (1969).

37. A.C.C. Tseung and S.Jasem, Electrochim. Acta, 22, 31 (1971).

38. M. de K. Thompson and A.L. Kaye, Trans. Electrochem. Soc., 60, 229 (1931).

39. G. Grube and W. Gaupp, Z. Elektrochem., 45, 290 (1939).

40. D.E. Hall, J. Electrochem. Soc., 128, 740 (1981).

41. M.de K. Thompson and G.H. Sistare Jr., Trans. Electrochem. Soc., 78, 259 (1940).

42. D.A. Thompson, J.A. Davies and W.W. Smeltzer, in "Ion Implant. Met.", 3rd Int. Conf. Modif. Surf. Prop. Met. Ion Implant., (1981).

43. J. Haenen, W. Visscher and E. Barendrecht, Electrochim. Acta, 31, 1541 (1986).

44. S. Trasatti and G. Lodi, in "Electrode of conductive metallic oxide" Part A, p.301, Ed. S. Trasatti, Elsevier Sci. Pub. Co., N. Y. (1981).

45. H. Miles, Y. H. Huang and S. Srinivasan, J. Electrochem. Soc., 125, 1931 (1978).

46. H.B. Beer, in "Electrochemistry in Industry - New Direction" Ed. U.Landau *et al.*,Plenum Press, N.Y. (1982).

47. Y. Matsumoto, H. Yoneyama, and H. Tamura, J. Electroanal. Chem., 83, 167 (1977).

48. A.G.C. Kobussen, F.R. van Buren, T.G.M. van den Belt and H.J.A. van Wees, J. Electroanal. Chem. 96, 123 (1979).

49. R. Kötz and S. Stucki, Electrochim. Acta,31, 1311 (1986).

50. G. Singh, M. H. Miles and S. Srinivasan, in "Special Publication No.455", p. 203, National Bureau of Standards USA, (1976).

51. Y. Matsumoto et al., J.Electrochem. Soc., 133, 2257 (1986).

52. D.K. Kyriacou and D.A. Jannakoudakis,in "Electrocatalysis for Organic Synthesis", John Wiley & Son, N. Y. (1986).

53. T. Loucka, J. Appl. Electrochem. 7, 211 (1977) and 11, 143 (1981).

54. L.D. Burke and M. McCarthy, Electrochim. Acta, 29, 211 (1984).

55. G.I. Volkov, E.L. Babayan and E.P. Siusheva, Khim. Prom., 46, 864 (1970).

56. M.U. Kieinke, M.A.B. de Moraes and O. Teschke, J. Electrochem. Soc., 133, 1815 (1986).

57. R. Parsons, Trans. Faraday Soc., 54, 1053 (1958).

58. "Modern Electrochemistry", Vol. 2., J. O'M. Bockris and A.K.N. Reddy. A Plenum, N. Y. (1970).

59. S. Motoo and M. Watanabe, J. Electroanal. Chem., 110, 103 (1980) and 111, 261 (1980).

60. M. Boudart, AIChE J., 18, 465 (1972) and Adv. Catal., 20, 153 (1969).

61. G. Lodi, E. Sivieri, A. de Battisti and S. Trasatti, J. Appli. Electrochem. 8, 135 (1978).

62. T. Erdey-Gruz and I. Vajasdy, Magy.Kem.Folyoirat, 67, 90 (1961).

63. S.A. Cronstedt, Trans. Electrochem. Soc., 15, 38 (1754).

64. Thenard, Ann. Chim. Phys.,9, 441 (1818); 10, 335 (1819) and 11, 85 (1819).

65. Brit. Pat. 12,608 (1888).

66. O.B.J. Fraser, Trans. Electrochem. Soc., 71, 425 (1937).

67. Foerster, Z. Elektrichem., 13, 414 (1907).

68. Haber, in "Die Elektrolytischen Prozesse der Organischen Chemie", p.59, (1910).

69. Brand and Ramsbottom, J. prakt. Chem., 82, 336 (1910).

70. G. Singh, M. H. Miles and S. Srinivasan, in "Special Publication No. 455", National Bureau of Standards USA, (1975).

71. Mellor, in "Comprehensive Treatise on Inorganic and Theoretical Chemistry", 15, 373 (1936).

72. J. Labat, J. Chim. Phys., 60, 1253 (1963).

73. O. Glemser and J. Einerhand, Z. Anorg. Allgem. Chem., 261, 26 (1950).

74. O. Glemser and J. Einerhand, Z. Anorg. Allgem. Chem., 261, 43 (1950).

75. A.I. Krasilschikov, Zh. Fiz. Khim., 37, 531 (1963).

76. P.C. Milner, J. Electrochem. Soc., 111, 438 (1964).

77. A. Damjanovic, A. Dey and J. O'M. Bockris, Electrochim. Acta, 11, 791 (1966).

78. J.P. Hoare, Nature, 241, 44 (1973).

79. S. Gottesfeld and S. Srinivasan, J. Electroanal. Chem., 86, 89 (1978).

80. J. O'M. Bockris, J. Chem. Phys., 24, 817 (1957).

81. T.P. Hoar, in "Proc. 8th Meeting CITCE", p.439, Madrid, (1965).

82. B.E. Conway and P.L. Bourgault, "Electrochemistry of the Nickel Oxide Electrode", Can. J. Chem., 40, 1690 (1960).

83. A. C. Riddiford, Electrochim. Acta, 4, 170 (1961).

84. W. H. Wade and N. Hackerman, Trans. Faraday Soc., 53, 1636 (1957).

85. L. M. Elina, Zh. Fiz. Khim., 28, 785 (1954).

86. T. Arikado, Electrochim. Acta, 23, 9 (1978).

87. "Techniques of Electrochemistry", p.293, Ed. E. Yeager and A. J. Salkind, Wiley-Intersci. N. Y. (1972).

88. R.S. Yeo, J. Orehotsky, W. Visscher, and S. Srinivasan, J. Electrochem. Soc., 128, 1900 (1981).

89. R.J. Brodd and N. Hackerman, J.Electrochem Soc.,104, 704 (1957).

90. E.G. Gagnon, J. Electrochem. Soc., 121, 512 (1974).

91. D.C Girchame, Chem. Rev., 41, 44 (1947).

92. F.P.Bowden and K.E.W.Grew,Dic. Faraday Soc.,1, 91 (1947).

93. J.G.D. Haenen *et al*, J. Appl. Electrochem.,15, 29 (1985).

94. H. Brown and Knapp, B, in "Modern Electroplating", ch.12 Ed. Lowenheim, F.C., John Wiley & Sons, Inc., N.Y.(1974).

95. E. Yeager, in "Special Publication No. 455", p. 203, National Bureau of Standards USA, (1976).

96. J. Kupka and A. Budniok, *J. Appl. Electrochem.* 20, 1015 (1990).

97. K. Lian, D. W. Kirk and S. J. Thorpe, *Electrochim. Acta*, 36, 537 (1991).

98. Y. Choquette, H. Ménard and L. Brossard, *Int. J. Hydrogen Energy*, 15, 21 (1990).

99. Y. Kunugi, T. Nonaka, Y. Chong, and N. Waunabe, *Electrochim. Acta*, 37, 353 (1992).

100. H. Kronberger, CH. Fabjan and G. Frithum, *Int. J. Hydrogen Energy*, 16, 219 (1991).

101. W.G. Moffatt, in "The Hand Book of Binary Phase", Genium Pub. Inc., (1988).

102. C. Manders, Ann. Phys.,5, 181 (1936).

103. E. Raub and D. Menzel, Z. Metallkd., 52, 831 (1961).

104. I.I. Kornilov and K.P. Myasnikova, TR: Russ. Met. Min., 4, 95 (1964).

105. D. Galizzioli, F. Tantardini and S. Trasatti, J. Appl. Electrochem. 4, 57 (1974).

106. D. Dobos, "Electrochemical Data", Elsevier Science, N. Y. (1975).

107. J.R. Macdonald, "Complex Nonlinear Least Squares Immittance Fitting Program", University of North Carolina, Chapel Hill, NC 27599-3255 USA.

108. J.R. Macdonald and B. Johnson, in "Impedance Spectroscopy", J.R. Macdonald, Ed., John Wiley & Sons Inc., N.Y. (1987), 1-26.

109. A. Brenner, in "Electrodeposition of Alloys-Principles and Practice", Vol.II, p.239, Academic Press, N. Y. (1963).

110. J. St-Pierre and D.L. Piron, J. Appl.Electrochem. 20, 163 (1990).

111. M. Pourbaix, "Atlas of Electrochemical Equilibria in Aqueous Solution", NACE, Houston, USA (1974).

112. G.J. Brug, A.L.G. Van Den Eeden, M. Sluyters-Rehbach and L.H. Slurters, *J. Electroanal. Chem.*, 176, 275 (1984).

113. I. Arul Raj and K.I. Vasu, J. Appl. Electrochem. 20, 32 (1990).

114. K. Appelt, Z. Dominiczak, A. Nowacki and M. Paszkiewick, Electrochim. Acta, 20, 617-625 (1965).

115. R.M. Khalil, "Electrodeposition of Catalytically Active Nickel Powders from Electrolytes of Various Anionic Compositions", J. Appl. Electrochem. 18, 292-297 (1988).

116. M. Kuroda and G. Yto, Japanese Patent, No. 5166 (1953).

117. C.D. Mantell, "Electrodeposition of Powders for Powder Metallurgy", J. Electrochem. Soc. 106, 70-74 (1959).

118. H.L Pinkerton and F.X. Carlin, in "Electroplating Engineering Handbook", 3rd Edition, pp.523-524, Ed. by A. Kenneth Graham, Van Nostrand Reinhold Co., N.Y. (1971).

119. M.W. Shafer et al., J. Electrochem. Soc., 126, 1625 (1979).

120. B.C. Banerjee and A. Goswami, "The Structure of Electro-deposited Nickel", J. Electrochem. Soc.,106, 20-23 (1959) and "Effects of Chloride on the Orientation of Nickel Deposits", J. Electrochem. Soc., 106, 590-592 (1959).

121. C.L. Fan, D.L. Piron, H.J. Miao and M. Rojas, "Hydrogen Evolution in Alkaline Solution on Cobalt Electrodeposits Prepared from Baths of Different Anionic Compositions", (submitted to J. Appl. Electrochem., December 1992).

122. R. Kötz, H.J. Lewerenz and S. Stucki, J. Electrochem. Soc., 130, 825 (1983).

123. R. Kötz, H. Neff and S. Stucki, J. Electrochem. Soc., 131, 72 (1984).

124. CH. Comninellis and G.P. Vercesi, J. of Appli. Electrochem., 21, 335 (1991).

125. Yu. B. Makarychev, E.K. Spasskaya, S.D. Khodkevich and L.M. Yakimenko, Electrokhimiya 12, 994 (1976).

126. J. O'M. Bockris and T. Otagawa, J. Electrochem. Soc., 131, 290 (1984).

127. S. Brunauer, P.H. Emmett and Edward Teller, Adsorption of gases in multimolecular layers, J. Amer. Chem. Soc., 60, 309 (1938).

128. D.G. Evans and D.J. Allardice, in "Analytical Methods for Coal and Coal Products", Vol.1, pp.83-124, Ed.C. Karr, Jr., Academic Press, N. Y. (1978).

129. S. Brunauer, in" The Adsorption of Gases and Vapors", p.511, Princeton University Press, Princeton, N. J. USA, (1943).

130. R.J. Brodd and N. Hackerman, J. Electrochem. Soc., 104, 704 (1957).

131. P. Delahay, in "The Double Layer and Electrode Kinetics", p.129, Interscience, N. Y. (1965).

132. W. Scheider, *J. Phys. Chem.* 79, 127 (1975).

133. R. de Levie, Electrochim. Acta, 9, 1231 (1964) and 10, 113 (1965).

134. D.A. Denton, J.A. Harrison and R.I. Knowles, *Electrochim. Acta*, 26, 1197 (1981).

135. J.A. Harrison, D.L. Caldwell and R.E. White, *Electrochim. Acta*, 29, 1139 (1984).

136. J.A. Harrison, *J. Appl. Electrochem.*. 15, 495 (1985).

137. L. Nyikos and T. Pajkossy, *Electrochim. Acta*, 30, 1533 (1985).

138. R. de Levie, *J. Electroanal. Chem.*, 261, 1 (1989).

139. B.B. Mandelbrot, in "The Fractal Geometry of Nature", Freeman, San Francisco (1982).

140. A. Le Méhauté and G. Crépy, Compt. Rend., 294, 685 (1982).

141. B.B. Mandelbrot, D.E. Passoja and A.J. Paullay, *Nature*, 308, 721 (1984).

142. C. Gabrielli, "Use and Application of Electrochemical Impedance Techniques," Schlumberger Technical Report, p.322, March (1990).

143. J.P. Candy, P. Fouilloux, M. Keddam and H. Takenouti, *Electrochim. Acta*, 26, 1029 (1981).

144. J.P. Candy, P. Fouilloux, M. Keddam and H. Takenouti, *Electrochim. Acta*, 27, 1585 (1982).

145. T. Pajkossy and L. Nyikos, *J. Electrochem. Soc.*, 133, (1986) 2061.

146. R.G. Compton and A.M. Waller, *J. Appl. Electrochem.* 20, 23 (1990).

147. R. de Levie, *J. Electroanal. Chem.*, 281, 1 (1990).

148. W.H. Mulder and J.H. Sluyters, Electrochim. Acta, 33, 303 (1988).

149. A. le Méhauté and G. Crepy, *Solid State Ionics*, 9-10, 17 (1983).

150. T. Pajkossy, *J. Electroanal. Chem.*, 300, 1 (1991).

151. L. Brossard, *J. Hydrogen Energy*, 16, 13 (1991).

152. H.J. Miao and D.L. Piron, Electrochim. Acta, 38, 1079 (1993).

153. H.J. Miao and D.L. Piron, Electrochim. Acta, (paper submitted, 1993).

APPENDIX I

PREPARATION METHODS OF OXIDE MATERIALS

A. Preparation of Rutile-type oxides

SUGGESTED PROCEDURES FOR PREPARATION OF RUTILE-TYPE OXIDE ELECTRODES (FROM 44)

PROCEDURE	SUPPORT	MORPHOLOGY
RuO_2		
$RuCl_3.nH_2O$ dissolved in 20% HCl, dried by heating. Residue dissolved in isopropanol. Deposition layer by layer by brushing. After each layer, dried at 50 °C, kept at 300-550 °C for 10 min in air or O_2. After final cooling, annealing at the same temperature for a few hours in air, O_2, N_2.	Ti, Ta, Pt. 0.1 mm thick plates. Sandblasted, treated with aqua-regia or 20% HCl, washed, rinsed in H_2O, dried.	Films (cracked) 2 μm
Plates are dipped for some minutes in 2 wt. % $RuCl_3.nH_2O$ solutions in isopropanol. Dried at 120 °C for 30 min. Pyrolysis carried out in a quartz crucibile heated in a vertical furnace. Air or O_2 flowing from the bottom through a porous diaphragm. Heating time after each immersion, 15 min, 300-800 °C on quartz.	Ti, silica glass, borosilicate glass, 0.5 mm thick, treated with abrasive and detersive in ultrasonic cleaner. Ti dipped in 20% HCl at room temperature. Glass degreased by refluxing in isopropanol.	Films (compact) 1-3 μm
Same procedure.	Glass microspheres of various porosity. Support is first dehydrated at 300-400 °C	Films
$RuCl_3$ was dissolved in 20% HCl to give 0.1 mol dm^{-3} solutions. Addition of few drops of H_2O_2 found without effect. Solution applied to the support in 6 sequential coatings. After each, dried at moderate temperature, fired at 450 °C for 10 min. Final annealing at 450 °C for 1 h.	Ti plates and rods (disk electrodes). Polished with emery paper and cleaned by immersion in concd. NaOH and concd. HCl.	Films
$RuCl_3$ in propanol brushed onto the support. Each layer fired at 400 °C for 5 min. Final layer 6 h at 400 °C.	Ti plates. Etched in 10% oxalic acid for 30 min at 100 °C.	Films

(contd.)

PROCEDURE	SUPPORT	MORPHOLOGY
$RuCl_3.nH_2O$ dissolved in 1 mol dm^{-3} HCl to give about 0.01 mol dm^{-3} solutions oxidized with 100-fold excess $K_2S_2O_8$ in 0.5 mol dm^{-3} NaOH. RuO_2 deposited on Pt by electrolysis at 0.75 V(sce). Layer used as such or thermally treated at 380 °C.	Pt	
1% $RuCl_3$ in isopropanol deposited on the support kept at 70 °C as a spray prepared in an atomizer under controlled and reproducible conditions. Spray strikes Ti for 5 s. Film dried for 30 s. Another layer deposited then fired at 400 °C for 2 h.	Ti cylinders polished with diamond pastes of corn sizes down to 0.25 μm. Washed with acetone and boiling H_2O. Side-walls insulated with thin teflon-tape. Used as disk electrodes.	Films (compact) 0.1 μm
$RuCl_3.3H_2O$ in n-butylacetate atomized onto the hot support (unspecified temperature). Heated in air at 475 °C for 20 min. Repeated 3-4 times.	Ti metal disk. Polished	Films (compact?)
$RuCl_3.nH_2O$ in isopropanol to give 0.4 mol dm^{-3} solutions. Applied to substrate by a pencil brush. Solvent allowed to evaporate, heating at 400 °C for 5 min. Final annealing at the same temperature for 6 h.	Ti, SiO_2 plates. Ti degreased with acetone and etched in boiling HCl for 30 min. SiO_2 optically flat degreased prior to application.	Films (cracked) 2 μm
Ru + O_2 deposited on the support by chemical vapor transport (*cf.* Table 4)	Fused SiO_2	Crystallites
Ruthenium acetylacetonate sublimed at 190 °C and carried by a dry N_2 stream is mixed with H_2O-satd. N_2 (50 °C) in a concentric delivery tube arrangement positioned approximately 2 cm over the heated (250 °C) Ti disk substrate. Deposition is continued until a thin red brown coating appears, which is baked at 450 °C for 30 min. The procedure may be repeated.	Ti is polished with 5 μm Al_2O_3 and 1 μm diamond paste to a mirror finish, and cleaned ultrasonically.	Films (compact?)
RuO_2 + TiO_2		
The same procedures as above can be used to prepare mixed oxides by employing mixed solutions of $RuCl_3$ + $TiCl_4$ or $TiCl_3$ or $Ti(OBu)_4$ in butanol or HCl or $Ti(OEt)_4$ in propanol.		

(contd.)

PROCEDURE	SUPPORT	MORPHOLOGY
IrO_2		
0.1 mol dm^{-3} $IrCl_4$, 20% HCl with few drops of 30% H_2O_2. Fired at 450 °C. (*cf.* RuO_2).	Ti	Films
Iridium chloride in isopropanol brushed on the support. Heated at 400 °C for 5 min. (*cf.* RuO_2).	Ti	Films
Ir + O_2 deposited on the support by chemical vapor transport (*cf.* Table 4).	Fused SiO_2.	Crystallites
PtO_2		
$H_2PtCl_6.6H_2O$ dissolved to give 0.1 mol dm^{-3} aqueous solutions. Few drops of 30% H_2O_2. Applied on the support in sequential layers. Dried at T < 100 °C. Heated at 350 °C for 10 min. Final heating at 450 °C for 1 h.	Ti plates, polished with emery paper, cleaned including degreasing by refluxing in isopropanol vapor.	Films
MnO_2		
Electrodeposited from 0.5-0.7 mol dm^{-3} $MnSO_4$ + 0.5-0.7 mol dm^{-3} H_2SO_4 at about 90 °C with a current density of 2-12 mA cm^{-2} for a few minutes.	Graphite, RuO_2, Pb, Pt.	
Vacuum impregnation with $Mn(NO_3)_2$ followed by heat treatment. Repeated.	Disks or plates. Porous TiN. Reactive sintering of Ti in H_2 or NH_3 at 1000-1100 °C.	
Thermal decomposition of $Mn(NO_3)_2$ at 190-200 °C. Applied to the support by repeated soaking with the solution. Loading and porosity varied by varying number of soakings.	Porous Ti, sintered from powder.	
0.1 mol dm^{-3} $Mn(NO_3)_2$ in H_2O. Applied to the support, dried at T < 100 °C, decomposed at 170 °C for 10 min. Final heating at 450 °C for 1 h.	Ti, Pt plates.	

B. Preparation of Spinel-type oxides (from 44)

Ceramic technique--The starting materials are metallic oxides. The initial compounds are pulverized and then subjected to a prolonged calcination at a high temperature ranging from 1000 to 1300°C. During calcination, the surface area of the specimen is considerably reduced, and there is consequently no advantage in using them as an electrocatalytic electrode.

Thermal decomposition of mixed nitrates--The starting materials are nitrates. The mixed nitrates are thermally decomposed at 300 to 400°C for 1 to 24 hours. The temperature should be below 450°C(44); at higher temperatures, the system may decompose, with a separation into individual oxide phases.

Co-precipitation of hydroxides or oxalates--The starting material is a mixture of nitrate solutions. The precipitation process is either in a potassium hydroxide or an ammonium oxalate solution, followed by thermal decomposition of precipitates.

Cryochemical method--The starting materials are mixtures of nitrate solutions. The nitrate solutions are sprayed into liquid nitrogen, evacuated, and finally decomposed in air or oxygen. As a result, a uniform mixture of components is obtained.

C. Preparation of Perovskite-type oxides

PREPARATION CONDITIONS FOR $LaNiO_3$ (FROM 44)

STARTING MATERIALS	CONDITIONS	STRUCTURE
$La(NO_3)_3$ $Ni(NO_3)_3$	Decomposition at 500-600 ^0C	Cubic
NiO or $NiCO_3$ $La_2(CO_3)_3$	Heated in a Na_2CO_3 flux at 800 ^0C in air, 72 h.	Hexagonal
$Ni(COOH)_2$ $La(COOH)_2$	Heated at 800 ^0C in pure oxygen	Cubic
$La_2(CO_3)_3$ $Ni(NO_3)_2\ 6H_2O$	Heated at 900 ^0C for 80 h.	Cubic

APPENDIX II

EVALUATION OF IR DROP

A 100 mA/cm^2 current density is applied to the working electrode in 5M KOH solution at 25°C. Then the current is interrupted, and the potential decay on the working electrode is recorded by an oscilloscope connected to the system. The IR drop between the working electrode and the reference electrode in the electrochemical cell is calculated from the potential decay curve as shown below.

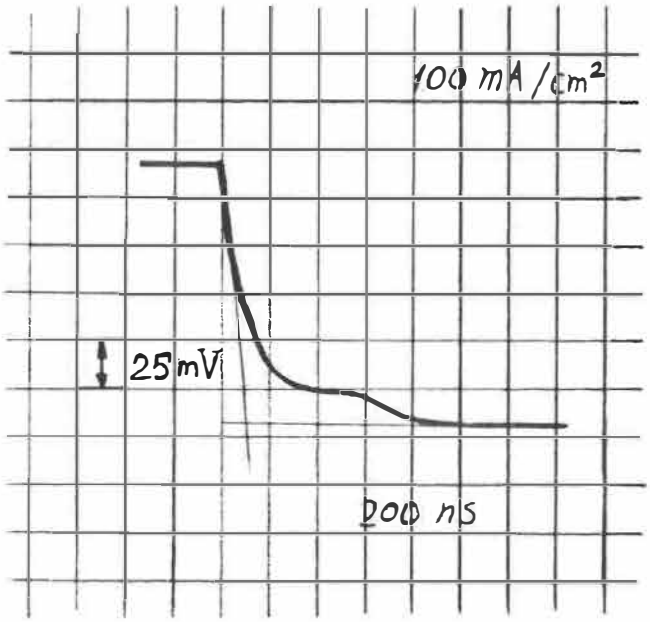

IR = 25 (mV) x 5.5 = 137.5 (mV).